TODA SOLITONS: PROPERTIES AND APPLICATIONS IN DATA TRANSMISSION

By
RONG CHAI
NOVEMBER 2007

A Thesis
Submitted to the Department of Electrical & Computer Engineering
and the School of Graduate Studies
in Partial Fulfilment of the Requirements
for the Degree of
Doctor of Philosophy

McMaster University

DOCTOR OF PHILOSOPHY (2007) McMaster University

(Electrical & Computer Engineering) Hamilton, Ontario

TITLE:	Toda Solitons: Properties and Applications in Data Transmission
AUTHOR:	Rong Chai M.Sc., B.Sc., University of Electronic Science and Technology, Chengdu, China
SUPERVISOR:	Dr. Kon Max Wong Professor, Department of Electrical and Computer Engineering
NUMBER OF PAGES:	xv, 155

Dedications

To my parents, my husband and my son

Abstract

Solitons are solutions to a special class of nonlinear partial differential equations representing certain nonlinear systems. Solitons possess some very interesting transmission properties through nonlinear systems. In this thesis, we examine the properties of Toda solitons and Toda circuits. The time-frequency characteristics, time-bandwidth product, and energy of the *single* and *composite* solitons are studied. The response of the Toda circuit to both deterministic and stochastic inputs are analysed and examined via Volterra series and Runge-Kutta method. The application of the Toda solitons as a message carrier in a data communication system is then proposed. Both single user transmission and a multiplexing scheme exemplified by a two-user transmission scenario are considered. The bandwidth efficiency of the soliton communication system is studied and compared with other systems. The detection performance of the soliton communication system is studied and compared with traditional signalling schemes. Theoretical analysis and numerical results demonstrate that soliton system offers high bandwidth efficiency and high robustness against channel noise for amplitude detection due to the special properties of the soliton and the Toda circuit. The response of mismatched Toda circuit to input soliton is studied and the detection performance of soliton system with mismatched Toda circuit is also examined. It is shown that the slightly mismatched Toda circuit may not affect the detection performance of soliton system, while the mismatched Toda circuit with large mismatch coefficient may deteriorate the system performance seriously.

Acknowledgements

I would like to express my sincere gratitude to my supervisor Dr. Kon Max Wong for his guidance, encouragement and support throughout the development of this project. I wish to thank my co-supervisor Dr. Xun Li for his guidance and very valuable help. I also wish to thank my supervisor committee members: Dr. S. Hranilovic, Dr. S. Kumar and Dr. D. Pelinovsky for their expert guidance and supervision.

I am sincerely grateful to Dr. Jian-kang Zhang for his many insightful discussions. Special thanks go to Cheryl Gies, Helen Jachna and other staff members in the department for providing administrative supports.

I would like to thank my friends Haiyan Tang, Xuan Wang, Yunyu Yi and Sherry He for their friendship which are my lifetime treasures. Thanks also go to many other friends in the digital processing group and network group for their friendship and valuable help.

Finally I would like to thank my parents Yuqi Chai and Peihua Nian for their love, encouragement and for being my best teachers and friends. Thanks to my parents-in-law Zi'an Yang and Cunfang Dong for their encouragement and great assistance. Most importantly, special thanks to my husband Shaojun Yang for his encouragement, support and love.

List of Abbreviations

ASK	Amplitude Shift Keying
AT	Amplitude Detection
AWGN	Additive White Gaussian Noise
BER	Bit Error Rate
BPSK	Binary Phase Shift Keying
DC	Direct Current
DSP	Digital Signal Processing
EO	Electrical-to-Optical
FDM	Frequency Division Multiplexing
FPU	Fermi, Pasta and Ulam
ISM	Inverse Scattering Method
IST	Inverse Scattering Transform
KdV	Korteweg-de Vries
LPF	Low Pass Filter
ML	Maximum Likelihood
NLS	Nonlinear Schrödinger
OE	Optical-to-Electrical
OOK	On-Off Keying
PDE	Partial Differential Equations
PDF	Probability Density Function

PSD	Power Spectral Density
PSK	Phase Shift Keying
SADM	Soliton Amplitude Division Multiplexing
S-G	Sine-Gordon
SNR	Signal-to-Noise Ratio
T-B	Time-Bandwidth
TL	Toda Lattice
WDM	Wave Division Multiplexing

Notations

$\sum_n$	Summation over n
$\int_x$	Integration w.r.t. y
$E[x]$	Expectation of x
$\max(x, y, z)$	Maximum among $x,\ y,\ z$
$\frac{\mathrm{d}y}{\mathrm{d}x}$	Derivative of y w.r.t. x
y_x	Partial derivative of y w.r.t. x
$\dot{x}$	Derivative of x w.r.t. time
$O(x)$	Order of x

Contents

List of Tables

List of Figures

Chapter 1

Introduction

1.1 History of Solitons

Solitons[13] are stable solitary waves, which are exact solutions to a class of nonlinear partial differential equations (PDE) representing some particular nonlinear systems. The phenomena of solitons was first observed by a Scottish engineer named J. S. Russell on the Edinburgh-Glasgow canal in 1834. The discovery was described in his own words as following [46]:

"I was observing the motion of a boat which was rapidly drawn along a narrow channel by a pair of horses, when the boat suddenly stopped - not so the mass of water in the channel which it had put in motion; it accumulated round the prow of the vessel in a state of violent agitation, then suddenly leaving it behind, rolled forward with great velocity, assuming the form of a large solitary elevation, a rounded, smooth and well-defined heap of water, which continued its course along the channel apparently without change of form or diminution of speed. I followed it on horseback, and overtook it still rolling on at a rate of some eight or nine miles an hour, preserving its original figure some thirty feet long and a foot to a foot and a half in height. Its height gradually diminished, and after a chase of one or two miles I lost it in the

windings of the channel. Such, in the month of August 1834, was my first chance interview with that singular and beautiful phenomenon which I have called the Wave of Translation".

Russell made some further experimental investigations of these waves and he noticed some key properties of these waves:

(1) Unlike normal waves which would tend to either flatten out, or steepen and topple over, the waves are stable, and can travel over very large distances without distortion .

(2) Assuming the depth of water is h, the velocity of the wave having amplitude a is given by $v = \sqrt{g(a+h)}$, where g is the acceleration of gravity.

(3) A sufficiently large initial mass of water produces two or more independent solitary waves.

The observation of J. S. Russell appeared to contradict the wave theory at the time, which predicted that a wave of finite amplitude could not propagate without distortion and it could tend to steepen or break. This contradiction was resolved by J. Boussinesq and L. Rayleigh in 1880, who showed that a wave might propagate stably if the velocity increase of the local wave resulted from the nonlinearity was compensated by the decrease from the dispersion.

Later in 1895, the mathematical model of the water wave Russel observed, i.e. the unidirectional propagation of long waves in shallow water region was derived by D. J. Korteweg and G. de Vries and named after the authors. This was the Korteweg-de Vries equation or KdV equation for short, the solution of which turned out to be a stably propagating pulse.

Since the derivation of the KdV equation, few further research work on soliton had been done until 1955 when Fermi, Pasta and Ulam (FPU) investigated how the equilibrium state could be approached in a one-dimensional nonlinear lattice. It was expected that the nonlinear interactions among the normal modes of the linear system

would lead to the energy of the system being evenly distributed throughout all the normal modes. Surprisingly, the system did not tend to share the energy among different modes, but returned to the initial state after some periods.

To pursue an explanation of the FPU experiment, Zabusky and Kruskal studied the continuum limit of the experiment in 1965 and obtained the Korteweg-de Vries equation. More importantly, they found that the solitary wave solutions of the KdV equation exhibited extremely stable properties and preserved their identities even after nonlinearly interacting with each other. To emphasize this particle-like property, they named the nonlinear wave "Soliton".

1.2 Solitons in Nature and Technology

During the long history of the development of soliton theory, many solitons phenomena have been observed in a variety of areas. The water wave observed by Russell can be classified as a type of surface solitary wave which rises from the shallow water region. Other solitary waves have also been observed in different water regions. In deep water region, for instance, in the ocean, internal solitary waves [41] which are generated by the nonlinear deformation of internal tides have been observed. These waves vertically displace the thermocline and cause internal currents with near-surface flow convergence and divergence. A well-known ocean phenomena, the Tsunami has also been shown to be related to soliton [15]. It is indeed generated by a large enough sea soliton.

Besides water region, solitons can also be observed in plasma and fluid. In plasma of hot electrons and cold ions, the ions with low-frequency fluctuate near the ion plasma frequency, while the electrons follow the motion of the ion and preserve an approximate local charge neutrality. Due to the balance of the inertia of ions and the pressure of the electrons, an ion-acoustic solitary wave [5, 60], which describes the

density of the ions fluctuation, can be observed.

A typical example of long-surviving advection of materials in fluids is the motions of a single vortex filament in background fluid [21, 31], which have been observed to exhibit a stable propagation of a loop or a hump of helical motion along a line vortex. This is called vortex soliton, which is indeed a large class of solitons and have also been found in superfluid, superconductors, high energy physics and optical lattice, etc. Particularly, the vortex solitary waves formed while propagating along the lattices are classified as vortex lattice solitons or simply lattice solitons.

The first lattice soliton observed in a discrete lattice is the Toda soliton in the nonlinear Toda lattice [54], the soliton solution of which describes the local displacement of the equilibrium positions of particles in a one-dimensional lattice. Lattice solitons are also found in molecular chain with anharmonicity [12] and in the energy transport of protein chains [38], etc.

The most significant technical application of the soliton is as an information carrier along optical fibers. The optical soliton is governed by the nonlinear Schrödinger (NLS) equation, and exhibits a balance between the effects of optical dispersion and nonlinear self-phase modulation. In 1973, Hasegawa and Tappert [4, 20] were the first to show theoretically that in an optical fibre, solitary waves can be generated and that the NLS equation description of the combined effects of dispersion and nonlinearity self-phase modulation give rise to envelope solitons. Mollenauer and his co-workers first described the experimental realization of the optical soliton in a low loss single-mode fibers in 1980. Over the past twenty years, there has been rapid developments both in theoretical and experimental research on optical soliton communication [19, 52].

1.3 Motivation and Scope of Thesis

Solitons possess some very interesting transmission properties through nonlinear systems, e.g. (a) Solitons propagate stably through a nonlinear medium properly matched to the characteristics of the solitons. (b) Solitons with different parameters propagate with different velocities along the nonlinear system. (c) Solitons preserve their identities after nonlinearly interacting with each other during the propagation. These and other properties of the soliton are explored in this thesis for their use in a wireless soliton communication system yielding advantages including high bandwidth efficiency and robustness against channel noise and timing error.

We employed the Toda soliton [53] in our consideration because of the ease with which it is generated and processed by a LC Toda circuit. The application of Toda solitons in communication was first proposed in [50] and [51] in which experimental investigations were reported on the modulation and multiplexing of a pair of soliton trains which are either amplitude or phase modulated. It was suggested that the recurrence phenomena could be used for secure communications. A much more detailed soliton multiplexing system model was presented and studied in [49] with particular consideration on applications in a wireless channel environment.

In this thesis, the properties of Toda solitons and Toda circuit are further studied. Applying these properties to data transmission, we propose an on-off keying Toda soliton system, which can be regarded as the special case of the system model proposed in [49]. We focus on the detection performance of a soliton transmission system through additive white Gaussian noise (AWGN) channel. The problem of mismatched Toda circuit response to input solitons are also studied.

In Chapter 2 of this thesis, we give a brief overview of solitons and soliton supporting systems. In Chapter 3, we discuss several properties of single solitons and

composite solitons, including the time and frequency domain characteristics, time-bandwidth characteristics and signal energy. In Chapter 4, the characteristics of Toda circuit response to deterministic and stochastic inputs are studied. We show that the circuit responses at early stages exhibit weak nonlinearity and can be analyzed by the third order Volterra series. If the Toda circuit is relatively long, at the later stages of the circuit, for higher accuracy, we should apply the Runge-kutta method to examine the circuit response to the combination of soliton and Gaussian noise. In Chapter 5, we apply Toda soliton in data transmission and propose the soliton communication system model, including the single user system and the multiplexed system. The detection performance of the soliton systems are studied and compared with other systems. In addition, the time bandwidth efficiency of soliton multiplexing system is also studied and compared with the other systems. In Chapter 6, the problem of mismatched Toda circuit response to input soliton is examined. In the case of small perturbation, the circuit output can be assumed to be a soliton. We study the dependence of the output soliton parameters on the input soliton, mismatch coefficient and circuit stages. The detection performance of soliton system with mismatched Toda circuit is also examined. In Chapter 7, we draw main conclusions and discuss possible extensions of our work.

1.4 Main Contributions of Thesis

A soliton multiplexing system model was proposed and studied in [49] and [48] with particular consideration on applications in a wireless channel environment. In the proposed two-user multiplexing and binary modulation system, the information of each user is represented by two single solitons with different amplitudes. The composite solitons formed from two constituent solitons representing information of each user are applied as information carrier and the detection are performed on each single

soliton after the composite is separated into two individual solitons while propagating along the Toda circuit at the receiver. The Cramér-Rao bound for the single soliton detection was derived and that for the composite soliton was evaluated numerically.

The properties of both the Toda solitons and Toda circuit are not fully studied in [49] and [48]. The examination of the Cramér-Rao bound is based on the assumption that the composite soliton will separate into two individual solitons without distortion after passing through the Toda circuit. However, this is only satisfied under the noise-free scenario. In this thesis, we will show that under the effect of channel noise, the composite soliton may not be able to separate into original two constituent solitons; even though the composite soliton separates to two solitons, the distortion of each soliton may be large resulting in detection errors.

In this thesis, after a quick review of several commonly-used solitons and soliton supporting systems, we start the study of the properties of the Toda solitons. We examine the time and frequency domain characteristics of the single and the composite Toda soliton and show the dependence of the characteristics on its parameters. The time-bandwidth (T-B) product of both single and composite Toda soliton are studied. We proved that the T-B product of the single Toda soliton turns out to be a constant independent on the parameter of the soliton. The closeness between this constant and the optimal T-B product achieved by Gaussian pulse indicates that the single Toda soliton has high energy localization and therefore, is suitable to be carrier of information. The T-B product of the composite soliton is examined numerically and we show that the optimal T-B product of the composite soliton can be as small as that of the single soliton. The condition for the composite Toda solitons achieving the optimal T-B product is also described. We also calculate the energy of the Toda solitons. The exact energy formula of the single Toda soliton is given. The energy of the composite soliton is calculated numerically and we show that the energy of the composite soliton is always smaller than the sum of two single solitons. The condition

of the maximum energy saving of the composite soliton is examined.

We then turn to the examining of the properties of Toda circuit. In particular, we study the circuit responses to stochastic inputs, i.e., the combination of the single and the composite soliton with Gaussian noise. We propose to apply Volterra series in the Toda circuit analysis. Volterra series is known to be an efficient mathematical tool in calculating responses of weakly nonlinear circuits. We verify that at the early stages, Toda circuit exhibits weak nonlinearity and can be analyzed by the third order Volterra series. Applying this method, the statistical characteristics of the circuit outputs are calculated and the circuit output noise is modelled. We also observe that the nonlinearity of Toda circuit becomes stronger as the stage number increases resulting in large approximation error of the Volterra series. Therefore, for high accuracy, Runge-Kutta method is applied in this case. We show that for circuit input being noise corrupted solitons, high nonlinearity of the circuit results in the circuit output being the combination of soliton(s), transients and oscillations.

Applying Toda solitons in data transmission, we propose the on-off keying soliton communication system model, including the single soliton system and the soliton multiplexing system. While this system can be regarded as a special case of the system model proposed in [48], we can show that this system achieves much better detection performance compared to that proposed in [48]. The time bandwidth efficiency of the soliton multiplexing system is studied and compared with that of other systems. The results show that the new multiplexing system enjoys much higher bandwidth efficiency than the FDM system. Applying both maximum likelihood (ML) detection and amplitude detection (AT) methods, we study the detection performance of soliton system and compare the results with that of traditional amplitude shift-keying (ASK) system. We show that while the ML detection performance of soliton system is similar to that of the ASK scheme, the AT detection performance of the soliton system is better than that of the ASK scheme. This is resulted from the high bandwidth

efficiency of the soliton pulse and the special filtering effects of the receiver Toda circuit. We also study the detection performance of the ASK scheme using soliton pulse under small timing error. We show that compared to other pulses, such as Raised Cosine and Rectangular, soliton is more robust in performance against timing error.

As we will show in later chapters, Toda circuit with linear inductors and nonlinear capacitors supports the stable propagation of the Toda solitons with same inductor and capacitor parameters. If the parameters of the input soliton are different from those of the Toda circuit, an input soliton might be distorted while propagating along the Toda circuit. In this case, we designate this to be a mismatch between Toda circuit and input soliton occurs. The problem of examining the mismatched Toda circuit response to input Toda soliton is of particular importance because in practice, due to circuit technology or imperfect knowledge of the Toda circuit, the parameters of the inductors and the capacitors of the Toda circuit may not be exactly accurate. In this thesis, we study a relatively common situation, such that the parameters mismatch in the Toda circuit is relatively small. In this case, the circuit output can still be assumed to be a soliton. Based on KdV approximation method, Runge-Kutta method and inverse scattering transform, we study the dependence of the parameters of the output soliton on the characteristics of the input soliton, mismatch coefficient and circuit stages. We show that for small mismatch coefficient and for input soliton with small amplitude, the perturbation only results in small distortion of the output phase shift, while the amplitude of input soliton remains unchanged. For large mismatch or large input soliton, both the amplitude and phase shift are distorted and the amplitude distortion increases with the increase of input soliton amplitude and mismatch coefficient, thereby will affect the accuracy of detection. The detection performance of the soliton system with mismatched Toda circuit is also examined. We show that for both single user and multiplexing soliton system, the

effects of the slightly mismatched Toda circuit on the system detection performance is relatively small, while the mismatched Toda circuit with large mismatch coefficient may deteriorate the system performance seriously.

Chapter 2

Solitons and Soliton Supporting System

Similar to the KdV equation, many other nonlinear equations have been shown to support soliton solutions, including the Nonlinear Schrödinger (NLS) equation, Sine-Gordon (S-G) equation and the Toda lattice (TL) equation, etc. These equations are key equations describing a wide variety of physical phenomena and are called "Integrable Equations" as the solutions of these equations can be obtained exactly by means of inverse scattering transform (IST) [8]. These solutions typically consist of solitons plus some transients decaying to zero as time goes to infinity. In this chapter, we will discuss the mathematical expressions of some of these typical soliton equations, then we focus on the IST of the KdV soliton and the TL soliton and study their relationship.

2.1 Mathematical Descriptions of Solitons

2.1.1 Korteweg-de Vries Equation

As we have mentioned in Chapter 1, the KdV equation was derived by Korteweg and de Vries in 1895 to describe weakly nonlinear shallow water waves [28]. It is a nonlinear, dispersive partial differential equation (PDE) for a function u of two real variables, x and t:

$$u_t - 6uu_x + u_{xxx} = 0 \tag{2.1}$$

where $u(x,t)$ is the amplitude of the travelling wave and $u_t = \frac{\partial u}{\partial t}$, $u_x = \frac{\partial u}{\partial x}$ and $u_{xxx} = \frac{\partial^3 u}{\partial x^3}$. In Eq. (2.1), the second and third terms represent the nonlinear and dispersion effects respectively. The nonlinear effect causes the steepening of the waveform, while the dispersion effect makes the waveform spread. The waveform steepening or dispersion may occur both in time and space, such that if the time is fixed, we observe the waveform change in space, conversely, if the space is fixed, we would be able to observe the change of the waveform in time. Due to the compensation of these two effects, a stationary solitary waveform called the KdV soliton exists and can be expressed as:

$$u(x,t) = \frac{\beta^2}{2}\mathrm{sech}^2\big(\frac{\beta}{2}(x - \beta^2 t - \phi_0)\big) \tag{2.2}$$

where β is a parameter characterizing both the amplitude and the width of the soliton and ϕ_0 is an arbitrary constant representing the initial phase shift of the soliton.

It is clear from Eq. (2.2) that if at $t = 0$, if input an initial waveform $u(x,0) = \frac{\beta^2}{2}\mathrm{sech}^2\big(\frac{\beta}{2}(x - \phi_0)\big)$ into the system characterized by the KdV equation, then at any $t = t_0$, there exists a stable propagation of the input wave without any distortion. For an arbitrary initial condition, the solutions of the KdV equation can be exactly specified by means of the inverse scattering transform, as we will show in Section 2.2.1.

2.1.2 Nonlinear Schrödinger Equation

The nonlinear Schrödinger (NLS) equation [62] is a nonlinear version of Schrödinger's equation. It was first proposed and solved by Zakharov and Shabat in 1972. The equation is expressed as:

$$ju_t + \frac{1}{2}u_{xx} + |u|^2 u = 0, \quad -\infty < x < \infty, \ t > 0 \tag{2.3}$$

where $j = \sqrt{-1}$. In contrast to the KdV equation, where the real travelling wave solution is obtained, the dependent variable in NLS equation can be complex, that is, the evolutions of two quantities, i.e magnitude and phase, are governed by the equation. It can be shown that the localized stationary single soliton solution of the NLS equation is given by:

$$u(x,t) = \beta \text{sech}(\beta(x - x_0)) \exp\left(j\frac{\beta^2}{2}t + j\phi_0\right) \tag{2.4}$$

where β is the parameter characterizing the amplitude and width of the soliton, x_0 is the central position of the soliton pulse and ϕ_0 denotes the phase.

NLS soliton has been observed in fluids, such as the shallow water wave and the motion of the vortex filament. It is also observed in optical fibre [4, 20] and has shown promising application in optical communication [19].

2.1.3 Sine-Gordon Equation

The sine-Gordon equation [31, 32] is a partial differential equation in two dimensions. For a function u of two real variables, x and t, it is

$$u_{tt} - u_{xx} + \sin u = 0. \tag{2.5}$$

While Eq. (2.5) cannot be solved analytically in general, several classes of solutions can be found by making the assumption that the solution is of the form $u(x,t) =$

arctan $\frac{\phi(x)}{\psi(t)}$. The single soliton solution can be expressed as:

$$u(x,t) = 4\arctan\left(\exp\left(\frac{x-\beta t}{\sqrt{1-\beta^2}}\right)\right) \tag{2.6}$$

where $\beta = \frac{\sqrt{m^2-1}}{m}$, $|m| > 1$ is a constant. For m being positive, the solution is a soliton known as the "kink solution". For m being negative, a similar solution can be obtained by replacing x by $-x$. This solution is known as "antikink solution".

Sine-Gordon equation arises in a variety of problems including the propagation of ferromagnetic domain walls, self-induced transparency in nonlinear optics, and the propagation of magnetic flux quanta in long Josephson transmission lines, etc.

2.1.4 Toda Lattice

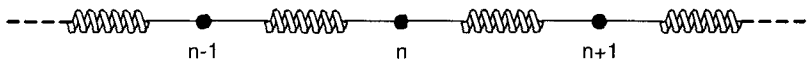

Figure 2.1: Model of Spring Toda Lattice

The Toda lattice [53] as shown in Fig. 2.1, is a nonlinear one-dimensional model which describes the motion of a chain of particles with nearest neighbor interactions. Denoting Q_n the displacement of the nth particle, m_n denotes the mass of the nth particle. Defining $r_n = Q_{n+1} - Q_n$ The equations of motion for the lattice of particles can be written as:

$$m_n \frac{d^2 r_n}{dt^2} = f_{n-1} + f_{n+1} - 2f_n, \quad n = 1, 2, ... \tag{2.7}$$

where f_n is the force of the spring on the nth particle. In 1966, Morikazu Toda [54] found the nonlinear lattice with exponential potential admit analytical solutions. Choosing the force to be

$$f(n) = a(\mathrm{e}^{-br_n} - 1)$$

where a, b are constants s.t. $ab > 0$, Eq. (2.7) transforms into:

$$m_n \frac{d^2 r_n}{dt^2} = a(2e^{-br_n} - e^{-br_{n-1}} - e^{-br_{n+1}}) \tag{2.8}$$

or equivalently, we obtain

$$\frac{\mathrm{d}^2}{\mathrm{d}t^2} \log\left(1 + \frac{f_n(t)}{a}\right) = \frac{b}{m}(f_{n-1}(t) - 2f_n(t) + f_{n+1}(t)) \tag{2.9}$$

It can be proved [53] that Eq. (2.9) supports soliton solution, as shown in the following:

$$f_n = a\beta^2 \mathrm{sech}^2(\beta t\sqrt{\frac{ab}{m}} - Pn - x_0) \tag{2.10}$$

where $\beta = \sinh P$, P is the parameter determining both the amplitude and the width of the soliton, x_0 is an arbitrary constant representing the initial phase shift of soliton. Eq. (2.8) describes a single bump travelling trough the lattice stably with constant speed $\frac{sinh(P)}{P}$.

2.2 Solution of Soliton Equations - Initial Value Problem of Soliton Equation

A systematic development of the mathematical theory of solitons began in 1967 when Gardner et al. [8] devised a method for constructing solutions of the KdV equation emerging from arbitrary initial conditions. Known as the inverse scattering transform (IST), this approach was later extended to solve the initial-value problem of many other soliton supporting equations [16, 39, 62]. While the mathematical manipulation of applying IST for treating different soliton equations are quite different, the basic procedures are very similar and can be summarized in following three steps.

Step 1: The nonlinear dynamics of the soliton equations are mapped onto an associated linear scattering equation, each discrete eigenvalue of which corresponds to a particular soliton. Given the initial condition of the soliton equation, i.e. the

solution at time $t = 0$, the scattering data of the linear scattering equation can be calculated.

Step 2: The time evolution of the associated linear scattering data is computed.

Step 3: Applying the inverse scattering calculation, the time evolved solution of the soliton equation can be obtained from the evolved scattering data.

In this chapter, we introduce the IST of the KdV equation and the TL equation, since they are of particular importance to this thesis. For a detail description of the IST and applying IST for solving some other soliton equations, interested readers can refer to [2].

2.2.1 Inverse Scattering Transform of the KdV Equation

The IST of the KdV equation starts from relating the KdV equation to the one-dimensional Schrödinger equation. After some tedious mathematical manipulations, it can be shown [8] that the solution of the KdV equation is the compatability condition of a pair of linear equations (Lax) on $\psi(x,t)$ satisfying:

$$-\psi_{xx} + u(x,t)\psi = \lambda\psi \tag{2.11}$$

$$\psi_t = A\psi \tag{2.12}$$

where λ and ψ are the eigenvalue and the eigenfunction of Eq. (2.11) and Eq. (2.12) respectively and A is the operator. It can be proved that the spectrum of the Schrödinger operator consists of the continuous spectrum corresponding to $\lambda > 0$ and a finite-dimensional discrete spectrum, i.e. $\lambda_n < 0,\ n = 1, 2 \cdots, N$. The continuous spectrum characterizes the oscillation and transient component of the solution, while the discrete spectrum represents the soliton component of the solution with each eigenvalue characterizing a soliton.

Taking into account the boundary condition of the equation, i.e. $u(x,t) \to 0$ as $x \to \infty$, we can obtain the eigenfunctions corresponding to both continuous and

discrete eigenvalues. For the continuous spectrum, we define $k = \sqrt{\lambda}$, the solution of the eigenfunction $\psi(x;k)$ can be written as following:

$$\psi(x;k) \sim \begin{cases} \mathrm{e}^{-jkx} + b(k)\mathrm{e}^{jkx} & \text{as } x \to \infty \\ a(k)\mathrm{e}^{-jkx} & \text{as } x \to -\infty \end{cases}$$

where $a(k)$ and $b(k)$ are complex constants for a fixed k and are referred to as the transmission and reflection coefficients respectively. Similarly, defining $\kappa_n = \sqrt{-\lambda_n}$, $n = 1, 2 \cdots, N$, the discrete eigenfunction $\psi_n(x)$ can be written as:

$$\psi_n(x) \sim c_n \mathrm{e}^{-\kappa_n x} \qquad \text{as } x \to \infty$$

where c_n is the normalization coefficient, such that $\int_{-\infty}^{\infty} \psi_n^2(x) = 1$. For a given initial condition $u(x,0)$, the scattering data, $b(k), \kappa_n, c_n, n = 1, 2 \cdots, N$ can be determined uniquely.

It can be shown that when $u(x,t)$ evolves obeying Eq. (2.1), the discrete eigenvalue λ_n does not depend on time, that is κ_n also remains constant. The time-dependence of other scattering data can be determined from Eq. (2.12):

$$\begin{aligned} b(k;t) &= b(k;0)e^{-8jk^3t} \\ c_n(t) &= c_n(0)e^{4\kappa_n^3 t} \end{aligned}$$

Based on these scattering data, the solution of the KdV equation at arbitrary time t, i.e. $u(x,t)$ can be determined uniquely. It can be shown that $u(x,t)$ can be obtained by:

$$u(x;t) = -2\frac{\partial K(x;x;t)}{\partial x} \tag{2.13}$$

where $K(x;z;t)$ is the solution of the Marchenko equation [8]:

$$K(x;z;t) + F(x+z;t) + \int_x^{\infty} K(x,y;t)F(y+z;t)dy = 0 \tag{2.14}$$

and $F(x;t)$ is defined as

$$F(x;t) = \sum_{n=1}^{N} c_n^2(t) \exp\left(4\kappa_n^3 t - \kappa_n x\right) + \frac{1}{2\pi}\int_{-\infty}^{\infty} b(k;t) \exp\left(jkx\right)dk \tag{2.15}$$

2.2.2 Inverse Scattering Transform of the Toda Soliton

The normalized Toda lattice equation Eq. (2.8) can be rewritten as:

$$\frac{dQ_n}{dt} = P_n \tag{2.16a}$$

$$\frac{dP_n}{dt} = \mathrm{e}^{-(Q_n - Q_{n-1})} - \mathrm{e}^{-(Q_{n+1} - Q_n)} \tag{2.16b}$$

where $n = 1 \cdots N$. The initial value problem for the TL equation solves the problem of given all the lattice states Q_n at time $t = 0$, obtaining Q_n at arbitrary time t. Similar to the KdV equation, an inverse scattering transform exists for the TL equation and it was developed by H. Flaschka in 1974 [16].

The IST of the TL equation starts from the connecting of the soliton equation with a pair of Lax equations by introducing new variable a_n and b_n, such that

$$a_n = \frac{1}{2}\mathrm{e}^{-(Q_{n+1} - Q_n)/2} \tag{2.17a}$$

$$b_n = \frac{1}{2}P_n \tag{2.17b}$$

Introducing $N \times N$ matrix L and B, we obtain an eigenvalue problem for a discrete Schrödinger equation and an evolution problem for the eigenvector φ:

$$(L\varphi)(n) = a_{n-1}\varphi(n-1) + b_n\varphi(n) + a_n\varphi(n+1) = \lambda\varphi(n) \tag{2.18}$$

$$\frac{d\varphi(n)}{dt} = (B\varphi)(n) = a_{n-1}\varphi(n-1) - a_n\varphi(n+1) \tag{2.19}$$

where scalar λ is the eigenvalue of Eq. (2.18), and $N \times 1$ vector φ is the eigenfunction of the equation, $\varphi(n)$ is the nth element of φ.

The expression of an infinite Toda lattice can be obtained from Eq. (2.18) and Eq. (2.19) by letting $|N| \to \infty$. Assuming that the motion of the lattice is confined in a finite region $|n| \leq N_0$, we obtain the boundary condition of the TL equation:

$$a_n = \frac{1}{2}, \qquad b_n = 0, \qquad \text{for } |n| > N_0$$

For convenience, introducing variable z, such that $\lambda = \frac{z+z^{-1}}{2}$, it can be proved that the corresponding boundary solution of the eigenfunction $\varphi(n)$ can be expressed as:

$$\varphi(n,z) = \begin{cases} \phi(n,z)\mathrm{e}^{-\jmath\omega t}, & n \to \infty \\ \psi(n,z)\mathrm{e}^{\jmath\omega t}, & n \to -\infty \end{cases}$$

where $\omega = \frac{z-z^{-1}}{2\jmath}$. $\phi(n,z)$ and $\psi(n,z)$ are denoted as wave functions and for $|z| = 1$, satisfy:

$$\begin{aligned} \phi(n,z) &\to z^n, \quad n \to \infty \\ \psi(n,z) &\to z^{-n}, \quad n \to -\infty \end{aligned}$$

Defining the scattering function as:

$$S(n,z) = \frac{\psi(n,z)}{\alpha(z)} = \phi(n,z^{-1}) + R(z)\phi(n,z)$$

The asymptotic forms of $S(n,z)$ are:

$$S(n,z) \to \begin{cases} z^{-n} + R(z)z^n, & n \to \infty \\ z^{-n}/\alpha(z) \quad , & n \to -\infty \end{cases}$$

where $1/\alpha(z)$ is defined as transmission coefficient. The poles of $\alpha(z)$ correspond to the discrete eigenvalues of the TL equation and are denoted by z_i, $i = 1 \cdots N$, where N is the total number of the solitons. $R(z)$ is defined as the reflection coefficient. Defining $\xi(n,z_i) = c_i\phi(n,z_i)$ as the normalized wave function, the normalization constants c_i can be obtained from $\sum_{n=-\infty}^{\infty}[\xi_i(n,z_i)]^2 = 1$.

The scattering data of the TL equation include $R(z)$, z_i and c_i, $i = 1 \cdots N$. Given lattice states, i.e. $a(n)$, $b(n)$ at $t = 0$, the scattering data can be determined. It can be proved that the time evolution of the scattering data can be expressed as:

$$\begin{aligned} z_j(t) &= z_j(0) \\ c_j(t) &= c_j(0)\mathrm{e}^{t(z_k^{-1}-z_k)/2} \\ R(z,t) &= R(z,0)\mathrm{e}^{t(z^{-1}-z)} \end{aligned}$$

Lattice states at arbitrary time t can then be obtained based on time evolution of scattering data. Defining function $F(m,t)$ as:

$$F(m,t) = \frac{1}{2\pi j}\oint R(z,t)z^{m-1}dz + \sum_{i=1}^{N} c_i(t)^2 z_i^m$$

$\kappa(n,m,t)$ can be obtained by solving the following discrete integral equation:

$$\kappa(n,m,t) + F(n+m,t) + \sum_{n'=n+1}^{\infty} \kappa(n,n',t)F(n'+m,t) = 0, \qquad m > n$$

Defining $K(n,m,t)$ such that

$$K(n,n,t)^{-2} = 1 + F(2n,t) + \sum_{n'=n+1}^{\infty} \kappa(n,n',t)F(n'+m,t)$$

$$\kappa(n,m,t) = \frac{K(n,m,t)}{K(n,n,t)}$$

Lattice states $a_n(t)$, $b_n(t)$ can then be computed from

$$a_n(t) = \frac{K(n+1,n+1,t)}{2K(n,n,t)}$$

$$b_n(t) = \frac{K(n,n+1,t)}{2K(n,n,t)} - \frac{K(n-1,n,t)}{2K(n-1,n-1,t)}$$

Based on $a_n(t)$ and $b_n(t)$, lattice displacement at time t, i.e. $Q_n(t)$ can then be obtained.

2.3 From KdV Soliton to Toda Soliton

Both the KdV and the TL equations are integrable and the form of the solutions is quite similar indicating some close relation between them. In fact, it can be shown that KdV equation is a continuous approximation of the Toda lattice equation.

Under the condition of small $f_n(t)$, the nonlinear term in TL equation, i.e. Eq. (2.9) can be approximated to

$$\log\left(1 + \frac{f_n(t)}{a}\right) \approx \frac{f_n}{a} - \frac{f_n^2}{2a^2} \tag{2.20}$$

Denoting $v_m = \sqrt{\frac{ab}{m}}$, $u = -\frac{2}{va}V$ and applying the Gardner-Morikawa transformation [8]:

$$\xi = \epsilon^{1/2}(n - v_m t), \quad \tau = \epsilon^{3/2}\frac{v_m}{24}t \tag{2.21}$$

Substituting Eq. (2.20) and Eq. (2.21) into Eq. (2.9), and choose $v = 1$, we obtain the original KdV equation [36]:

$$u_\tau - 6uu_\xi + u_{\xi\xi\xi} = 0 \tag{2.22}$$

Comparing Eq. (2.9) and Eq. (2.22), it is clearly seen that the governing equation of the Toda circuit can be transformed into the KdV equation by introducing new time variable τ and displacement variable ξ. We have shown that the single KdV soliton solution of Eq. (2.22) is [13]:

$$u = -2\beta^2 \text{sech}^2(\beta\xi - 4\beta^3\tau) \tag{2.23}$$

Using Eq. (2.21), the corresponding Toda soliton solution of Eq. (2.22) can be expressed as:

$$f_n(t) = a\beta^2 \text{sech}^2((\beta + \frac{\beta^3}{6})t\sqrt{\frac{ab}{m}} - \beta n) \tag{2.24}$$

Under the condition of small input, i.e., $\beta \ll 1$, we obtain, $\beta + \frac{\beta^3}{6} \approx \beta$ and $\beta \approx \text{asinh}(\beta) = P$, Eq. (2.24) reduces to the Toda soliton of Eq. (2.10), which means the KdV soliton can approximate Toda soliton accurately in this case.

2.4 Summary

In this chapter, we introduce the mathematical description of several classes of common solitons, including KdV soliton, NLS soliton, Sine-Gordon soliton and Toda soliton. The corresponding supporting equations, i.e., the KdV equation, the NLS equation, Sine-Gordon equation and the governing equation of the Toda lattice are

also introduced. The method of solving initial value problem of soliton equation, i.e., IST is then discussed through the examples of the KdV equation and the Toda lattice. The relationship of the KdV soliton and the Toda soliton is then studied. We show that the KdV soliton is indeed a continuous approximation of the Toda soliton.

Chapter 3

Signal Properties of the Toda Soliton

Solitons enjoy rich transmission properties through nonlinear systems. In this thesis, we apply these properties in data transmission and propose a soliton communication system. In this soliton system, Toda soliton is employed as information carrier in linear channel and the corresponding soliton supporting system is employed as both the transmitter and the receiver.

Among many kinds of solitons [40], Toda soliton is chosen to be the carrier of information in our soliton communication system for its being relatively easily generated and processed. Motivated by Toda's work on the particles chain with exponential interaction, Hirota and Suzuki proposed a nonlinear LC electrical network [23] equivalent to the original Toda lattice and verified the generation and propagation of Toda soliton through the circuit. In this chapter, the structure of the LC Toda circuit and its soliton solutions will be discussed.

To apply the Toda soliton as information carriers, we need to examine some signal properties of the Toda solitons important to applications to communications. In this chapter, we examine the time and frequency domain characteristics, the time duration

and frequency bandwidth and the signal energy of both single and composite Toda soliton [10].

3.1 The LC Toda Circuit and Toda Solitons

We now introduce the LC Toda circuit which can be used to generate and propagate Toda solitons [23]. The LC Toda circuit is a multi-stage circuit comprised of cascaded individual sections of linear inductor and nonlinear capacitor as shown in Fig. 3.1 where I_n and V_n denote respectively, the current passing through the inductor with constant inductance L and the voltage across the nonlinear capacitor at the nth stage.

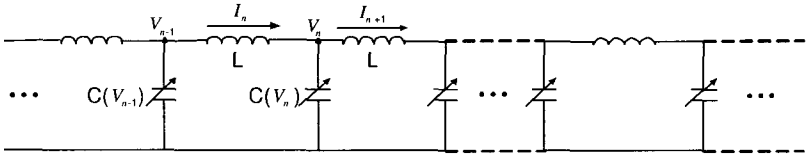

Figure 3.1: The LC Toda circuit

The charge of the nth nonlinear capacitor in Fig. 3.1 is of the form

$$Q_n = C_0 V_0 \log(1 + \frac{V_n}{V_0}) \tag{3.1}$$

where V_0 and C_0 are constants representing the DC bias voltage and the nominal capacitance, respectively. In practice, the bias voltage V_0 is usually chosen to be around 10 Volts [50, 51], thus hereafter, we will assign $V_0 = 10$V unless specifically indicated. The governing equation of LC Toda circuit is given by [23, 53]

$$\frac{\mathrm{d}^2}{\mathrm{d}t^2} \log\left(1 + \frac{V_n(t)}{V_0}\right) = \frac{V_{n-1}(t) - 2V_n(t) + V_{n+1}(t)}{LC_0V_0} \tag{3.2}$$

Comparing this nonlinear LC circuit with the Toda lattice introduced in Section 2.1.4, it is clear that these two systems are equivalent. More specifically, the charge of the nonlinear capacitor in the LC circuit is equivalent to the particle displacement of the

original lattice and the voltage across the capacitor is equivalent to the force between two nearest particles.

It can be easily verified that the single soliton solution of this system representing the voltage at the nth stage of the Toda circuit is given by:

$$V_n(t) = V_n(\tau) = V_0\beta^2 \text{sech}^2\left(\beta\tau - n\,\sinh^{-1}\beta - \phi\right) \tag{3.3}$$

where $\tau = t/\sqrt{LC_0}$ is the normalized time variable, β is the parameter governing the behavior of the soliton represented by Eq. (3.3), and ϕ is the initial phase shift of the soliton. It can be shown [53] that Eq. (3.3) is the only class of single solitons supported by the Toda circuit. Hence we call this class *Toda solitons.* Similar to most other soliton supporting systems, the Toda circuit can be employed to generate Toda solitons simply by having narrow rectangular pulses as its input. It has been shown [53] that after a number of stages of the Toda circuit, the pulse is a close approximation to that given in Eq. (3.3). $V_n(\tau)$ in Eq. (3.3) also tells us that the soliton propagates along the Toda circuit without changing its shape or its amplitude. This is a fundamental property of the propagation of a soliton in a nonlinear medium matched to its characteristic. Fig. 3.2 shows the soliton of amplitude $V_0\beta^2 = 4$ measured at different stages of the Toda circuit, and it can be seen that the pulse measured at a later stage is merely a delayed version of the earlier ones.

From Eq. (3.3), we see that $V_0\beta^2$ governs the amplitude of the Toda soliton, the parameter β also governs the spread of the soliton in the time domain and the velocity of propagation which can be calculated to be $\beta/\sinh^{-1}\beta$. Thus, β characterizes not only the amplitude and width of the Toda soliton, but also its velocity of propagation along the Toda circuit. The larger is β, the faster the soliton propagates along the circuit. Consider two solitons having different parameters β_1 and β_2 ($\beta_1 > \beta_2$) such

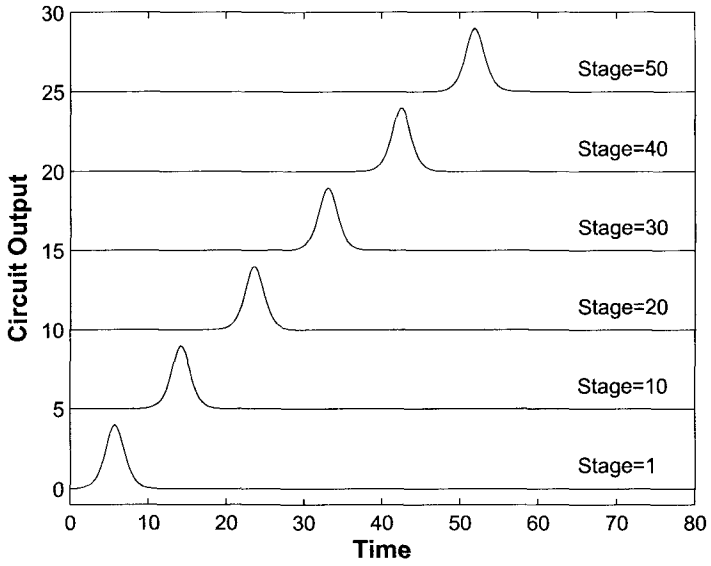

Figure 3.2: Circuit response to single soliton, $V_0\beta^2 = 4$

that at the nth stage of the circuit, they are given by

$$V_n^{(1)}(\tau) = V_0\beta_1^2 \text{sech}^2\left(\beta_1\tau - n\,\sinh^{-1}\beta_1 - \phi_1\right)$$
$$V_n^{(2)}(\tau) = V_0\beta_2^2 \text{sech}^2\left(\beta_2\tau - n\,\sinh^{-1}\beta_2 - \phi_2\right)$$

where ϕ_1 and ϕ_2 are the respective phase shifts of the two solitons. Now, if the two solitons propagate along the Toda circuit starting at the input $n = 0$, with $V_{20}(\tau)$ preceding $V_{10}(\tau)$, then at some subsequent stages of the circuit, Soliton 1 will catch up with Soliton 2, since it propagates with higher speed along the circuit. Under such condition, the two solitons will start "merging", forming an *interacting* soliton. The general interacting soliton can be represented by the equation [23, 53]:

$$V_n(t) = s_a(\tau, n, \phi_1, \phi_2) = \frac{V_0\left[\beta_1^2\text{sech}^2\theta_1 + \beta_2^2\text{sech}^2\theta_2 + A_0\text{sech}^2\theta_1\text{sech}^2\theta_2\right]}{\left[\cosh(\varphi/2) + \sinh(\varphi/2)\,\tanh\theta_1\,\tanh\theta_2\right]^2} \tag{3.4}$$

where

$$\begin{aligned}\theta_m &= \beta_m\tau - n\sinh^{-1}\beta_m - \phi_m, \qquad m = 1, 2\\ \varphi &= \frac{1}{2}\log\left(\frac{\sinh^2[(\sinh^{-1}\beta_1 - \sinh^{-1}\beta_2)/2]}{\sinh^2[(\sinh^{-1}\beta_1 + \sinh^{-1}\beta_2)/2]}\right)\\ A_0 &= \sinh\frac{\varphi}{2}\left[(\beta_1^2+\beta_2^2)\sinh\frac{\varphi}{2} + 2\beta_1\beta_2\cosh\frac{\varphi}{2}\right]\end{aligned}$$

When $\frac{\phi_1+n\sinh^{-1}\beta_1}{\beta_1} = \frac{\phi_2+n\sinh^{-1}\beta_2}{\beta_2}$, the two solitons will completely merge and the interacting soliton in Eq. (3.4) will become a *composite* soliton denoted by

$$s_c(\tau) = s_a(\tau, n, \phi_1, \phi_2)\Big|_{\frac{\phi_1+n\sinh^{-1}\beta_1}{\beta_1}=\frac{\phi_2+n\sinh^{-1}\beta_2}{\beta_2}} \tag{3.5}$$

This complete merging will happen at the stage

$$n = \frac{\beta_1\phi_2 - \beta_2\phi_1}{\beta_2\sinh^{-1}\beta_1 - \beta_1\sinh^{-1}\beta_2} \tag{3.6}$$

Therefore, if ϕ_1 and ϕ_2 are properly chosen such that n is an integer, we will be able to extract a composite soliton at the output of the nth stage circuit. We note that the composite soliton is symmetric at the instant $\tau_0 = \frac{\phi_1+n\sinh^{-1}\beta_1}{\beta_1} = \frac{\phi_2+n\sinh^{-1}\beta_2}{\beta_2}$. The amplitude of this composite soliton is defined as the maximum point of its function in time. Now, as the composite soliton so formed is allowed to further propagate along the circuit, the two constituent solitons start to separate since soliton 1 propagates with higher speed than soliton 2. This separation continues until the two constituent solitons separates completely returning to their original individual forms.

Fig. 3.3 illustrates the propagation of two solitons of amplitudes $V_0\beta_1^2 = 9$ and $V_0\beta_2^2 = 1$ along the Toda circuit. It can be seen that at stage $n = 1$, the two solitons start to interact with each other as they propagate along the circuit. The interaction is complete at stage $n = 72$ when the composite soliton is formed. The merged solitons then start separating as they further propagate along the circuit and at stage $n = 143$, the two constituent solitons can be clearly recognized in their original forms. For this pair of constituent solitons whose difference in amplitudes is relatively large,

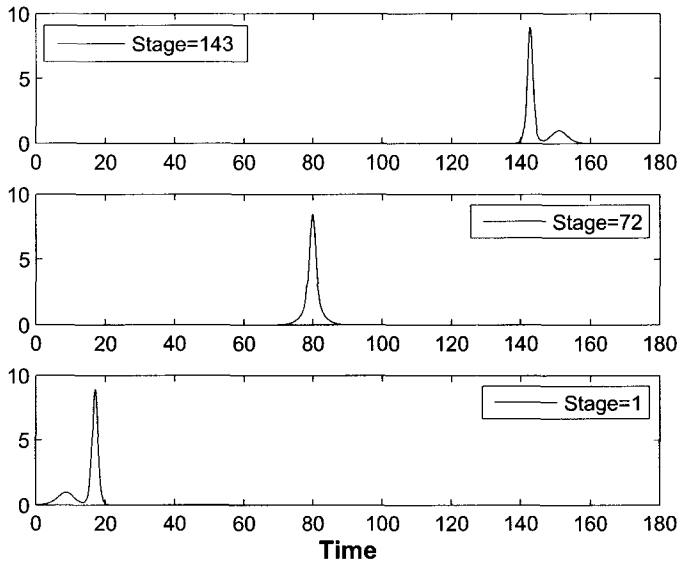

Figure 3.3: Circuit response to composite soliton, $V_0\beta_1^2 = 9$, $V_0\beta_2^2 = 1$

it takes approximately 72 stages of circuit for the composite soliton to form and completely re-separate. On the other hand, when the difference in the amplitudes of the two constituent solitons are relatively small, since the velocities of propagation of the two are close, it will take a much larger number of circuit stages for them to catch up and merge and again take a large number of circuit stages to re-separate. This is illustrated in Fig. 3.4. Here, we observe that for the constituent solitons of amplitudes 5 and 4, the forming of the composite soliton takes a total of 397 stages of the circuit and then takes another 397 stages to separate again into the constituent solitons.

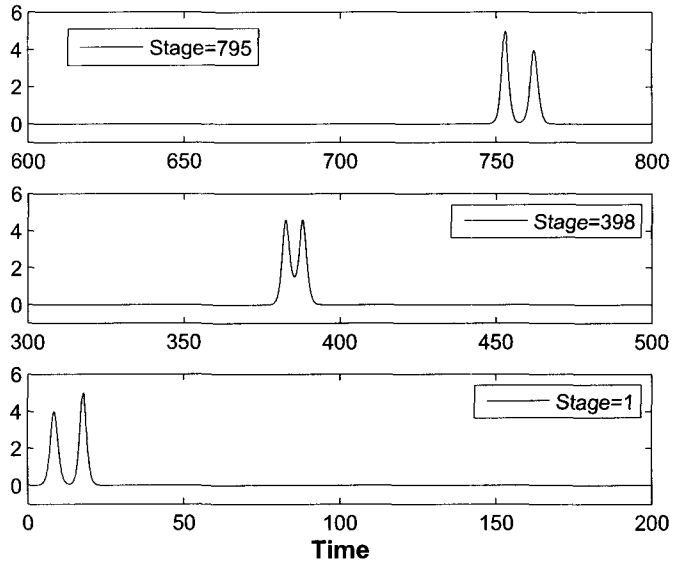

Figure 3.4: Circuit response to composite soliton, $V_0\beta_1^2 = 5$, $V_0\beta_2^2 = 4$

3.2 Time and Frequency Characteristics of the Toda Soliton

In this section and next section, we examine some signal properties of the Toda solitons important to applications to communications. From Eq. (3.3), the single soliton with zero phase shift at the initial stage ($n = 0$) of the Toda circuit is

$$s(\tau) = V_0\beta^2 \text{sech}^2(\beta\tau) \tag{3.7}$$

which is an even function symmetric to $\tau = 0$. Applying the Fourier transform to this soliton, the frequency characteristic of this soliton is given by

$$S(f) = V_0 \frac{2\pi^2 f}{\sinh(\pi^2 f/\beta)} \tag{3.8}$$

where $f = 1/\tau$ is the normalized frequency. The waveform of the soliton with amplitude $V_0\beta^2 = 2$ in the normalized time domain and its characteristics in the normalized

frequency domain are shown in Fig. 3.5. It can be seen that the Toda soliton has a "low-pass" frequency characteristic.

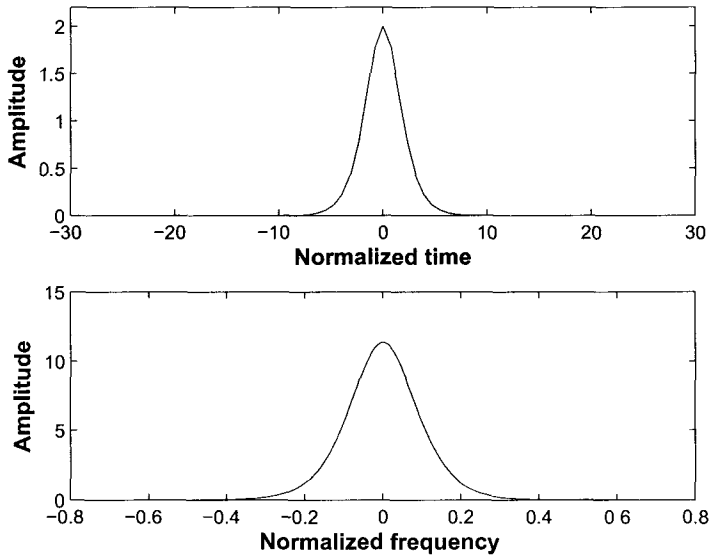

Figure 3.5: Time and frequency characteristics of a single soliton, $V_0\beta^2 = 2$

Now, let us examine the time and frequency characteristics of the composite soliton $s_c(\tau)$. Since the formation of a composite soliton is a result of nonlinear interaction between two single solitons, the superposition principle does not apply to either the time or the frequency domain characteristics of the composite soliton. As an illustration, we show in Figs. 3.6 and 3.7 the normalized time and normalized frequency characteristics of two different composite solitons formed from the combination of constituent solitons having amplitudes 3 and 2, and 8 and 2 respectively. It is evident that the results of the merging are entirely different in the two cases, depending on the relative parameters of the constituent solitons.

From Fig. 3.6, we observe that if the parameters of the two constituent solitons are close in value, the resulting composite soliton may have multiple peaks in both

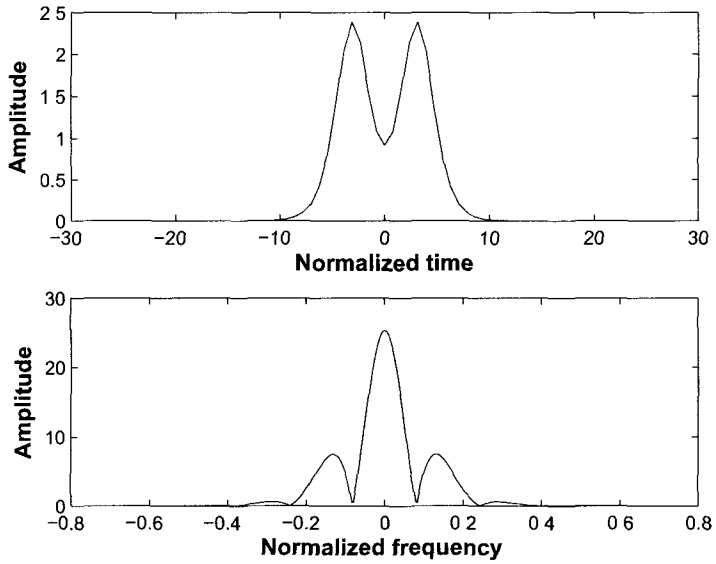

Figure 3.6: Time and frequency characteristics of a composite soliton, $V_0\beta_1^2 = 3$, $V_0\beta_2^2 = 2$

the time and the frequency characteristics. Since the time- and frequency-domain expressions of the composite soliton are symmetric, the twin peaks are always equal in amplitude. It is also observed that the amplitude of the twin peaks always lies between the values of the two constituent soliton peaks, i.e., $V_0\beta_2^2 < A_c < V_0\beta_1^2$ with A_c being the value of one of the twin peaks. This fact is used later in our application of the solitons as a message-carrying signal. On the other hand, if the parameters are very different, the resulting composite soliton may turn out to be unimodal as shown in Fig. 3.7. Thus, the resulting composite soliton shape depends on the ratio of β_1/β_2: Let $\beta_2 < \beta_1$, in general, it can be shown that for a fixed β_2, a threshold of β_1, denoted by β_{th}, exists such that for $\beta_1 < \beta_{th}$, the composite soliton will have twin peaks as exemplified in Fig. 3.6, while for $\beta_1 > \beta_{th}$, the composite soliton has only a single peak in time and frequency similar to that in Fig. 3.7. It should be noted that for different fixed values of β_2, the value of β_{th} will be correspondingly different. This

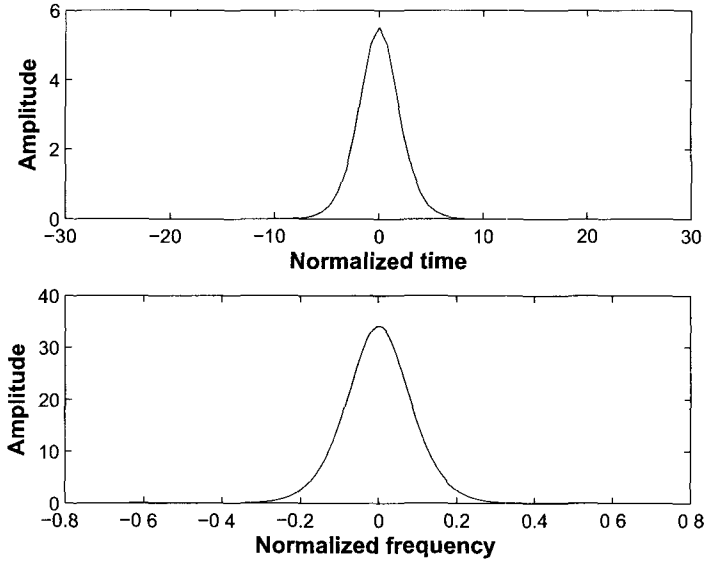

Figure 3.7: Time and frequency characteristics of a composite soliton, $V_0\beta_1^2 = 8$, $V_0\beta_2^2 = 2$

is shown as a ratio β_{th}/β_2 plotted against the amplitude $V_0\beta_2^2$ in Fig. 3.8 for the usual biased voltage $V_0 = 10$. However, for a different choice of the biased voltage, this ratio of β_{th}/β_2 will be different.[1] This is also illustrated in Fig. 3.8 for $V_0 = 1$. We note that for $\beta_1 < \beta_{th}$, while the resulting composite soliton maintains its twin-peak structure, as β_1 is increased and approaches β_{th}, the separation between the two peaks of the composite soliton decreases and the peaks become less pronounced. Finally, when $\beta_1 = \beta_{th}$, the two peaks merge to form a single peak. This is illustrated in Fig. 3.9 in which $V_0\beta_2^2 = 4$ and $V_0\beta_1^2$ is varied from 5 to beyond $V_0\beta_{th}^2$. The effect of the merging twin peaks are clearly demonstrated.

[1]Similar result has been shown in KdV(Korteweg-de Vries) soliton, which is the continuous version of Toda soliton (having n replaced by a continuous variable). The threshold ratio β_{th}/β_2 for KdV soliton has been proved to be a constant equal to 2.6.

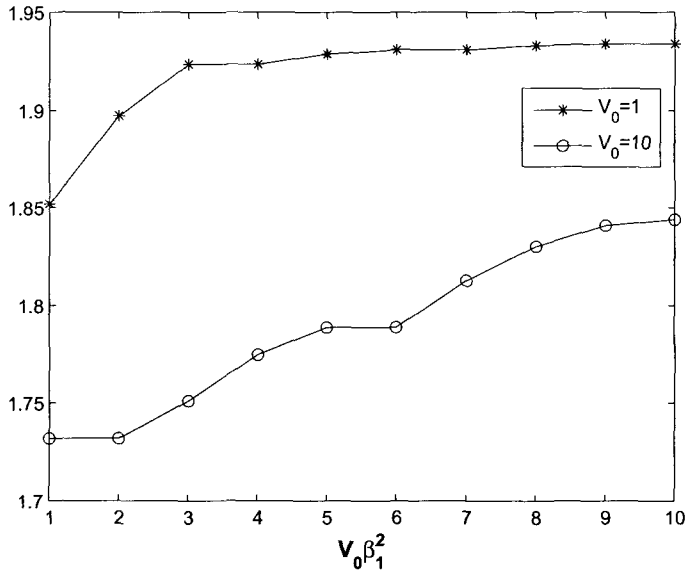

Figure 3.8: β_{th}/β_2

3.3 Energy and Time-Bandwidth Product of the Toda Soliton

In the application of solitons to communications, another important characteristic to consider is the pulse energy defined as

$$E_s = \int_{-\infty}^{\infty} s^2(t)dt = \int_{-\infty}^{\infty} |S(f)|^2 df \tag{3.9}$$

Substituting the expression of the single soliton in Eq. (3.3) into Eq. (3.9), we obtain the energy of the Toda soliton $s(\tau)$:

$$\begin{aligned} E_s &= \int_{-\infty}^{\infty} s^2(\tau)d\tau = V_0^2\beta^4 \int_{-\infty}^{\infty} \text{sech}^4(\beta\tau)d\tau \\ &= V_0^2\beta^3 \int_{-\infty}^{\infty} \big(1-\tanh^2(\beta\tau)\big)d\tanh(\beta\tau) = \frac{4}{3}V_0^2\beta^3 \end{aligned} \tag{3.10}$$

It is clear from Eq. (3.10) that the energy of the single Toda soliton depends on its parameter β. For larger β, the soliton has larger energy.

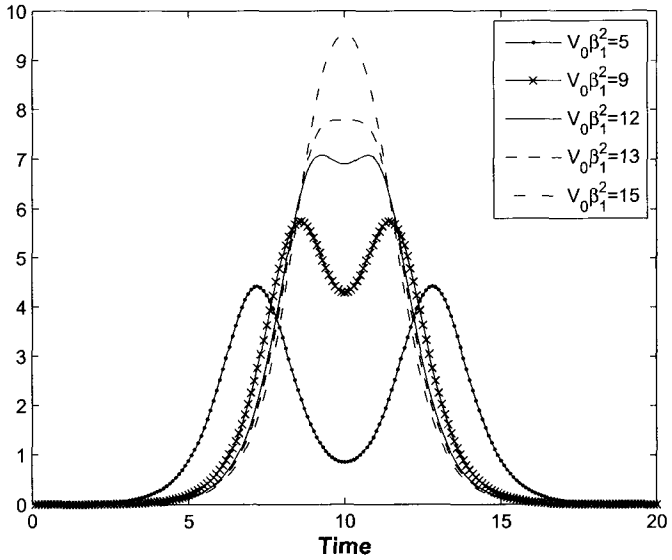

Figure 3.9: Composite soliton, $V_0\beta_2^2 = 4$, $V_0\beta_1^2 = [5\ 9\ 12\ 13\ 15]$

For a composite soliton, we can evaluate the energy in a similar way by substituting the square of $s_c(\tau)$ in Eq. (3.5) into Eq. (3.9). The resulting integral cannot be expressed in a closed form; however, it can be evaluated numerically by dividing the "duration" of the composite soliton into M segments of width $\Delta\tau$ and sum up such that $E_c \simeq \sum_{m=0}^{M} s_c^2(m\Delta\tau)\Delta\tau$. Since the composite soliton is not a linear sum of its constituent solitons, the superposition principle does not apply to the energy of the composite soliton. If we denote the energy of the individual solitons having parameters β_1 and β_2 by E_{s1} and E_{s2} respectively, then the energy ratio of the composite soliton to the two individual constituent solitons can be defined as: $r_E = E_c/(E_{s1} + E_{s2})$. It has been shown [23] that if the composite soliton is formed by having the constituent solitons merged while propagating in the same direction of the nonlinear medium, then $r_E \leq 1$. To find out a more detail relation of r_E and β_1, β_2, we fix $V_0 = 10$ and vary β_1 and β_2 ($\beta_1 > \beta_2$) in the region such that β_1/β_2 is between 1 to 10 and calculate the corresponding r_E. In Fig. 3.10, r_E is plotted

versus the ratio β_1/β_2 with $V_0\beta_2^2$ being 2, 5 and 8, respectively. It can be seen from Fig. 3.10 that while r_E varies for different β_1 and β_2, the ratio β_1/β_2 corresponding to the minimum r_E for different β_2 is very close to a constant, which is approximately equal to 2.94. Similar result can be obtained for different value of V_0. As an example, Fig. 3.11 shows r_E versus β_1/β_2 for $V_0 = 1$. It can be seen that for different β_2, the ratio β_1/β_2 corresponding minimum energy ratio is still a constant, but this ratio, i.e. 2.69 is slightly different as the case of $V_0 = 10$. It can also be shown that if the composite soliton is formed by merging two constituent solitons propagating through the nonlinear medium in opposite directions, then $r_E \geq 1$ [23].

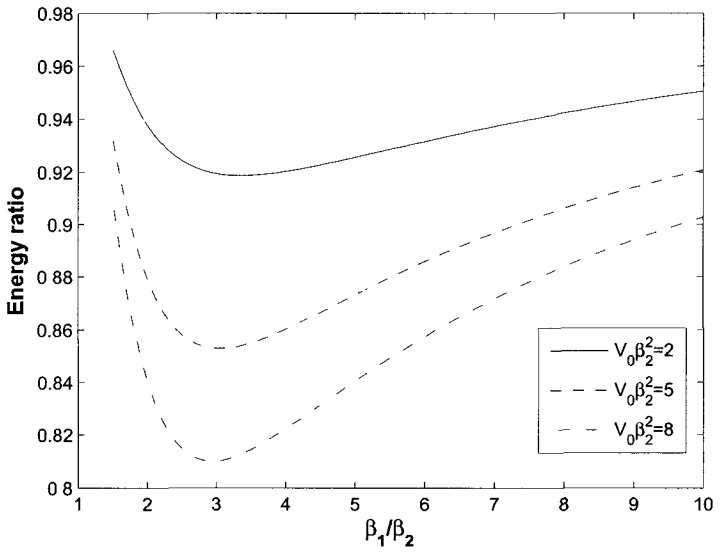

Figure 3.10: Energy ratio of composite soliton and constituent solitons, $V_0 = 10$

The fact that the energy of the composite soliton is always less than the sum of the energy of two constituent solitons may seem to violate the Law of Conservation of Energy. However, in the Toda circuit, the energy includes both the electrical energy of capacitors and the magnetic energy of inductors. Denoting the power on stage n by: $P_n = I_{n-1}V_n$, it can shown [23] that the energy of the nth stage, defined as

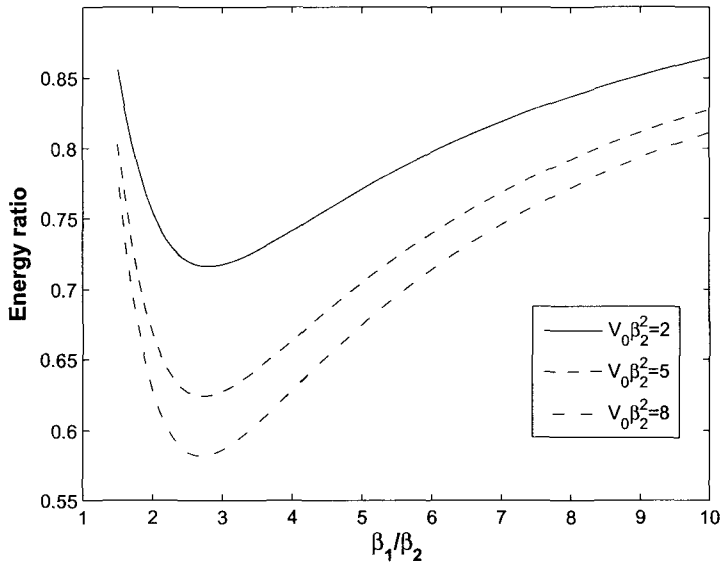

Figure 3.11: Energy ratio of composite soliton and constituent solitons, $V_0 = 1$

$E_n = \int_{-\infty}^{\infty} P_n dt$ is a constant independent on the circuit stage number, which is indeed the Energy Conservation Law of the Toda circuit.

Now, from the general expressions of the soliton and the composite soliton in Eqs. (3.3) and (3.5), we note that their supports range over the entire normalized time domain $\tau \in (-\infty, \infty)$ (and likewise in the normalized frequency domain). However, we also note that the signals approach zero very quickly (both in the time and frequency domains). Therefore, to come up with a definition of effective duration and bandwidth for the signals, we use the "99% energy" [42] concept such that the *essential duration* T_E of the signal centered at $\tau = 0$ is defined as

$$\int_{-T_E/2}^{T_E/2} |s(\tau)|^2 d\tau = 0.99\ E_s \tag{3.11}$$

where E_s is the total energy of the signal. Similarly. the *essential bandwidth* F_E of

the signal centered at $f = 0$ is defined as

$$\int_{-F_E}^{F_E} |S(f)|^2 df = 0.99\ E_s. \tag{3.12}$$

Substituting the time domain expressions of the soliton into Eq. (3.11), we obtain:

$$\int_{-T_E/2}^{T_E/2} V_0^2\beta^4 \mathrm{sech}^4(\beta\tau)d\tau = V_0^2\beta^3\big(2\tanh(\frac{\beta T_E}{2}) - \frac{2}{3}\tanh^3(\frac{\beta T_E}{2})\big) = 0.99 \times \frac{4}{3}V_0^2\beta^3 \tag{3.13}$$

Denoted $\tanh(\frac{\beta T_E}{2})$ by a new variable x, from Eq. (3.13), we obtain

$$x - \frac{1}{3}x^3 - 0.66 = 0 \tag{3.14}$$

Eq. (3.14) is a cubic function of x and can be solved analytically [55]. We obtain $x = 0.917$, from which the essential duration for a single Toda soliton can then be calculated, which is inversely proportional to the soliton parameter β:

$$T_E = \frac{3.14}{\beta}$$

Substituting the frequency domain expressions of the soliton into Eq. (3.12), we obtain

$$\int_{-F_E}^{F_E} |S(f)|^2 df = 4V_0^2\pi^4 \int_{-F_E}^{F_E} \frac{f^2}{\sinh^2(\pi^2 f/\beta)} df = 4V_0^2\frac{\beta^3}{\pi^2} \int_{-\frac{\pi^2 F_E}{\beta}}^{\frac{\pi^2 F_E}{\beta}} \frac{f^2}{\sinh^2(f)} df = \frac{4}{3}V_0^2\beta^3 \tag{3.15}$$

The analytical solution of the integral in Eq. (3.15) is unavailable, therefore, we solve the equation numerically using *fzero* function in mathematical software Matlab and obtain

$$\frac{\pi^2 F_E}{\beta} = 3.8797 \quad \Rightarrow \quad F_E = 0.3931\beta \tag{3.16}$$

It is clear that the essential bandwidth for a single Toda soliton is proportional to the soliton parameter β.

The exact 99% duration and 99% bandwidth of the composite soliton, however, do not have simple relationship with the β-parameters of the constituent solitons

and therefore have to be evaluated numerically from its expression. To evaluate the essential duration of the composite soliton, we divide the time domain "duration" of the composite soliton into M segments of width $\Delta\tau$ and find out the index C corresponding to the center of the waveform, that is

$$\sum_{i=0}^{C-1} s_c^2(i) \approx \sum_{i=C+1}^{M} s_c^2(i) \tag{3.17}$$

We then calculate the index l, such that

$$s_c^2(C) + \sum_{i=1}^{l} (s_c^2(C+i) + s_c^2(C-i)) \approx 0.99E_c$$

The essential duration of the composite soliton can then be calculated as $T_E = (2l+1)\Delta\tau$. The essential bandwidth of the composite soliton can be calculated in a very similar manner. As examples, the values of the essential duration and the essential bandwidth of the composite solitons shown in Figs. 3.6 and 3.7 are calculated and are given respectively by $T_E = 11.908, F_E = 0.174$ for the soliton shown in Fig. 3.6 and $T_E = 7.414, F_E = 0.171$ for that in Fig. 3.7.

Associated with the duration and bandwidth is the important factor of *time-bandwidth (T-B) product* which characterizes the time and frequency domain efficiency of a signal. The T-B product of a signal $s(t)$ is the product of the root-mean-square values of the duration and the bandwidth of a signal and is defined as [42]:

$$\Pi_{TBs} = \frac{1}{E_s}\sqrt{\int_{-\infty}^{\infty} t^2|s(t)|^2dt \int_{-\infty}^{\infty} f^2|S(f)|^2df} \tag{3.18}$$

where $S(f)$ is the Fourier transform of $s(t)$ and E_s is the total energy of the signal.

The T-B product of a single Toda soliton can be calculated by directly substituting the time and frequency expressions of the Toda soliton from Eqs. (3.7) and (3.8) into Eq. (3.18) as described in the following lemma:

Lemma 3.1 *For a Toda soliton, the T-B product is a constant and is equal to 0.5066.*

Proof: From the time and frequency expressions of the Toda soliton of Eqs. (3.7) and (3.8), the mean-square duration and mean-square bandwidth of the single Toda soliton are given respectively by:

$$\int_{-\infty}^{\infty} \tau^2 |s(\tau)|^2 d\tau = \int_{-\infty}^{\infty} \tau^2 V_0^2 \beta^4 \mathrm{sech}^4(\beta\tau) d\tau = V_0^2 \beta (\frac{\pi^2}{9} - \frac{2}{3}) \tag{3.19}$$

and

$$\int_{-\infty}^{\infty} f^2 |s(f)|^2 df = V_0^2 \int_{-\infty}^{\infty} f^2 \frac{(2\pi^2 f)^2}{\sinh^2(\frac{\pi^2 f}{\beta})} df = V_0^2 \frac{4\beta^5}{\pi^6} 2\pi^4 |B_4| = V_0^2 \frac{4\beta^5}{15\pi^2} \tag{3.20}$$

where $B_4 = \int_{-\infty}^{\infty} \frac{f_1^4}{\sinh^2(f_1)} df_1 = -\frac{1}{30}$ is a Bernoulli number [17]. Substituting Eqs. (3.19) and (3.20) together with the energy E_s given by Eq. (3.10) into the definition of T-B production of Eq. (3.18), we obtain $\Pi_{TBs} = 0.5066$. □

It is well-known [42] that, of all the signals, the Gaussian pulse possesses the smallest T-B product of 0.5. From Lemma 3.1, it can be seen that the single Toda soliton has a T-B product very close to that of the Gaussian pulse and thus, like the Gaussian pulse, it also has high time and frequency localization abilities, i.e., it has a high energy concentration in both time and frequency domains.

Unlike that for a single Toda soliton, the T-B product for a composite Toda soliton cannot be evaluated in a simple form because of the mathematical complexity in its time-domain expression, and therefore has to be calculated numerically. In spite of this, the composite Toda soliton can also be shown to enjoy a high energy concentration (i.e., a compact T-B product) as long as the parameters of constituent solitons are chosen properly. To calculate the values of the T-B product numerically, we divide the "duration" of the composite soliton into M_1 segments of width $\Delta\tau$ and also divide the "bandwidth" of the composite soliton into M_2 segments of width Δf. Similar to the calculating of index C in Eq. (3.17), we examine the indices

corresponding to the center of both the time and frequency waveform, denoted by C_1 and C_2 and then evaluate the discrete version of Eq. (3.18), i.e.

$$\Pi_{TBs} = \frac{1}{E_s}\sqrt{\Big(\sum_{i=1}^{\frac{M_1-1}{2}}(C_1 \pm i\Delta\tau)^2|s_c(C_1 \pm i\Delta\tau)|^2 + C_1^2|s_c(C_1)|^2\Big)\Delta\tau} \cdot \sqrt{\Big(\sum_{i=1}^{\frac{M_2-1}{2}}(C_2 \pm i\Delta\tau)^2|S_c(C_2 \pm i\Delta\tau)|^2 + C_2^2|S_c(C_2)|^2\Big)\Delta f}$$

where M_1 and M_2 are assumed to be odd numbers, for M_1 and M_2 being even number, similar calculation can be performed. For illustration of the variation of the T-B product of the composite Toda solitons, we form the composite solitons by having the amplitude of one of the constituent soliton being held at 1, 5 and 10 respectively, while having the amplitude of the other constituent soliton varying from 1 to 10. The values of the T-B product are shown in Fig. 3.12. For comparison, we also plot the constant T-B product of the single soliton. It can be easily seen from Fig. 3.12 that the T-B product of a composite soliton depends on the relative amplitudes $V_0\beta_1^2$ and $V_0\beta_2^2$ of the constituent solitons. For example, for $V_0\beta_1^2 = 1$, if $V_0\beta_2^2 \geq 3$, the two constituents will yield a composite soliton the T-B product of which is very close to that of a single soliton. On the other hand, for $V_0\beta_1^2 = 10$, then $V_0\beta_2^2 \leq 3$ will make the T-B product of the resulting composite soliton close to that of a single soliton. In contrast, if the amplitudes of the two constituent solitons are relatively close, say, $V_0\beta_1^2 = 5$ and $V_0\beta_2^2 = 4$, then the T-B product of resulting composite soliton is equal to 1.5, a value much larger than that of a single soliton which is 0.5066. In Fig. 3.13, we fix $V_0\beta_1^2$ to be 1, 5 and 10 and plot the T-B product of the composite soliton versus β_2/β_1. It can be see that for same β_2/β_1, the T-B product of the composite soliton is different for different $V_0\beta_1^2$, however, the trend of the curves are very similar, indicating the dependence of the T-B product of the composite soliton on the ratio β_2/β_1. From Fig. 3.13, we can also see that for composite soliton with the amplitude of

one constituent soliton, i.e., $V_0\beta_1^2$ being different, the optimal T-B product is achieved at similar condition, i.e., $\beta_2/\beta_1 \approx 2$.

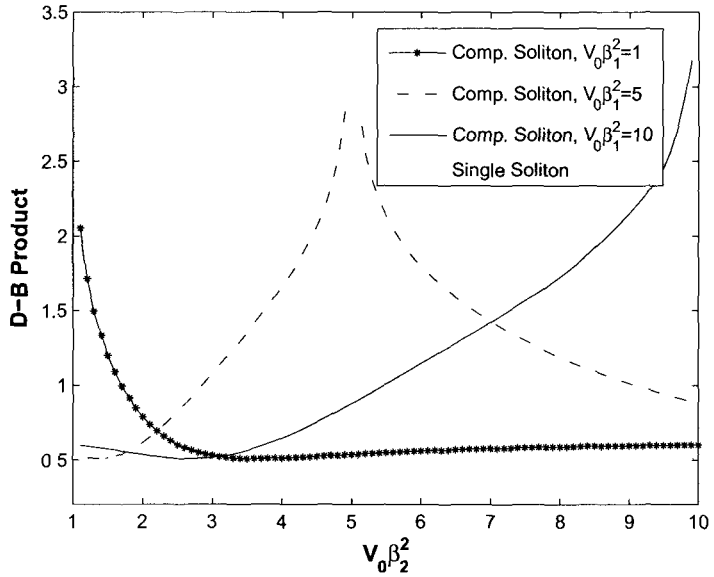

Figure 3.12: T-B product of composite soliton and single soliton (1)

3.4 Summary

In this chapter, we examine several signal properties of the Toda solitons important to the applications to communications. We show that while the single Toda soliton is having single peak in both the time and frequency domain, the composite soliton may have single peak or multiple peaks in both the time and frequency domain depending on the parameter of the constituent solitons. We also study the time and bandwidth efficiency of the Toda soliton by examining the T-B product of both single and composite Toda soliton. We show that the T-B product of the single Toda soliton is equal to 0.5066, which is close to the optimal value achieved by Gaussian pulse. By

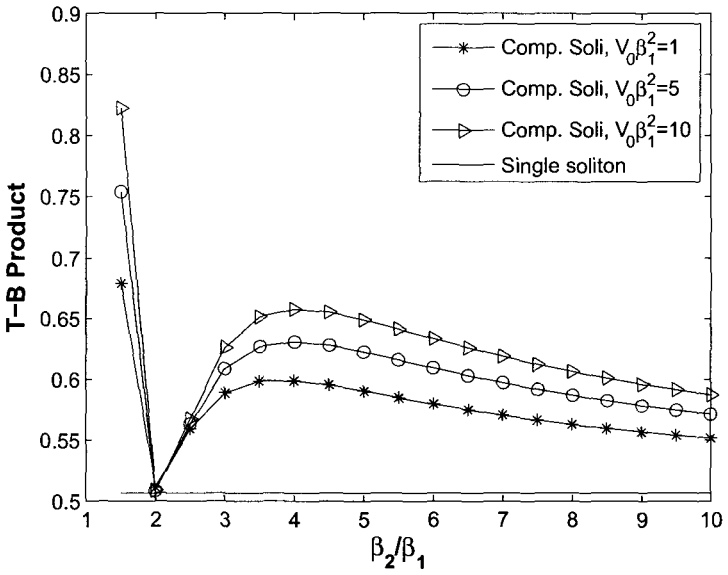

Figure 3.13: T-B product of composite soliton and single soliton (2)

numerically calculating the T-B product of the composite soliton, we show that the optimal T-B product of the composite soliton can be as small as that of the single soliton and it is achieved when $\beta_2/\beta_1 \approx 2$, where β_1 and β_2 are the parameters of the two constituent solitons. The energy of the Toda solitons is also examined. We show that the energy of the single soliton is a monotonic function of its parameter β. The energy of the composite soliton is always smaller than the energy sum of two consitituent solitons and the smallest energy of the composite soliton is achieved when $\beta_2/\beta_1 \approx 2.94$ (for $V_0 = 10$).

Chapter 4

Response Analysis of The Toda Circuit

In this chapter, we examine the processing of signals by the Toda circuit [10]. To this end, we seek for accurate representations of the response of the Toda circuit. We first assume that the circuit is weakly nonlinear and employ the Volterra series [45, 58] to calculate its response. We then take an alternative approach and apply the Runge-Kutta method to evaluate the complete response of the circuit. The accuracy of the two approaches are then compared using the known soliton solution.

4.1 Volterra Series Analysis

4.1.1 Introduction of Volterra Series

Volterra series is a functional expansion of a dynamic, nonlinear, time-invariant system. It was first developed around 1910 by Vito Volterra in [18]. In 1930's, Norbert Wiener [59] proposed to apply this series in analyzing the input-output relationship of certain nonlinear systems with memory. Since then, Volterra series has quickly

received a great deal of attention in the field of electrical engineering for its feasibility and efficiency in the modelling of nonlinear system behavior [6, 7, 47]. As a generalization of the linear convolution approach applied to linear, time-invariant systems, the theory of Volterra series states that the output of many time-invariant, nonlinear system can be modelled as an infinite sum of multidimensional convolution integrals of increasing order, i.e. given system input $x(t)$, the system response $y(t)$ can be calculated as:

$$y(t) = \sum_{k=1}^{\infty} y_k(t) \tag{4.1}$$

where

$$\begin{aligned} y_k(t) &= \int_{-\infty}^{\infty} \cdots \int_{-\infty}^{\infty} x(\tau_1)x(\tau_2)\cdots x(\tau_k)h_k(t-\tau_1, t-\tau_2, \cdots t-\tau_k)\mathrm{d}\tau_1\mathrm{d}\tau_2\cdots\mathrm{d}\tau_k \\ &\triangleq x \circ x \cdots \circ x \otimes h_k \end{aligned} \tag{4.2}$$

is the system output component of order k, and $h_k(\tau_1, \tau_2, \cdots \tau_k)$ is the kth-order system impulse response, the kth dimensional Fourier transform of which yields the kth order transfer function of the system given by,

$$H_k(f_1, f_2, \cdots f_k) = \int_{-\infty}^{\infty} \cdots \int_{-\infty}^{\infty} h_k(\tau_1, \tau_2, \cdots \tau_k)\mathrm{e}^{-j2\pi(f_1\tau_1+f_2\tau_2+\cdots+f_k\tau_k)}\mathrm{d}\tau_1\mathrm{d}\tau_2\cdots\mathrm{d}\tau_k$$

It should be noted that although Eq. (4.1) is a sum of an infinite number of terms, under the assumption of weak nonlinearity, the first few terms can approximate the system output accurately and the high order terms are negligible. Here the term "weak nonlinearity" means the nonlinearity departs from the linearity in a small and gradual manner and there is no abrupt change in system behavior [45].

It is clear from Eqs. (4.1) and (4.2) that the evaluation of the nonlinear system output can be viewed as the evaluation of the system impulse responses or, more conveniently in general, the transfer function of different orders. A commonly-used method for determining the transfer functions of nonlinear system is Harmonic Input method [58], by which the transfer functions of different orders are determined

recursively through having the sum of complex exponential function with different frequency components as input.

It is well known that the transfer function of a linear system can be calculated by exciting the system with the single complex exponential, i.e. $e^{j2\pi f_1 t}$ and examining the system output. For a linear system, the output only contains the frequency component $e^{j2\pi f_1 t}$. It can be shown easily that the coefficient of $e^{j2\pi f_1 t}$ of the system output is exactly the system transfer function. Applying Harmonic Input method to calculate different order transfer functions of a nonlinear system, the basic idea is very similar to that of linear system. The nonlinear system is first linearized and the linear transfer function of the system is determined. Then taking into account second-order nonlinearity of the system and choosing the system input to be $e^{j2\pi f_1 t} + e^{j2\pi f_2 t}$, the second order transfer function at frequency f_1 and f_2 can be determined by examining the coefficient of $e^{j2\pi(f_1+f_2)t}$ of the system output. Similarly, the nth order transfer function at frequency f_1, $f_2, \cdots f_k$ can be determined by inputting $e^{j2\pi f_1 t} + e^{j2\pi f_2 t} + \cdots + e^{j2\pi f_k t}$ and examining the coefficient of the term $e^{j2\pi(f_1+f_2+\cdots+f_k)t}$ of the system output.

In following sections, we apply Harmonic Input method to calculate the first three order transfer functions of the Toda circuit and then calculate circuit response to different input based on these transfer functions.

4.1.2 Transfer Function of Toda Circuit

To calculate the transfer function of a nonlinear system, it is the usual practice to replace a nonlinear device by a combination of a linear device and nonlinear sources. The only nonlinear devices in the Toda circuit are the nonlinear capacitors. The charge in the nth nonlinear capacitor is given by Eq. (3.1), for convenience it is

rewritten in the following:

$$Q(V_n) = Q_0 \log(1 + \frac{V_n}{V_0})$$

Differentiating $Q(V_n)$ respect to time variable t, we obtain the current through the nth capacitor, denoted as $i_c(V_n)$:

$$i_c(V_n) = C_0 \frac{1}{1 + \frac{V_n}{V_0}} \frac{\mathrm{d}V_n}{\mathrm{d}t} \tag{4.3}$$

Expanding Eq. (4.3) in a Taylor series, we obtain

$$i_c(V_n) = C_0 \frac{\mathrm{d}V_n}{\mathrm{d}t} - \frac{C_0}{2V_0} \frac{\mathrm{d}V_n^2}{\mathrm{d}t} + \frac{C_0}{3V_0^2} \frac{\mathrm{d}V_n^3}{\mathrm{d}t} + \cdots \tag{4.4}$$

It is clearly seen from Eq. (4.4) that under the condition of $\frac{V_n}{V_0} \ll 1$, first few terms can represent $i_c(V_n)$ with negligible error. Using first three terms to approximate $i_c(V_n)$, we obtain

$$i_c(V_n) \approx C_0 \frac{\mathrm{d}V_n}{\mathrm{d}t} - \frac{C_0}{2V_0} \frac{\mathrm{d}V_n^2}{\mathrm{d}t} + \frac{C_0}{3V_0^2} \frac{\mathrm{d}V_n^3}{\mathrm{d}t} \tag{4.5}$$

From Eq. (4.5), we can see that without affecting the topological structure of the circuit, the nonlinear capacitor in the Toda circuit can be replaced by the combination of the linear capacitor with capacitance C_0 and two voltage-controlled current sources with the current being $-\frac{C_0}{2V_0} \frac{\mathrm{d}V_n^2}{\mathrm{d}t}$ and $\frac{C_0}{3V_0^2} \frac{\mathrm{d}V_n^3}{\mathrm{d}t}$ respectively. The Toda circuit in Fig. 3.1 can then be redrawn as in Fig. 4.1, where, AC_1 represents the second order current

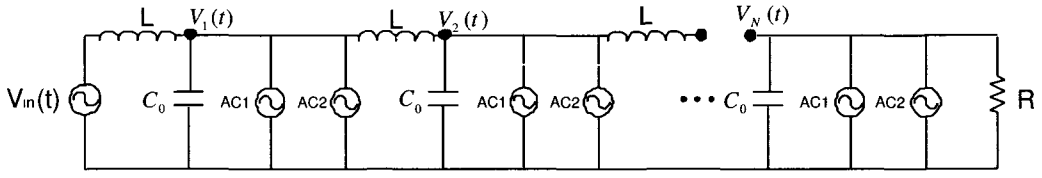

Figure 4.1: The Equivalent LC Toda Circuit

source, i.e. $i_1(t) = -\frac{C_0}{2V_0} \frac{\mathrm{d}V_n^2}{\mathrm{d}t}$, AC_2 represents the third order current source, i.e.

$i_2(t) = \frac{C_0}{3V_0^2}\frac{\mathrm{d}V_n^3}{\mathrm{d}t}$. In Fig. 4.1, $R = \sqrt{\frac{L}{C_0}}$ represents the equivalent load resistor chosen to truncate the circuit without introducing reflection [14, 23].

Applying the Harmonic Input method, we can calculate the first to third order transfer function of the circuit at different stages, $H_{1n}(f_1)$, $H_{2n}(f_1, f_2)$ and $H_{3n}(f_1, f_2, f_3)$, where $n = 1, \cdots, N$ denotes the nth stage of the Toda circuit, f_1, f_2 and f_3 are arbitrary frequency in the interested frequency region.

Defining the kth order transfer impedance matrix such that

$$\mathbf{Z}_k = \begin{pmatrix} 2+\frac{Z_{Lk}}{Z_{Ck}} & -1 & 0 & \cdots & \cdots \\ -1 & 2+\frac{Z_{Lk}}{Z_{Ck}} & -1 & 0 & \cdots \\ 0 & -1 & 2+\frac{Z_{Lk}}{Z_{Ck}} & -1 & \cdots \\ & \cdots & & & \cdots \\ 0 & \cdots & 0 & -1 & 1+\frac{Z_{Lk}}{Z_{Ck}}+\frac{Z_{Lk}}{R} \end{pmatrix} \tag{4.6}$$

where Z_{Lk}, Z_{Ck} are the kth order inductive and capacitative impedances defined respectively as

$$Z_{Lk} = j2\pi\left(\sum_{i=1}^{k} f_i\right), \qquad Z_{Ck} = \frac{1}{j2\pi\left(\sum_{i=1}^{k} f_i\right)C_0}, \qquad k = 1\cdots 3 \tag{4.7}$$

To calculate the linear transfer function of the circuit, we replace the nonlinear capacitor by linear capacitor with capacitance C_0 and ignore the two current sources. Choosing the circuit excitation to be $x(t) = V_{\text{in}}(t) = \mathrm{e}^{j2\pi f_1 t}$ and solving the node equations for circuit output $y(t) = V_i(t)$, $i = 1, \cdots N$, we obtain the linear transfer functions $H_{1i}(f_1), i = 1, \cdots N$:

$$\begin{pmatrix} H_{11}(f_1) \\ H_{12}(f_1) \\ \vdots \\ H_{1N}(f_1) \end{pmatrix} = (Z_{L1}\cdot\mathbf{Z}_1)^{-1}\begin{pmatrix} 1 \\ 0 \\ \vdots \\ 0 \end{pmatrix} \tag{4.8}$$

To calculate the second order transfer function at two incommensurable frequency f_1 and f_2, we replace the input by $x(t) = V_{\text{in}}(t) = e^{j2\pi f_1 t} + e^{j2\pi f_2 t}$ and replace the nonlinear capacitor by the combination of linear capacitor and current source AC_1. Calculating the output voltage, we can obtain the second order transfer function at frequency f_1 and f_2 as shown in the following:

$$\begin{pmatrix} H_{21}(f_1, f_2) \\ H_{22}(f_1, f_2) \\ \vdots \\ H_{2N}(f_1, f_2) \end{pmatrix} = (Z_{L2}\mathbf{Z}_2)^{-1}\mathbf{J}_2 \tag{4.9}$$

where, with $P_2 = j2\pi(f_1 + f_2)$, the equivalent input vector $\mathbf{J}_2$ is given by:

$$\mathbf{J}_2 = \frac{C_0}{2V_0} P_2 Z_{L2} \begin{pmatrix} H_{11}(f_1)H_{11}(f_2) \\ H_{12}(f_1)H_{12}(f_2) \\ \vdots \\ H_{1N}(f_1)H_{1N}(f_2) \end{pmatrix} \tag{4.10}$$

Similarly, choosing input $x(t) = V_{\text{in}}(t) = e^{j2\pi f_1 t} + e^{j2\pi f_2 t} + e^{j2\pi f_3 t}$ and replacing nonlinear capacitor by the combination of linear capacitor and current source AC_1 and AC_2, the third order transfer function at frequency f_1, f_2 and f_3 can be calculated as:

$$\begin{pmatrix} H_{31}(f_1, f_2, f_3) \\ H_{32}(f_1, f_2, f_3) \\ \vdots \\ H_{3N}(f_1, f_2, f_3) \end{pmatrix} = (Z_{L3}\mathbf{Z}_3)^{-1}\mathbf{J}_3 \tag{4.11}$$

where, with $P_3 = j2\pi(f_1 + f_2 + f_3)$, the vector $\mathbf{J}_3$ is given by:

$$\mathbf{J}_3 = \frac{C_0}{2V_0} P_2 Z_{L2} \begin{pmatrix} \overline{H_{11}(f_1)H_{21}(f_2,f_3)} \\ \overline{H_{12}(f_1)H_{22}(f_2,f_3)} \\ \vdots \\ \overline{H_{1N}(f_1)H_{2N}(f_2,f_3)} \end{pmatrix} - \frac{C_0}{3V_0^2} P_3 Z_{L3} \begin{pmatrix} H_{11}(f_1)H_{11}(f_2)H_{11}(f_3) \\ H_{12}(f_1)H_{12}(f_2)H_{12}(f_3) \\ \vdots \\ H_{1N}(f_1)H_{1N}(f_2)H_{1N}(f_3) \end{pmatrix} \tag{4.12}$$

The over-bar in Eq. (4.12) denotes the arithmetic average of the permuted terms. For example,

$$\begin{aligned} \overline{H_{11}(f_1)H_{21}(f_2,f_3)} = \tfrac{1}{6}[&H_{11}(f_1)H_{21}(f_2,f_3) + H_{11}(f_1)H_{21}(f_3,f_2) + H_{11}(f_2)H_{21}(f_1,f_3) \\ &+H_{11}(f_2)H_{21}(f_3,f_1) + H_{11}(f_3)H_{21}(f_1,f_2) + H_{11}(f_3)H_{21}(f_2,f_1)] \end{aligned}$$

The kth order impulse response of the circuit at stage n, denoted by h_{kn}, $k = 1 \cdots 3$, $n = 1 \cdots N$ can be obtained by applying the $k-$dimensional inverse Fourier transform on the transfer functions H_{kn}. For convenience, the index n denoting the stage number in h_{kn} is ignored hereafter and will be indicated specifically in the content. Based on $h_k, k = 1 \cdots 3$, the system output given an input can be calculated from Eqs. (4.1) and (4.2).

4.1.3 Toda Circuit Response Using Volterra Series

To illustrate the accuracy of employing the Volterra series, we apply a single soliton with amplitude $V_0\beta^2 = 5$ to the input of the Toda circuit. We calculate the exact response at the first stage of the circuit by evaluating Eq. (3.3) with $n = 1$ and this is shown in the top of Fig. 4.2. Together, at $n = 1$, we also plot the first order (y_1), the second order ($y_1 + y_2$), and the third order ($y_1 + y_2 + y_3$) Volterra series approximated outputs. If we let $y_0(m)$, $m = 0, \cdots, M$, be the theoretical output of the circuit, which can be obtained by evaluating Eq. (3.3) with $n = 1$. From Fig. 4.2, we can calculate the mean square error (MSE) of the kth order approximation of the

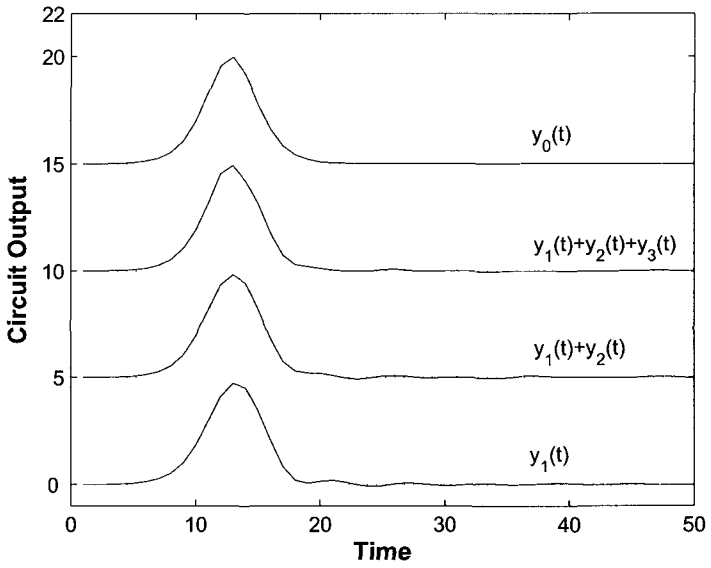

Figure 4.2: Circuit response to a single soliton, $V_0\beta^2 = 5$

circuit output, i.e. $\text{MSE}_k = \sum_{m=0}^{M} |(\sum_{i=1}^{k} y_i(m)) - y_0(m)|^2 \Delta t$. The results obtained, with $M = 100$, are: $\text{MSE}_1 = 0.6521$, $\text{MSE}_2 = 0.1201$, and $\text{MSE}_3 = 0.092$. From Eq. (3.10), we have the total energy of the exact output signal $E_s = \frac{4}{3} V_0^2 \beta^3 = 117.95$. Thus, the relative approximation errors are given by $\bar{e}_k = \text{MSE}_k / E_s$, $k = 1, 2, 3$, giving $\bar{e}_1 = .0055, \bar{e}_2 = .0010, \bar{e}_3 = 7.799 \times 10^{-4}$. It can be clearly observed that in the case of a small amplitude soliton input, i.e., $V_0\beta^2 = 5$, using the third order approximation of the circuit output yields a reasonably small error at the early stage of the circuit. Fig. 4.2 also verifies that the linear approximation of the output shows linear dispersion of the soliton which is compensated by the second-order and third-order nonlinearity resulting in a stable propagation. The responses at first stage and later stages of the Toda circuit to a single soliton with amplitudes 1, 4, and 8 are shown in Figs. 4.3 to 4.5. In each figure, the Volterra series output of order 3, i.e. $\sum_{i=1}^{3} y_i$ is compared with the theoretical outputs (again obtained by evaluating Eq. (3.3) with the corresponding values of n). The output stage numbers are chosen to be 1, 3, 5,

7 and 9. It is clear from these figures that in the case of small input amplitude and lower stage numbers, third-order Volterra series is an efficient approximation of the Toda circuit. The approximation error of Volterra series increases with the increase of the input amplitude and increase of circuit stages. This indicates that for larger input amplitude and for longer cascade of Toda circuit sections, nonlinearity of circuit increases.

Fig. 4.6 illustrates the third-order approximated output of the Toda circuit in response to the input of a *composite* soliton formed by two constituent solitons of amplitudes $V_0\beta_1^2 = 4$ and $V_0\beta_2^2 = 5$. Note that the composite soliton has two peaks of equal amplitude. We examine the approximated output at stages 1, 3, 5, 7 and 9. Theoretical outputs are obtained by evaluating Eq. (3.5) and are plotted for comparison. It can be seen from Fig. 4.6 that good approximation is obtained at the earlier stages (1 and 3), however, the approximation deteriorates as the stage number increases.

The increasing approximation error with the increase of stage number and input amplitude shows that higher order Volterra series is required to represent longer circuits with larger input. However, the exponentially increase in computation complexity makes this unrealistic. Therefore, in this thesis, the Volterra series approximation (3rd order) is only applied to the outputs at the first few stages. For circuit output at later stages of the circuit, we use the more accurate Runge-Kutta numerical method.

4.2 Runge-Kutta Integration Method

In this section, the output of the finite-length Toda circuit is evaluated using the numerical integration method of Runge-Kutta [33]. Runge-Kutta method was developed around 1900 by two German mathematicians C. Runge and M.W. Kutta for

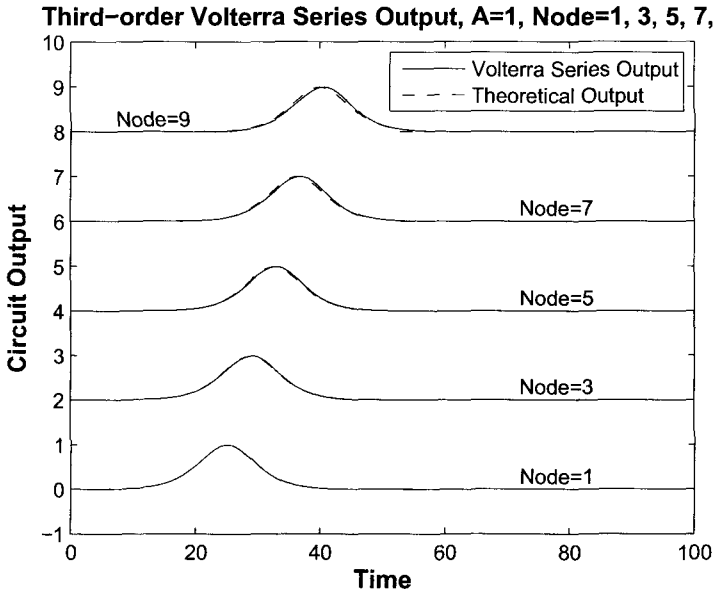

Figure 4.3: Circuit response to a single soliton, $V_0\beta^2 = 1$

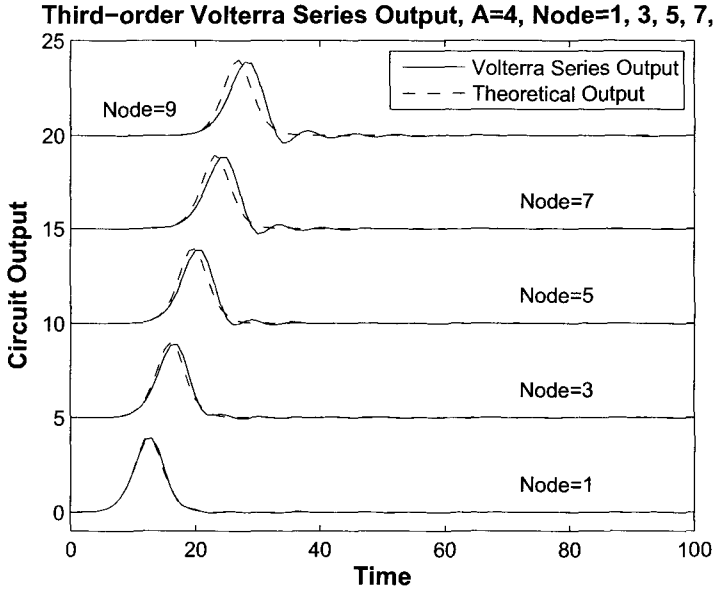

Figure 4.4: Circuit response to a single soliton, $V_0\beta^2 = 4$

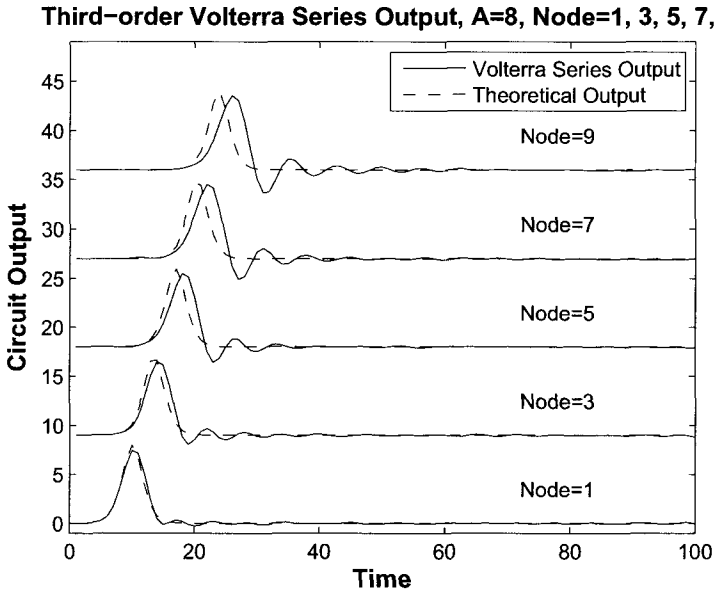

Figure 4.5: Circuit response to a single soliton, $V_0\beta^2 = 8$

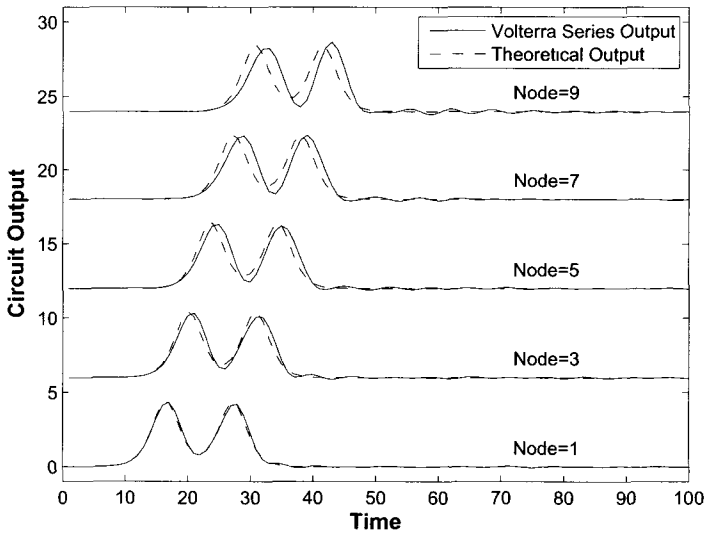

Figure 4.6: Circuit response to a composite soliton, $V_0\beta^2 = [4\ 5]$

solving the initial value problem of the ordinary differential equation:

$$y' = f(x, y), \quad y(x_0) = y_0$$

The basic idea of the Runge-Kutta Method is to approximate the solution of $y(x)$ at a set of points of x. For each point at step $n+1$, the approximation is constructed from a linear combination of approximations at step n and intermediate points. According to the number of the intermediate points, Runge-Kutta method can be classified by different orders, including order 2, 3 or 4. The commonly-used Runge-Kutta method is of the order 4, which is defined as follows:

$$\begin{aligned} k_1 &= hf(x_n, y_n) \\ k_2 &= hf(x_n + \frac{1}{2}h, y_n + \frac{1}{2}k_1) \\ k_3 &= hf(x_n + \frac{1}{2}h, y_n + \frac{1}{2}k_2) \\ k_4 &= hf(x_n + h, y_n + k_3) \\ y_{n+1} &= y_n + \frac{1}{6}k_1 + \frac{1}{3}k_2 + \frac{1}{3}k_3 + \frac{1}{6}k_4 + O(h^5) \end{aligned}$$

where, h is the prescribed step-size. In this thesis, we apply Runge-Kutta method of order 4 to solve the problem of the Toda circuit response to input.

To evaluate the response of the Toda circuit using Runge-Kutta method, we re-write the governing equation of the Toda circuit, i.e., Eq. (3.2) in terms of the variable Q_n which is the charge of the nth capacitor. As a result, we obtain:

$$\frac{d^2}{dt^2}Q_n(t) = \mathrm{e}^{Q_{n-1}(t)/Q_0} + \mathrm{e}^{Q_{n+1}(t)/Q_0} - 2\mathrm{e}^{Q_n(t)/Q_0} \tag{4.13}$$

Defining the new variables $U_n(t) = \frac{dQ_n(t)}{dt}$, $n = 1, \cdots, N$, with N being the total number of circuit sections, and taking into account the signal generator at the input section and the terminating load at the final section, then Eq. (4.13) can be

reformulated as pairs of first-order differential equations such that:

$$\begin{aligned}
\frac{dU_1(t)}{dt} &= (\frac{s_{\text{in}}(t)}{V_0} - 2\mathrm{e}^{Q_1(t)/Q_0} + \mathrm{e}^{Q_2(t)/Q_0} + 1)/(LC_0); \qquad n = 1 \\
\frac{dU_n(t)}{dt} &= (\mathrm{e}^{Q_{n-1}(t)/Q_0} - 2\mathrm{e}^{Q_n(t)/Q_0} + \mathrm{e}^{Q_{n+1}(t)/Q_0})/(LC_0); \qquad 1 < n < N \\
\frac{dU_n(t)}{dt} &= (\frac{R}{C_0} e^{Q_n(t)/Q_0} \frac{dQ_n(t)}{dt} + \frac{V_0}{L}(e^{Q_{n-1}(t)/Q_0} - e^{Q_n(t)/Q_0}))/(LC_0); \qquad n = N \\
\frac{dQ_n(t)}{dt} &= U_n(t) \qquad \forall\, n
\end{aligned} \tag{4.14}$$

Eq. (4.14) is now in the standard form ready to be evaluated by the Runge-Kutta integration method. To test the accuracy of the method, we choose the total number of stages in the Toda circuit to be $N = 100$. We normalize the circuit parameters such that $L = 1$ and $\mathrm{C}_0 = 1$. Given an input voltage signal $s_{\text{in}}(t)$, the output voltage at stage n is then $V_n(t) = V_0(\mathrm{e}^{Q_n(t)/Q_0} - 1)$, $n = 1, \cdots, N$, and can be obtained by solving the above $2N$ differential equations.

Fig. 4.7 shows the results of examining the accuracy of the Runge-Kutta method for the output of a relatively long Toda circuit with the amplitude of the input being relatively large. Here, the input is a single soliton with amplitude 8. The circuit response at stages 1, 10, 20, 30, 40 and 50 are plotted together with the theoretical outputs obtained, as in the case for the Volterra series approximation, by evaluating Eq. (3.3). It can be seen that the evaluation of the output at both lower and higher stages of the circuit is very accurate (relative error $e_i < 0.002$, $i = 1, \cdots 5$), showing that Runge-Kutta method is suitable to evaluate the output of the Toda circuit for both low and high stage numbers. Similar accuracies are observed if the input soliton is of relatively low amplitudes.

We also apply the Runga-Kutta method for the evaluation of the outputs at different stages of the Toda circuit when the input is a composite soliton, and similar accuracies as in the cases of single solitons are observed, showing that the Runga-Kutta method is also suitable for the calculation for such cases. Here, we repeat the examination of the two cases as shown in Figs. 3.3 and 3.4 in which separate constituent solitons of different amplitudes (1 and 9, 4 and 5) propagate along the

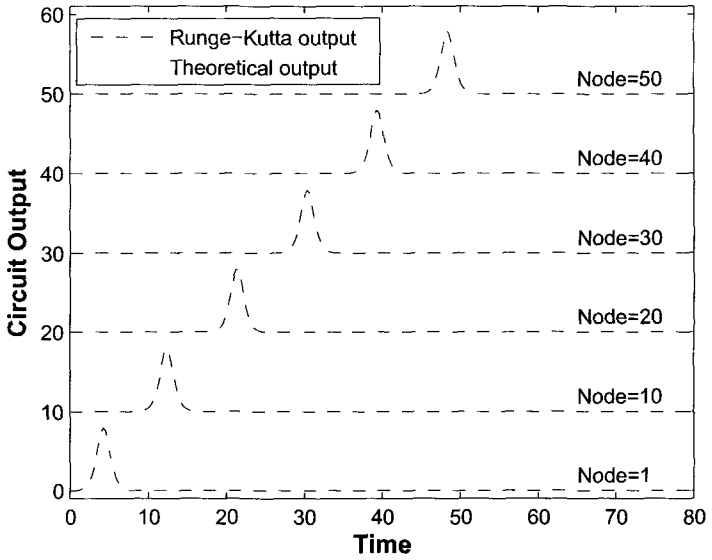

Figure 4.7: Circuit response to a single soliton, $V_0\beta^2 = 8$

Toda circuit, merge to form a composite soliton, and then re-separate after being allowed to further propagate. The observations are almost identical (relative error $e < 0.002$) to those theoretical results illustrated in Figs. 3.3 and 3.4, showing the high accuracy of the Runge-Kutta method in the evaluation of composite solitons.

In previous section and this section, we examine the response of the Toda circuit using both Volterra series and Runge-Kutta method. We show that Volterra series is valid for relative small input soliton amplitude and at the early stages of the Toda circuit, while Runge-Kutta method is accurate for both low and high input soliton amplitude and for both early and late stages of the circuit. It is obvious that in terms of accuracy, Runge-Kutta method is a better option than Volterra series. However, we also notice that for each circuit input, Runge-Kutta method has to perform numerical routines for calculating circuit output, which results in high computation complexity and difficulty in qualitative analysis especially for examining circuit response to

stochastic input. On the other hand, under the condition of weak nonlinearity, according to Volterra series, Toda circuit can be characterized by transfer functions of the circuit. Circuit response to any input can then be calculated based on these transfer functions. For stochastic input, the statistical characteristics of the circuit output, including mean, variance, correlation and power spectral density (PSD) can be calculated as a function of these transfer functions and the characteristics of the circuit input. This offers convenience in analyzing the circuit effects to stochastic input compared to that of the Runge-Kutta method, as we will show in next section and in the detection of the soliton system in next chapter.

In next section, we study the Toda circuit response to stochastic input and we employ the Volterra series to calculate circuit response at early stages and apply the Runge-Kutta method to evaluate the circuit response at both the early and the late stages.

4.3 Response of Toda Circuit to Stochastic Input

In this section, we consider the response of Toda circuit to stochastic inputs. Specifically, the inputs we considered are solitons accompanied by additive Gaussian white noise commonly encountered in a wireless communication environment. The input to the Toda circuit is written as $x(t) = s(t) + n(t)$, where $s(t)$ denotes a general soliton signal, i.e., $s(t)$ may represent a soliton of any amplitude, or a composite soliton as described in Section 3.1. The noise $n(t)$ is AWGN with zero mean and PSD $\mathcal{N}_0/2$.

4.3.1 Response at Early Stages of Circuit

As shown in Section 4.1, the Volterra series representation is sufficiently accurate for the response of the early stages of the Toda circuit. Therefore, we can employ the Volterra series for the analysis of the response of the Toda circuit to stochastic inputs

at its early stages. We limit the analysis to stages 1 - 5. From Eqs. (4.1) and (4.2), the output of the third-order approximation Toda circuit can be expressed as:

$$\begin{aligned} y(t) &= \sum_{k=1}^{3} \int_{-\infty}^{\infty} \cdots \int_{-\infty}^{\infty} (s(\tau_1) + n(\tau_1)) \cdots (s(\tau_k) + n(\tau_k)) h_k(t - \tau_1, \cdots t - \tau_k) \mathrm{d}\tau_1 \cdots \mathrm{d}\tau_k \\ &= \tilde{s}(t) + \tilde{n}(t) \end{aligned} \tag{4.15}$$

for which, using the notation of higher-order convolution in Eq. (4.2), the 3rd order approximation circuit response to $s(t)$ and the output noise sequence can be expressed as

$$\tilde{s}(t) = s \otimes h_1 + s \circ s \otimes h_2 + s \circ s \circ s \otimes h_3 \tag{4.16a}$$

$$\tilde{n}(t) = n \otimes h_1 + [(n \circ n) + 2(s \circ n)] \otimes h_2 + [(n \circ n \circ n) + 3(s \circ n \circ n + s \circ s \circ n)] \otimes h_3 \tag{4.16b}$$

where $\circ$ is defined by Eq. (4.2). It has been demonstrated in Section 4.1.3 (see Figs. 4.2-4.6) that if the input $s(t)$ is a single soliton or a composite soliton, the third order approximation of the early-stage circuit output $\tilde{s}(t)$ is very close to the theoretical output which is the delayed version of the original input signal $s(t)$. Here, we examine the statistical properties of the output noise by analyzing the first and second moments, the auto-correlation and the power spectral density of the output noise $\tilde{n}(t)$.

The mean of the output noise can be directly obtained from the expression of the output in Eq. (4.16b). At any instant t_0, the mean $\mu_{\tilde{n}}(t_0)$ of $\tilde{n}(t)$ is given by

$$\begin{aligned} \mu_{\tilde{n}}(t_0) &= \mathrm{E}[n \otimes h_1 + (n \circ n + 2s \circ n) \otimes h_2 + (n \circ n \circ n + 3s \circ n \circ n + 3s \circ s \circ n) \otimes h_3] \\ &= \frac{\mathcal{N}_0}{2} \int_{-\infty}^{\infty} h_2(\tau_1, \tau_1) d\tau_1 + 3 \cdot \frac{\mathcal{N}_0}{2} \int_{-\infty}^{\infty} \int_{-\infty}^{\infty} s(t_0 - \tau_1) h_3(\tau_1, \tau_2, \tau_2) d\tau_1 d\tau_2 \end{aligned} \tag{4.17}$$

where the facts that the input noise $n(t)$ is zero-mean and white such that $\mathrm{E}[n(t)] = 0$ and $\mathrm{E}[n(\tau_1)n(\tau_2)] = \frac{\mathcal{N}_0}{2}\delta(\tau_1 - \tau_2)$, and that convolution of a function with an impulse

results in the same function have been used. From Eq. (4.17), the mean $\mu_{\tilde{n}}(t_0)$ of the output noise of the Toda circuit can be evaluated at any instant t_0 given a particular input soliton. Consider the case of $s(t)$ being a single soliton or a composite soliton, we define the signal-to-noise ratio as the ratio of the energy of the single or composite soliton to the noise power such that $\rho = E/(\mathcal{N}_0/2)$ where E can represent either E_s or E_c. Under the condition $\rho > 1$dB, calculations from Eq. (4.17) show that for all $s(t)$ of amplitude A such that $0.5 \leq A \leq 10$, $\mu_{\tilde{n}}(t_0) < 10^{-2}\ \forall\ t_0$. This result indicates that $\mu_{\tilde{n}}(t_0)$ is very small compared to the amplitude of the output amplitude and we can make the approximation of $\mu_{\tilde{n}}(t_0) \approx 0$.

On the other hand, the variance of $\tilde{n}(t)$ at time instance t_0 can also be calculated from Eq. (4.16b) yielding:

$$\sigma^2_{\tilde{n}}(t_0) = \mathrm{E}[\tilde{n}^2(t_0)] = \frac{\mathcal{N}_0}{2}(\tilde{a}_1 + \tilde{V}_1(t_0)) + \left(\frac{\mathcal{N}_0}{2}\right)^2(\tilde{a}_2 + \tilde{V}_2(t_0)) + \left(\frac{\mathcal{N}_0}{2}\right)^3 \tilde{a}_3 \qquad (4.18)$$

where $\tilde{a}_i,\ i = 1, 2, 3$, are constants and $\tilde{V}_i(t_0),\ i = 1, 2$, are functions of $h_1,\ h_2,\ h_3$ and $s(t)$ (see Appendix A). Since $\tilde{V}_i,\ i = 1, 2$ are time-dependent functions, we expect $\sigma^2_{\tilde{n}}(t_0)$ to be time-varying if the input contains both signal and noise. However, if the input consist of Gaussian noise $n(t)$ only, then the output noise variance is a constant. The variance of the output signals at different time instants t_0 for various input signals are plotted in Fig. 4.8. Here, we plotted the variance of the outputs of the first stage $(n = 1)$ for which the input is $x(t) = s(t) + n(t)$ with $s(t)$ respectively being 0, single soliton of amplitude 4, single soliton of amplitude 5, and composite soliton formed from the two single solitons. The PSD of the input noise is chosen to be 1, i.e., $\frac{\mathcal{N}_0}{2} = 1$. It can be observed that, as expected from Eq. (4.18), the variance of output noise is a constant if the input is only Gaussian noise. For the cases when soliton signals are mixed with noise, the initial variances of the output noise are marginally higher, but quickly settle to the constant value of the variance of the output for which the input is noise only. As another example, Fig. 4.9 shows the variance of the first-stage

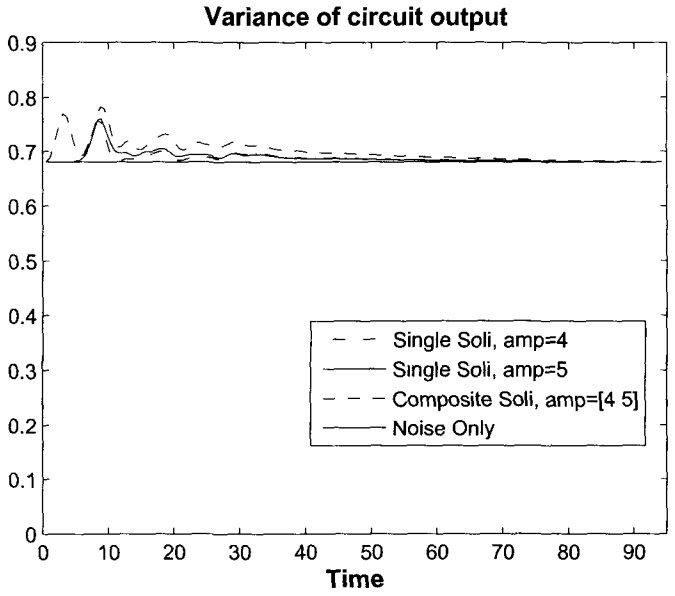

Figure 4.8: Variance of output signal, $V_0\beta^2 = [4\ 5]$

outputs of the circuit for which the input is $x(t) = s(t) + n(t)$ with $s(t)$ respectively being 0, single solitons of amplitude 1 and 10, and a composite soliton formed from the two single solitons. It is clear that for solitons with different amplitudes, similar results as shown in Fig. 4.8 can be observed.

Noise only input: In Section 4.1, we have illustrated that the short Toda circuit exhibits weak nonlinearity. Thus, we would expect the responses of the early stages of the Toda circuit to be not too different from those for linear circuits. Hence, if the input to a short Toda circuit is Gaussian noise only, we would expect the output to be almost Gaussian. Fig. 4.10 shows the distribution of the output $\tilde{n}(t_0)$ calculated from Eq. (4.16b) at $t_0 = 6.033$ for various zero-mean Gaussian noise $n(t)$ with $\frac{\mathcal{N}_0}{2} = 1, 3, 5$. The number of noise samples is chosen to be $1e4$. We also plotted the theoretical values of the Gaussian distribution with mean $\mu_{\tilde{n}}(t_0)$ and variance $\sigma^2_{\tilde{n}}(t_0)$ from Eqs. (4.17) and (4.18) with the various values of $\frac{\mathcal{N}_0}{2}$ again evaluated at $t_0 = 6.033$. From Fig. 4.10, the mean-square difference between the actual distribution and the

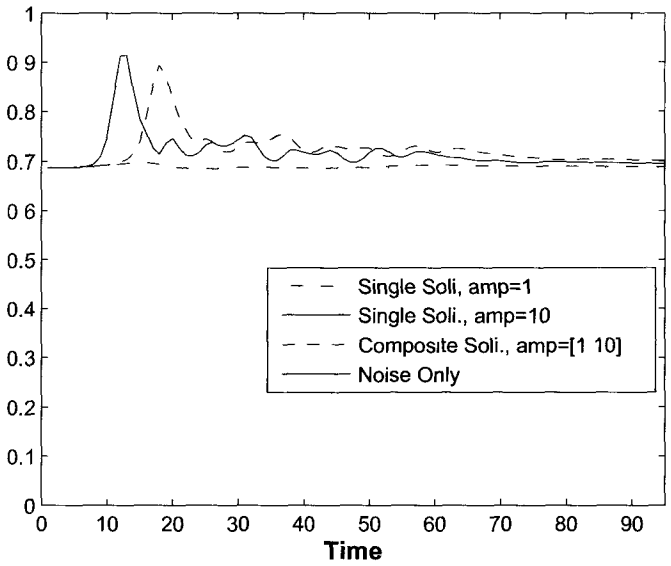

Figure 4.9: Variance of output signal, $V_0\beta^2 = [1\ 10]$

Input PSD	Numerical output mean	Numerical output variance	Theoretical Gaussian mean	Theoretical Gaussian variance
1	0.0002	0.675	0	0.68
3	0.0008	1.993	0	2.06
5	-0.0004	3.5180	0	3.52

Table 4.1: Mean and variance of output noise for input noise only

theoretical Gaussian curve for each of the values of $\frac{N_0}{2}$ is $\bar{\epsilon}^2 < 0.001$ showing that each of the distribution can be accurately approximated by a Gaussian distribution. We also note that the mean value of the output noise distribution is approximately zero, thus confirming our previous observation. The following table shows the comparison of the measured means and variances with the theoretical Gaussian approximation for different input PSD $\frac{N_0}{2}$. It can be observed that the means and variances are indeed very close.

We now examine the autocorrelation of the output noise when the input is white

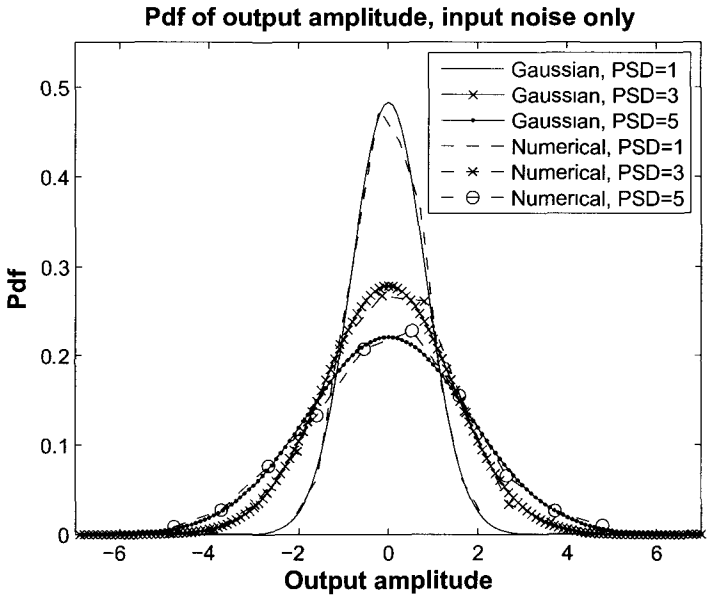

Figure 4.10: PDF output noise, input noise only

Gaussian noise. From the expression of the output noise in Eq. (4.16b), the autocorrelation function of the output noise can be written as

$$r_{\tilde{n}\tilde{n}}(t_1,t_2) = \mathrm{E}[\tilde{n}^2(t_1)\tilde{n}^2(t_2)] = \frac{\mathcal{N}_0}{2}\tilde{R}_1(t_1,t_2) + \left(\frac{\mathcal{N}_0}{2}\right)^2 \tilde{R}_2(t_1,t_2) + \left(\frac{\mathcal{N}_0}{2}\right)^3 \tilde{R}_3(t_1,t_2) \tag{4.19}$$

where $\tilde{R}_i(t_1,t_2)$, $i = 1,2,3$, are functions involving the convolutions of h_1, h_2, h_3 and $s(t)$ (see Appendix A). Since $\tilde{R}_i$, $i = 1,2,3$ are non-stationary functions, we expect $r_{\tilde{n}\tilde{n}}(t_1,t_2)$ to be non-stationary. However, in a practical Toda circuit, the first term in Eq. (4.19) is dominant rendering the auto-correlation function approximately stationary. Fig. 4.11 shows the autocorrelation function of the output noise for $s = 0$ and it can be observed that along the line $t_1 - t_2 = K$ for K being a constant, the autocorrelation function is essentially constant. Thus, if we take the Fourier transform of the autocorrelation function along the line $t_1 = K$ we obtain the spectral power density of the output noise. Fig. 4.12 depicts the spectral power density function of

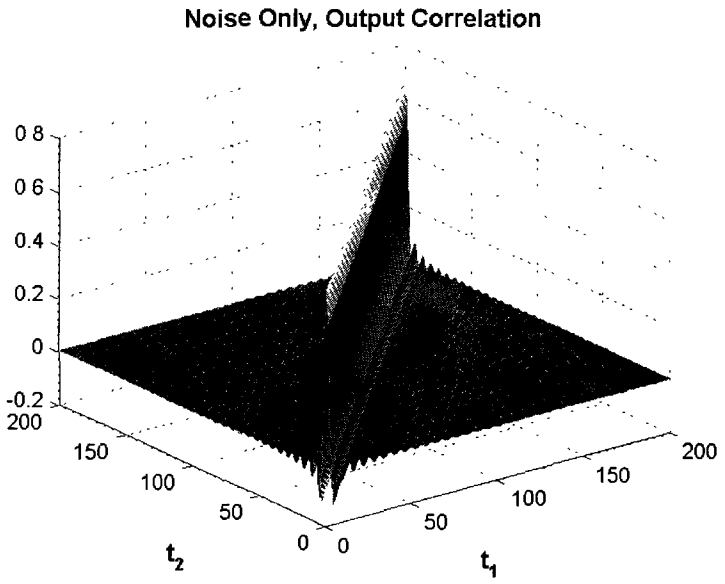

Figure 4.11: Correlation of output noise, input noise only

the output noise and it can be observed that within the normalized bandwidth, the noise is essentially white.

Signal plus noise input: We now examine the output of the circuit when the input is $s(t) + n(t)$ where $s(t)$ is a single soliton. Solitons of various amplitudes and noise of different power have been tested as input. The general properties of the output can be exemplified by the following case in which a single soliton of amplitude 4 accompanied by additive white Gaussian noise of PSD $\frac{N_0}{2} = 1, 3, 5$ is chosen to be the input. The output of the first stage ($N = 1$) of the Toda circuit at t_0 chosen to be the instant corresponding to the peak of $\tilde{s}(t)$ is examined. We calculated $t_0 = 6.033$ by substituting $n = N = 1$ in Eq. (3.3). Choosing the number of noise samples being $1e4$, the histograms of the corresponding outputs at t_0 is plotted in Fig. 4.13 juxtaposed with a Gaussian distribution with mean $\mu = s(t_0) = 4$ and variances calculated from Eq. (4.18) with the respective input PSD. It can be observed that the distribution of the output noise $\tilde{n}(t_0)$ is very close to a Gaussian distribution. The mean-square

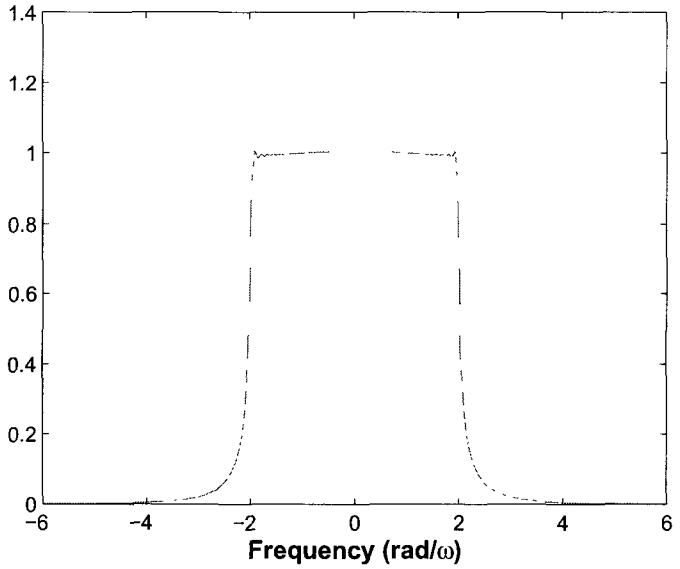

Figure 4.12: Power spectral density, input noise only

Input PSD	Numerical output mean	Numerical output variance	Theoretical Gaussian mean	Theoretical Gaussian variance
1	3.982	0.698	4	0.708
3	3.999	2.098	4	2.104
5	3.989	3.552	4	3.540

Table 4.2: Mean and variance of output noise for input soliton and noise

difference between each of the histogram and its Gaussian approximation is $\varepsilon^2 < 0.003$ which is negligibly small. Table 2 shows the comparison of the measured means and variances with the theoretical Gaussian approximation for different input noise PSD. Again, it can be observed that the means and variances are indeed very close.

The autocorrelation function $r_{\tilde{n}\tilde{n}}(t_1, t_2)$ of the output noise $\tilde{n}(t)$ with input to the circuit being $s(t) + n(t)$ is shown in Fig. 4.14. It is again observed that along the line $t_1 - t_2 = K$ for K being a constant, the autocorrelation function is almost constant, making the process close to stationary. Taking the Fourier transform of the

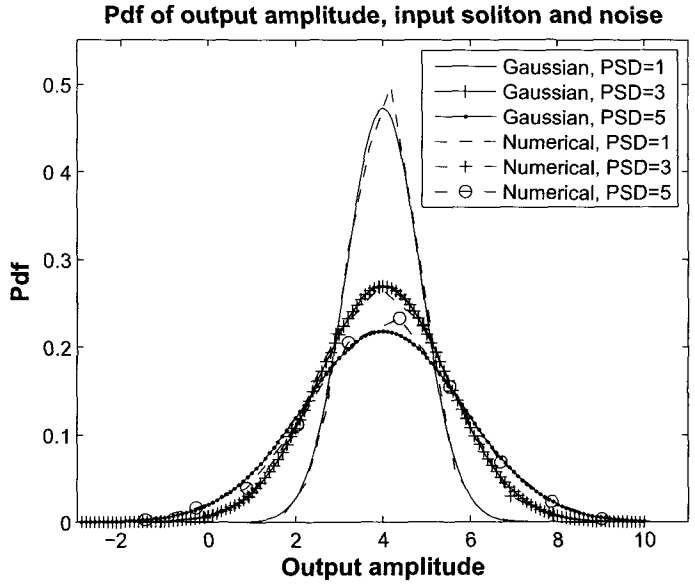

Figure 4.13: PDF output noise, input signal and noise

autocorrelation function along the line $t_1 = K$ we obtain the spectral power density of the output noise and this is shown in Fig. 4.15. Even though there are small ripples within the passband of the noise, the power spectral density function of the output noise can still be regarded as essentially flat, indicating that the output noise is reasonably white.

Similar properties are exhibited by the output noise for the input signal $s(t)$ being chosen from single solitons of different amplitudes or from different composite solitons.

4.3.2 Response at Later Stages of the Circuit

In this subsection, the response of the later stages of the Toda circuit will be examined. For large n, the long circuit exhibits strong nonlinearity. As pointed out in Section 4.2, the Runge-Kutta method is suitable for the evaluation of the responses under such conditions. Again, we study the effects of various inputs including white Gaussian noise only, single soliton and noise, and composite soliton and noise.

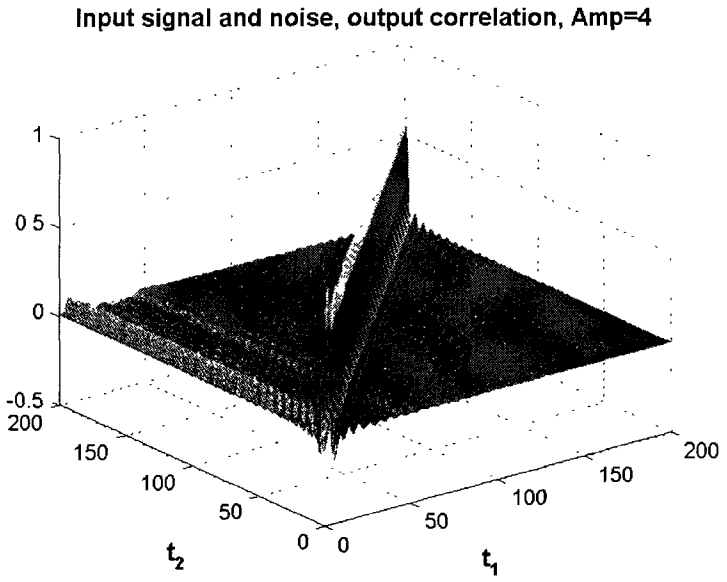

Figure 4.14: Correlation of output noise, input signal and noise

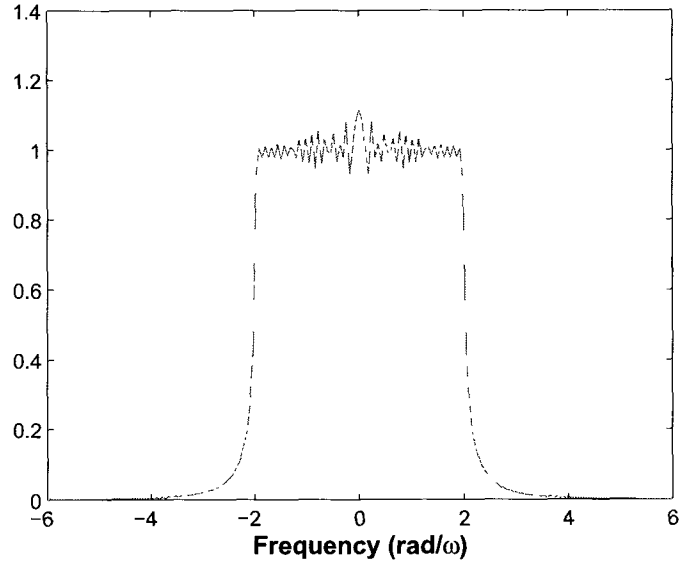

Figure 4.15: Power spectral density, input signal and noise

Noise-only input: The fact that solitons can be generated from rectangular inputs indicates the ability of Toda circuit, or more generally, soliton supporting systems, transforming a rectangular pulse input into solitons [9]. As a matter of fact, the rectangular pulse is not the only input that can be applied to generate solitons. In general, we found that under certain conditions, an irregular input such as a noise sequence, can also give rise to a soliton. Finding the exact nature of these conditions proved to be difficult. In this thesis, we only demonstrate some special cases such that the DC component (time average) of the input signal is a) very close to zero, b) negative, and c) positive.

a) DC component approximately zero: Here, we study the effect of a burst of random pulses which have an overall mean approximately equal to zero. We vary the variance of these random pulses and observe the output of the Toda circuit at the relatively early stages and also at the later stages. Fig. 4.16 shows an example of a burst of random pulses with mean $\mu = 0$, PSD $\frac{N_0}{2} = .01$. We can observe that the output at the various stages are decaying oscillation. At the earlier stages, the initial transient is much larger in amplitude while the subsequent oscillations are much smaller in amplitude. However, at the later stages, the initial transient decreases in amplitude in comparison to those at the earlier stages whereas the subsequent oscillations increase in amplitude. Fig. 4.17 shows input bursts of random pulses with mean $\mu = 0$, PSD $\frac{N_0}{2} = 1$. Comparing Fig. 4.16 and Fig. 4.17, we can observe that, the outputs of the Toda circuit to these different random inputs have similar structures, a sequence of oscillations preceded by a transient, the larger is the input variance, the larger are the oscillations. Other bursts of random pulses of approximately zero DC components have been used for input to the circuit and responses of similar structures are observed.

b) Negative DC component: Now, we test the output responses at different stages of the Toda circuit to an input of random pulses with overall mean being negative.

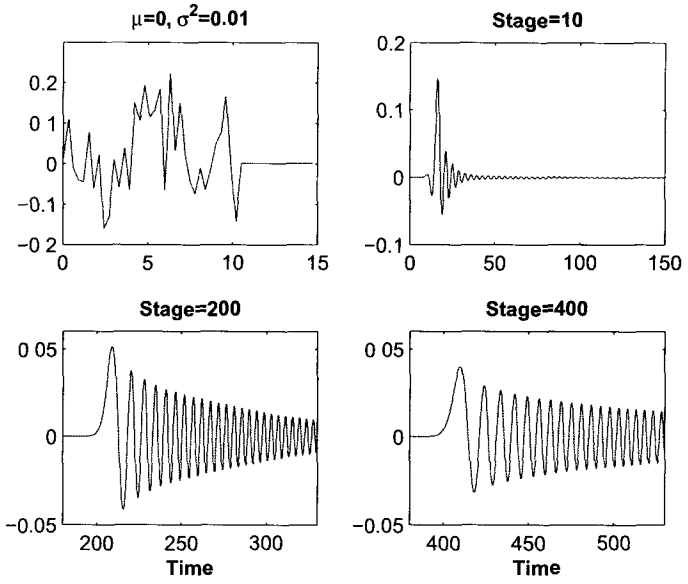

Figure 4.16: Circuit response to noise-only input, $\mu = 0$, $\frac{\mathcal{N}_0}{2} = 0.01$

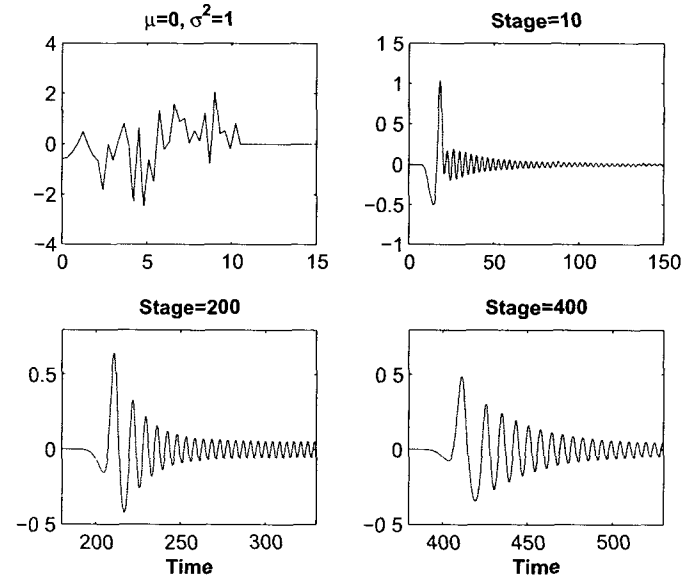

Figure 4.17: Circuit response to noise-only input, $\mu = 0$, $\frac{\mathcal{N}_0}{2} = 1$

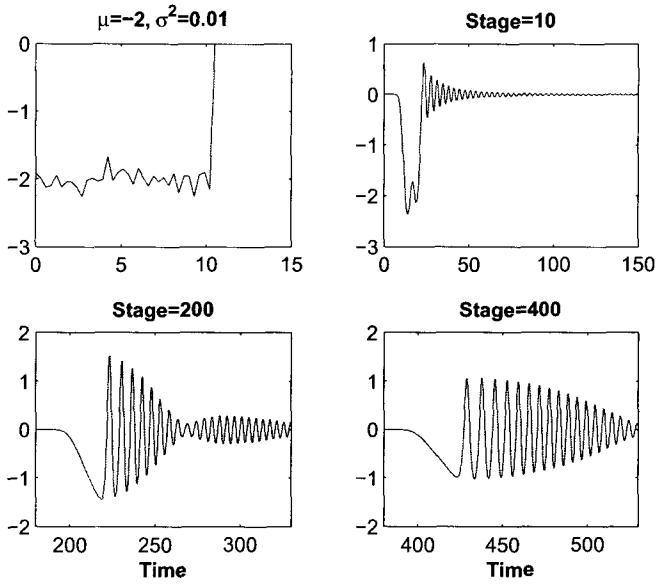

Figure 4.18: Circuit response to noise-only input, $\mu = -2$, $\frac{\mathcal{N}_0}{2} = 0.01$

Fig. 4.18 shows the response of the circuit at different stages for the input burst of random pulses with overall mean $\mu = -2$ and PSD $\frac{\mathcal{N}_0}{2} = .01$. Here, we observe that at the earlier stages, the response invariably starts with a negative transient followed by decaying oscillations. At later stages, the amplitude of the negative transient decreases substantially whereas the amplitudes of the oscillations increase significantly in comparison to those at the earlier stages. Fig. 4.19 shows the bursts of random pulses of negative overall mean $\mu = -2$ and PSD $\frac{\mathcal{N}_0}{2} = 1$. It can be seen that similar transient and oscillations occurring at earlier and later stages of the circuit are observed as in the previous case in Fig. 4.18. The larger is the variance of the random pulses, the higher is the amplitudes of the oscillations. Other bursts of random pulses of different overall mean and variances have also been used as input, and similar observations obtained.

c) Positive DC component: Here, we examine the output responses at different stages of the Toda circuit to an input of random pulses with overall mean being

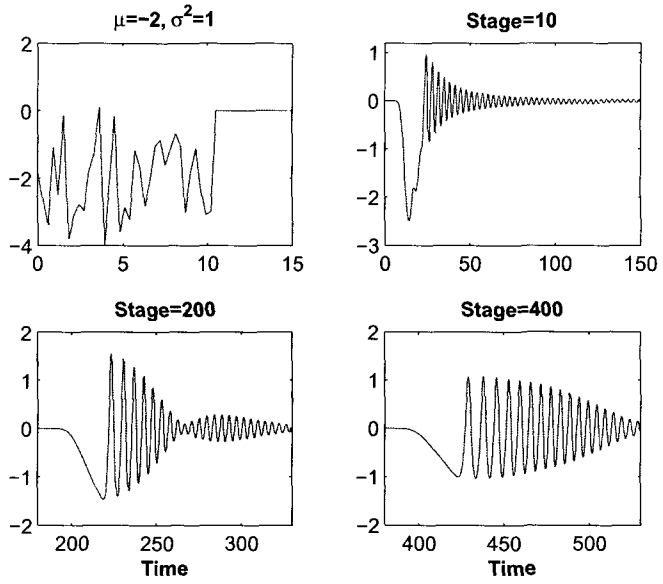

Figure 4.19: Circuit response to noise-only input, $\mu = -2$, $\frac{\mathcal{N}_0}{2} = 1$

positive. Fig. 4.20 shows the response of the circuit at different stages for the input burst of random pulses with overall mean $\mu = 2$ and PSD $\frac{\mathcal{N}_0}{2} = .01$. It can be observed in this case, that the output is not only comprised of transient and oscillations, but also there is a soliton-like pulse preceding them. Unlike the transient and the oscillations as in previous two cases, this soliton-like response propagates through the various stages of the circuit and, in the stationary state, does not subside nor change in shape. Fig. 4.21 shows circuit response to the input random pulse with mean $\mu = 2$ and PSD $\frac{\mathcal{N}_0}{2} = 1$. It can be observed that, similar to Fig. 4.20, there is an additional soliton-like pulse preceding the transient and the oscillations. In both Figs. 4.20 and. 4.21, the soliton-like pulse at the early stages is very similar to an interacting soliton which will then separate into its constituent solitons at the later stages. It can be shown that depending on the input random pulses, the soliton-like pulse in the response of the early stages may also be a single soliton which will then propagate without dispersion along the circuit. These additional soliton-like pulses in the circuit

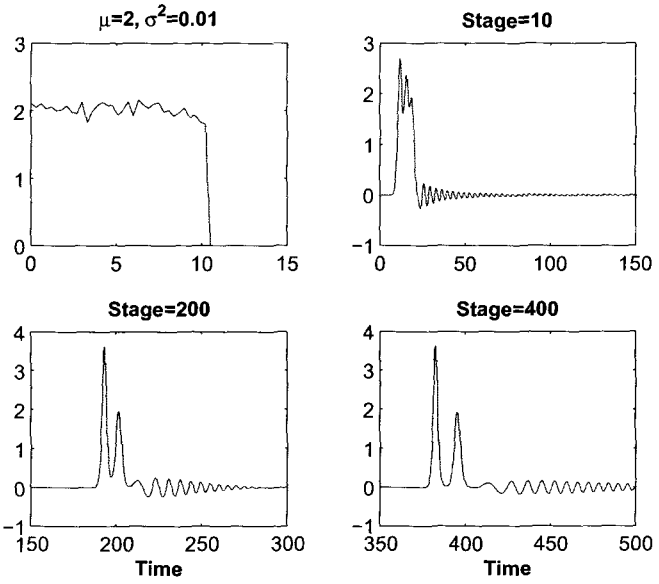

Figure 4.20: Circuit response to noise-only input, $\mu = 2$, $\frac{N_0}{2} = 0.01$

response is an important observation and is entirely different from the previous two cases of a) and b). Random pulses of different positive mean and different variance have also been used as input for the test and similar observations persist.

The reason why the DC component of the input signal affects the amplitude of output signal can be explained by the property of Toda circuit. Let $V_i(t)$ denote the voltage at the ith stage of the Toda circuit. It has been proved [23] that

$$\int_0^\infty V_i(t)dt = \text{Constant} \tag{4.20}$$

Eq. (4.20) indicates the DC component is conserved in the Toda circuit output. As observed in the examples here, all outputs consist of oscillations of which the DC component is very small. Since the DC component of a soliton is positive, therefore, to generate an output consisting of a soliton necessitates an input of positive DC component. Hence, outputs containing solitons are only observed if the input signals are of positive mean values. For input signals of negative mean values, the DC

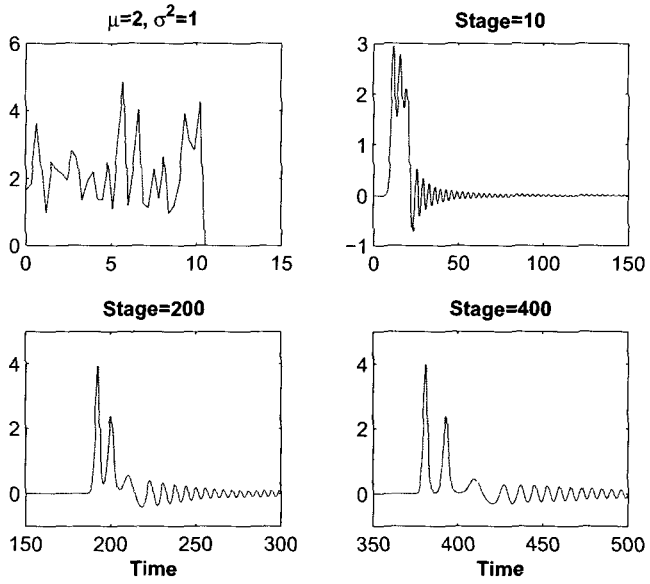

Figure 4.21: Circuit response to noise-only input, $\mu = 2$, $\frac{\mathcal{N}_0}{2} = 1$

conservation of Eq. (4.20) also holds. Therefore, the outputs of the Toda circuit for inputs having negative mean values will also have a negative DC component. This can be observed by the large negative part of the output just before the start of the oscillations. However, since the Toda circuit only supports positive-valued solitons of the form as shown in Eq. (3.3), this negative part is not supported by the circuit and will gradually disperse as the output is propagated along the circuit. This is evident in comparing the negative parts of the outputs at the different stages of the circuit in Figs. 4.18 and 4.19 in which the negative part gradually stretches out to be longer and longer in duration.

Input consisting of soliton and random noise: Since the amplitude of a soliton is positive, under higher signal-to-noise ratio (SNR), the input mixture of soliton and zero-mean Gaussian noise will have positive mean. Thus, the input is similar to that of Case c) above. Therefore, the output response of the Toda circuit to such an input will also be similar to those observed in Case c).

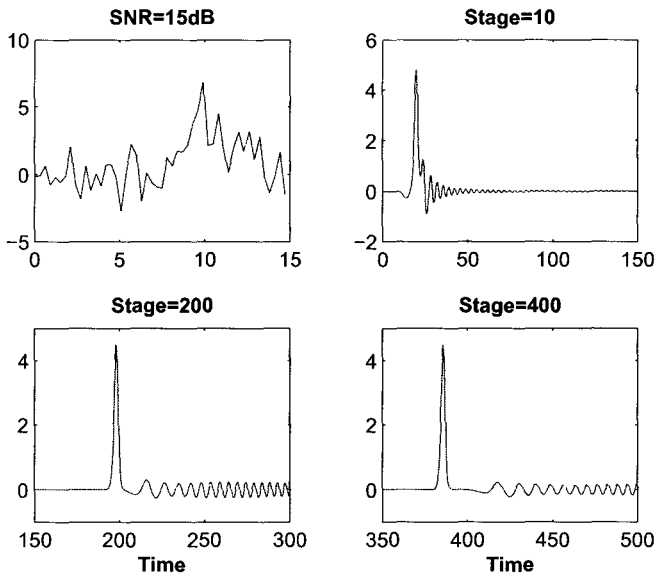

Figure 4.22: Circuit response to single soliton with noise input, SNR= 15dB

a) Single soliton with noise: Figs. 4.22 and 4.23 illustrate the various responses at different stages of the circuit for an input being a single soliton mixed with zero-mean Gaussian noise. The input soliton in both cases is of amplitude 4. The input SNR are respectively 15dB and 5dB. It can be observed that in each case, a soliton-like pulse exists at the output followed by transients and oscillations. We also observe that in Fig. 4.22, the soliton-like pulse at the output is no longer the same as the input soliton, having amplitude of 4.75 instead. For SNR higher than 20dB, it is observed that the output soliton remains the same as the input soliton and the effect of the Gaussian noise is reduced to small oscillations following the soliton. Other experiments have been carried out with different mixtures of single solitons and zero-mean Gaussian noise and similar observations are obtained.

b) Composite soliton with noise: Figs. 4.24 and 4.25 show the various responses at different stages of the circuit for an input being a composite soliton mixed with zero-mean Gaussian noise. The input composite soliton in both cases is made up of

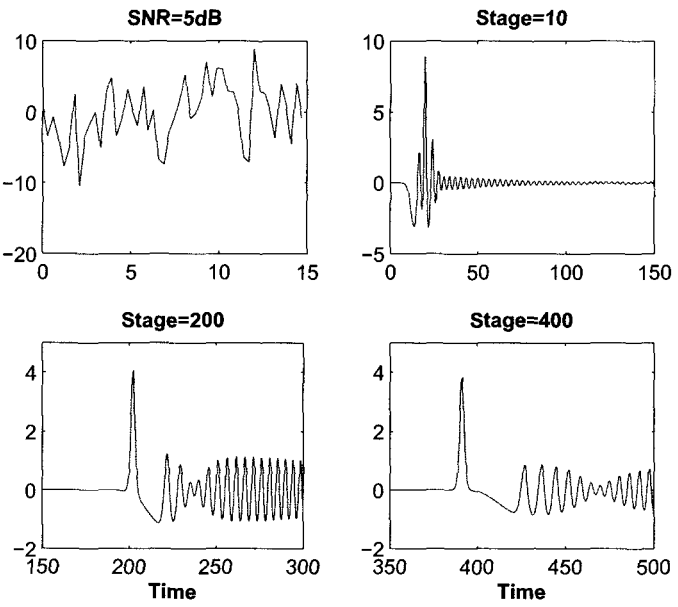

Figure 4.23: Circuit response to single soliton with noise input, SNR= 5dB

constituent solitons having amplitudes 4 and 5. The input SNR are respectively 15dB and 5dB. It can be observed that in each case, the output consists of a composite soliton which, after a number circuit stages, separates into the constituent solitons. However, as shown in Fig. 4.25 , under lower SNR, the constituent solitons at the output are not necessarily the same as those making up the input composite soliton. Indeed, it can also be observed that an additional small soliton-like pulse also exists at the outputs of both Figs. 4.24 and 4.25 . Due to the much lower amplitude, this additional soliton propagates much more slowly than the two other solitons. Inputs containing other composite solitons mixed with zero-mean Gaussian noise have also been used and similar output responses have been obtained.

The result that additive input noise sequence may corrupt soliton(s) into soliton(s) of different parameters together with some oscillations is indeed a general one. This result is parallel to the propagation of an exact soliton in impure nonlinear lattices [29,

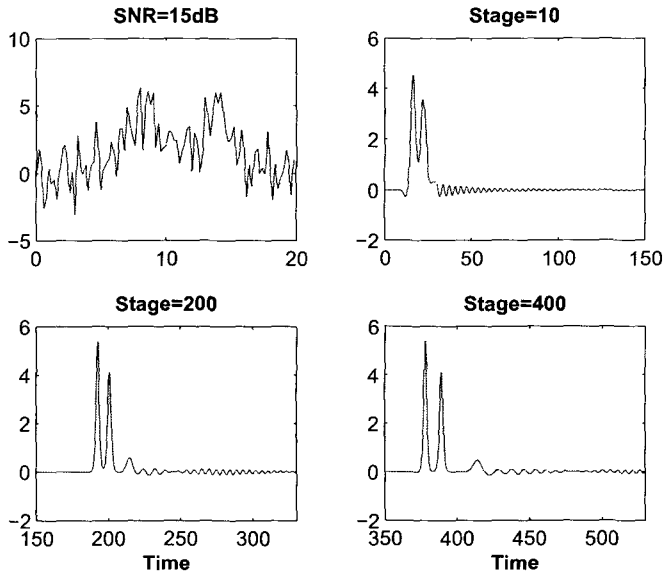

Figure 4.24: Circuit response to composite soliton with noise input, SNR= 15dB

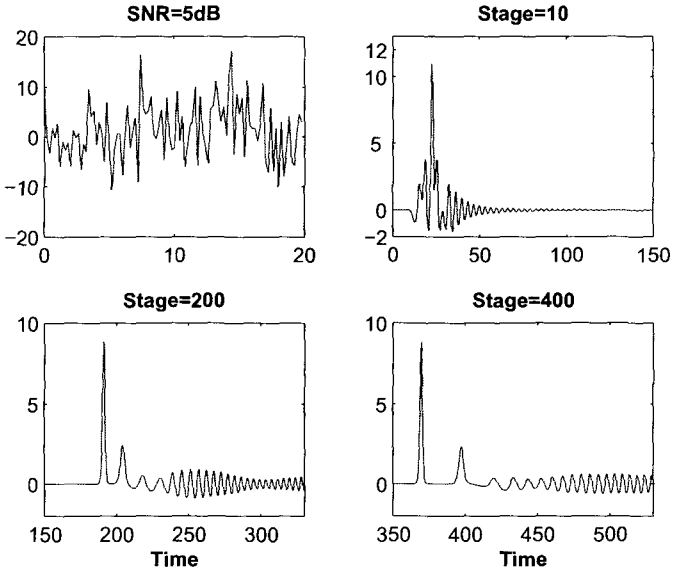

Figure 4.25: Circuit response to composite soliton with noise input, SNR= 5dB

35, 57] indicating the inherent similarity between the circuit perturbation and initial input perturbation.

4.4 Summary

In this chapter, we examine the properties of the Toda circuit and focus on the circuit response to stochastic input. We show that the Toda circuit response at early stage exhibits weak nonlinearity and can be analyzed by Volterra series. For circuit response at late stags, the approximation error of the Volterra series increases due to the increase of the nonlinearity of the circuit. To seek for better accuracy, we apply the Runge-Kutta method to study the circuit response at both early and late stages. Applying Volterra series, the Toda circuit response to stochastic input, including the Gaussian noise and the mixture of the noise and soliton signal is studied. The mean, variance, correlation and PSD of the circuit output are calculated. Applying the Runge-Kutta method, we examine the Toda circuit response to noise input only and to noise corrupted soliton signal. We show that for noise only input, the mean of the noise plays an important role in generating solitons. The noise with positive mean may excite soliton(s), while noise with zero or negative mean may only transform into oscillations. For input being the combination of both soliton and noise, we show that the noise may distort input soliton to solitons with other parameters.

Chapter 5

Application of Soliton in Data Communication

In previous chapters, we examined the properties of Toda solitons and Toda circuits. In this chapter, we apply these properties in data transmission and propose a data communication system in which Toda solitons are employed as information carriers [11]. The application of solitons in data communications was first proposed in [50] and [51] in which experimental investigations on the multiplexing of a pair of soliton trains that were either amplitude or phase modulated were reported. It was suggested that the multiplexing effected by the transmission of a composite soliton could be used for secure communications. A more detailed soliton multiplexing system model was presented and studied in [49] with particular consideration given to applications in a wireless channel environment and to the system detection and estimation performance under an additive Gaussian channel. The Cramér-Rao bound for single soliton detection was derived and that for the composite soliton was evaluated numerically.

In this thesis, we propose a soliton communication system and examine the use of solitons for both the single-user and multi-user cases. For the single-user case, we employ, at least in concept, the Toda circuit as a signal generator and a modulator at

the transmitter, and focus our attention on an On-Off Keying (OOK) scheme which, as a special case of the general soliton amplitude modulation schemes [48], yields the best detection performance. For the multi-user case, we employ, again in concept, the Toda circuit as a signal generator, a multiplexer and a modulator at the transmitter, and use the *composite* soliton formed by the nonlinear interaction of constituent solitons as a multiplexed signal. At the receiver, a Toda circuit is also employed as a de-modulator. As solitons with different amplitudes represent information of different users, we call this scheme Soliton Amplitude Division Multiplexing (SADM). In both the single-user and multi-user soliton systems proposed here, we employ the OOK scheme. The OOK signals are transmitted through a linear communication channel corrupted by additive white Gaussian noise (AWGN) and are detected at the receiver. Besides wireless communications, the proposed soliton system can also find particular applications in wireless optical and optical fibre systems. In a wireless optical system, wide field-of-view point-to-point links in short-range can be assumed to be loss-free and the associated noise can be modelled as AWGN [24]. OOK scheme is commonly used in the transmission of optical carriers through these channels. In optical fibre system [3], a dispersion compensated and low-loss fibre can also be modelled as an ideal linear channel with the only noise source (modelled as AWGN) being the optical receiver. Both OOK and BPSK modulation-detection schemes can be employed [25] in the optical fiber system. While BPSK performs better than OOK, its complexity is much higher since coherent homodyne detection must be applied for the BPSK scheme. In this thesis, in conjunction with the properties of single and composite solitons studied in Chapter 3 and Chapter 4, we examine the bandwidth efficiency of the proposed soliton communication system in comparison with other multiplexing systems. Two detection schemes for the system are proposed and, applying some of the properties of stochastic signals to Toda circuits, the detection performance of soliton system is analyzed and evaluated via computer simulations.

5.1 Soliton Data Transmission System

In this section, we propose a data transmission system which employs the soliton as a carrier of information. For a single-user system, an on-off keying system using a single soliton is employed. For a two-user system, a multiplexed scheme using both single and composite solitons is proposed. This multiplexed scheme can be extended conceptually for $M > 2$ users.

5.1.1 Transmitted Signals

According to the discussion in Chapter 3, at the nth stage of the Toda circuit, the voltage of a Toda soliton can be described by

$$V_n(\tau) = V_0\beta^2 \text{sech}^2\left(\beta\tau - n\ \sinh^{-1}\beta - \phi\right) \tag{5.1}$$

where V_0 is a constant bias voltage and chosen to be 10 Volts, $\tau = t/\sqrt{LC_0}$ is the normalized time variable, β is the parameter governing the behavior of the soliton, and ϕ is the initial phase shift of the soliton. Eq. (5.1) represents a positive pulse. Its shape and amplitude do not change as the soliton propagates along the Toda circuit, which was observed in Chapter 3. Therefore, different solitons with different parameters β can be used to represent different signal levels in a pulse amplitude modulated (PAM) system. In this thesis, we consider binary signalling. Since the binary signal is distinguished by the relative amplitudes of the two solitons, it can be easily seen from a signal space viewpoint [43] that the larger is the distance between the two amplitudes, the better will be the detection performance in noise. Since negative amplitudes are not admissible for solitons, in this thesis, we propose the use of the on-off keying such that the maximum distance between the two soliton amplitudes is achieved.

Single User Transmission: For the on-off keying here, the binary message of a single user is represented such that a soliton s with parameter β is assigned if user

information $b = 1$, and zero (no soliton) is assigned when $b = 0$, i.e., the transmitted signal is represented by

$$x_0(t) = 0 \quad \text{for} \quad b = 0 \tag{5.2a}$$

$$x_1(t) = s(t) \quad \text{for} \quad b = 1 \tag{5.2b}$$

where b is the transmitted bit. At the transmitter, a Toda soliton of a prescribed amplitude (and therefore a prescribed value of $\beta = \beta_1$) is stored, i.e., for simplicity of implementation, such a soliton does not have to be generated by a Toda cirucit, rather a ready-made soliton waveform is kept ready to be transmitted when needed. For a sequence of 1 and 0, a sequence of solitons of this particular parameter and zeros representing 1 and 0 of the message respectively are selected to be transmitted through an AWGN channel. At the receiver, the Toda circuit is employed to restore the transmitted sequence of solitons which will then be detected by a maximum likelihood (ML) detector or a threshold detector. (In optical communication systems, electrical-to-optical (EO) and optical-to-electrical (OE) converters are employed for processing information carrying signals [25]. In employing the Toda soliton scheme proposed here in optical communications, the Toda circuit at the receiver is applied after the OE converter. In this thesis, both the EO and OE converters employed in optical system are assumed to be ideal so that the system performance will not be affected.)

Multiplexed Signal Transmission: Messages from several users represented by sequences of solitons of different parameters of course, can be time multiplexed, giving rise to the SADM system. In a general binary SADM system shared by M users [48], the signal of the mth user has two levels represented by two solitons of specified values of β such that

$$\beta_m = \begin{cases} \beta_{m1} & \text{if } b_m = 1 \\ \beta_{m0} & \text{if } b_m = 0, \end{cases}$$

where b_m is the binary data of the mth user and $[\beta_{m1}, \beta_{m0}]$, $m = 1, \cdots, M$ are suitably chosen values for the mth user parameter β_m to result in non-overlapping ranges of amplitudes for the two solitons. In the case of on-off keying system, $\beta_{m0} = 0$, $\forall\, m$, i.e., no soliton is sent if $b_m = 0$. Although M can be chosen as any number, in this paper, for simplicity, we will mainly discuss the case for $M = 2$. Most of the properties of two-user multiplexing can be extended to the case of M users. The transmission of these multiplexed user solitons through a linear communication channel can be effected by using the composite soliton formed by the merging of the individual solitons which represent the different user signals. Consider a two user system employing two soliton binary on-off keying signalling, for User m, $m = 1, 2$, soliton s_m with parameter β_m is assigned when $b_m = 1$, while zero (no soliton) is assigned when $b_m = 0$. If the transmitted bits from the two users are time multiplexed, then a sequence of bit pairs $\{b_1 b_2\}$ is formed. These bit pairs can take on values of $\{00,\ 01,\ 10,\ 11\}$ in which the first and the second digits of each word are from the first and second multiplexed users respectively. In the On-Off SADM system, these bit pairs can be represented such that for the sequence '00', no soliton is transmitted; for '01', a 0 followed by s_2; for '10', s_1 followed by a 0; and for '11', instead of transmitting the linear combination of s_1 and s_2, we propose to transmit the *composite* soliton of which s_1 and s_2 are the constituent solitons, i.e., to represent $\{11\}$, we transmit the signal $s_c(\tau)$, which can be expressed as:

$$s_c(\tau) = s_a(\tau, n, \phi_1, \phi_2)\Big|_{\frac{\phi_1 + n\sinh^{-1}\beta_1}{\beta_1} = \frac{\phi_2 + n\sinh^{-1}\beta_2}{\beta_2}} \tag{5.3}$$

where $s_a(\tau, n, \phi_1, \phi_2)$ is the general form of the interacting soliton as given in Eq. (3.4). It has been shown in Chapter 3 that the composite soliton is symmetric at the instant $\tau_0 = \frac{\phi_1 + n\sinh^{-1}\beta_1}{\beta_1}$. Assuming $\beta_1 > \beta_2$, it has also been shown that for a fixed β_2, a threshold, β_{th}, of β_1 exists such that for $\beta_1 < \beta_{th}$, the composite soliton will have twin peaks on either side of the symmetric point in its time characteristics. Since $s_c(\tau)$

is symmetric, the two peaks are equal in amplitude. Strictly, the duration of $s_c(\tau)$ is infinite, thus we measure its *essential* duration using the time interval containing 99% of the energy of the pulse,

$$\int_{-T_E/2}^{T_E/2} |s_c(\tau)|^2 d\tau = 0.99\ E_c \tag{5.4}$$

where $E_c = \int_{-\infty}^{\infty} s_c^2(\tau)d\tau$ is the total energy of the composite soilton. These integrals can be evaluated numerically as shown in Chapter 3.

We designate these signals representing {00, 01, 10, 11} by $\{x_0(t), x_1(t), x_2(t), x_3(t)\}$, i.e.,

$$x_0(t) = 0 \quad \text{for} \quad b_1b_2 = [0\ 0] \tag{5.5a}$$

$$x_1(t) = [0\ s_2(t)] \quad \text{for} \quad b_1b_2 = [0\ 1] \tag{5.5b}$$

$$x_2(t) = [s_1(t)\ 0] \quad \text{for} \quad b_1b_2 = [1\ 0] \tag{5.5c}$$

$$x_3(t) = s_c(t) \quad \text{for} \quad b_1b_2 = [1\ 1] \tag{5.5d}$$

where b_1b_2 denotes the transmitted bit pair with b_1 and b_2 being the bits from User 1 and User 2 respectively. For our two-user multiplexed system, the transmitter will store these four different waveforms and select the corresponding one to be transmitted.

5.1.2 Detection of On-Off Soliton Signals

For both single user and multiple user soliton system, we apply the amplitude threshold detection and the maximum likelihood detection methods on the signal that is transmitted. The two detection methods and the corresponding received signal alignment are discussed in this section and the system detection performance is studied in Sec. 5.3 and 5.4.

Amplitude Threshold Detection

The fact that a single information carrying soliton is characterized by its peak amplitude indicates the possibility of distinguishing different solitons according to their amplitudes. Thus, a receiver scheme can be derived by passing the received soliton signal and noise through a Toda circuit and detecting the peaks of the output solitons using a threshold decision. This is designated as amplitude threshold (AT) detection. Since the decision is made based on the peak value of the transmitted soliton signal, the timing of the detection is very important.

AT Detection for a Single-user System: For a single user, since the binary digits are represented by a soliton of parameter β or no soliton, we sample the signal at the output of the Toda circuit at the instant when the transmitted soliton is at its peak. Assuming that the transmitter and the receiver are synchronized such that the initial phase shift ϕ of the received soliton is known, from Eq. (5.1), the peak of the soliton at the output of the N-staged receiver Toda circuit occurs at $\tau_0 = (N \sinh^{-1} \beta + \phi)/\beta$. Thus, the sampling instant is at $t_0 = \tau_0 \sqrt{LC_0}$. The sample value of the received signal and noise is then compared with a threshold A_{th}, the choice of which will be discussed later in Section 5.3.

AT Detection of Multiplexed Soliton System: For a two-user multiplexed signal, there are four possible transmitted waveforms: one with no soliton, two with one soliton each (i.e., each waveform will have one peak) and one represented by a composite soliton. For the first three cases, AT detection is similar to that of detecting a single soliton. For the case when the composite soliton is transmitted, theoretically it can be received by a section of the cascaded Toda circuit resulting in the composite soliton being completely separated into its constituent parts which can then be detected separately by threshold detection as two single solitons. However, as we have seen in Chapter 3, the proper separation of a composite soliton depends on the relative amplitudes of the constituent solitons and may take hundreds of stages of the Toda

circuit. This causes unnecessary delay and complicates the implementation of the receiver. Hence we propose the following AT detection procedure for the composite soliton: it has been shown in Chapter 3 that twin peaks of equal amplitude on either side of the point of symmetry in a composite soliton will result if the constituent solitons have comparable parameters. Since AT detection of soliton signals are based on peak signal values, we will focus on the use of such composite solitons having twin peaks for representing a multiplexed bit pair of $\{11\}$. Thus, for receiving the two-user multiplexed signals, we will use an N-staged Toda circuit where N is stipulated to be a small number (say, < 5) which will cause very little change in the shape of the composite soliton at the output of the circuit compared to the received twin-peaked composite soiliton at the input. We can then apply a threshold at the instants of the twin peaks to distinguish the different signals transmitted. For AT detection at the twin peak instants, we need to align the transmitted pulses as follows:

Signal Alignment: For the four possible signals, we can align them such that at the output of the receiving N-staged Toda circuit, the peak of the soliton in $\{10\}$ occurs at the same instant as the first, whereas the peak of the soliton in $\{01\}$ occurs at the same instant as the second, of the twin peaks of the composite soliton representing $\{11\}$. The alignment of the waveforms can be realized by properly choosing their initial phase shifts at the transmitter. Let the parameters of two single solitons be respective β_1 and β_2 with $\beta_1 > \beta_2$. Then, we can form the composite soliton as indicated in Eq. (5.3). The 99%-energy duration of the composite soliton can be calculated numerically, and denoted by T_c as in Eq. (5.4). Assuming the transmission time of signals starts from 0, then, the transmitted composite soliton lies within the duration of 0 to T_c and the centre of this soliton is at $t_0 = T_c/2$. Therefore, to synthesize a composite soliton, we have to choose the initial phase shift parameters such that $\phi_{c1} = \beta_1 t_0$ and $\phi_{c2} = \beta_2 t_0$. Now, we need to find out the initial phase shifts of the two single solitons. To do that, for the given ϕ_{c1} and ϕ_{c2}, we first calculate the time

instants of the twin peaks of the composite soliton at the output of the N-staged Toda circuit by searching the numerical values of Eq. (5.3). Let these two time instants be denoted by t_1 and t_2 respectively. Then, the peak instants of the two single solitons s_1 and s_2 should also be t_1 and t_2 respectively at the output of the N-staged receiving Toda circuit. If we let the initial phase shifts of s_1 and s_2 at the transmitter be ϕ_{s1} and ϕ_{s2}, respectively, then, we have $\phi_{s1} = \beta_1 t_1 - N\sinh^{-1}\beta_1$ and $\phi_{s2} = \beta_2 t_2 - N\sinh^{-1}\beta_2$. In this thesis, this type of soliton alignment is designated SADM1, in which all the signals representing {00}, {01}, {10}, and {11} have their peaks properly aligned to be AT detected at the output of the N-stage Toda circuit. The two sets of ideally SADM1-aligned signals at the transmitter and at the output of the N-staged receiving Toda circuit are denoted respectively by $\{x_{1i}(t)\}$ and $\{\tilde{x}_{1i}(t)\}$, $i = 0, \cdots, 3$. Fig. 5.1 shows an example of a two-user soliton multiplexing system, in which the amplitudes of two single solitons are chosen to be respectively $V_0\beta_1^2 = 5$ and $V_0\beta_2^2 = 4$ and the receiving Toda circuit is chosen to have $N = 1$ stage. In Fig. 5.1, we show both $\{x_{1i}(t)\}$ and $\{\tilde{x}_{1i}(t)\}$, $i = 1, \cdots, 3$, the signals representing 01, 10 and 11 at the transmitter and at the receiver output. The duration of the composite soliton is calculated to be $T_c = 9.7707$ so that the initial phase shift of the two constituent solitons are respectively $\phi_{c1} = 3.4545$ and $\phi_{c2} = 3.0898$. The detection instants of the two peaks of the output signals are $t_1 = 3.01$ and $t_2 = 8.63$ respectively and the initial phase shifts of the two single solitons are calculated to be $\phi_{s1} = 1.4699$ and $\phi_{s2} = 4.8616$.

With additive white Gaussian noise (AWGN) during transmission, the output of the short ($N \leq 5$) receiving Toda circuit will no longer be the ideally SADM1-aligned signal, rather it can be approximated (see Chapter 4) by $\tilde{x}_{1i}(t) + \tilde{n}_{1i}(t)$, $i = 0, \cdots, 3$, where $\tilde{n}_{1i}(t)$ is the noise at the output of the receiver circuit when $x_{1i}(t)$ is transmitted. Our AT detector will make the decision of the transmitted signal by applying a threshold to the measured received signal at t_1 and t_2. Analysis of the performance

of the AT detector will be given in Section 5.4.

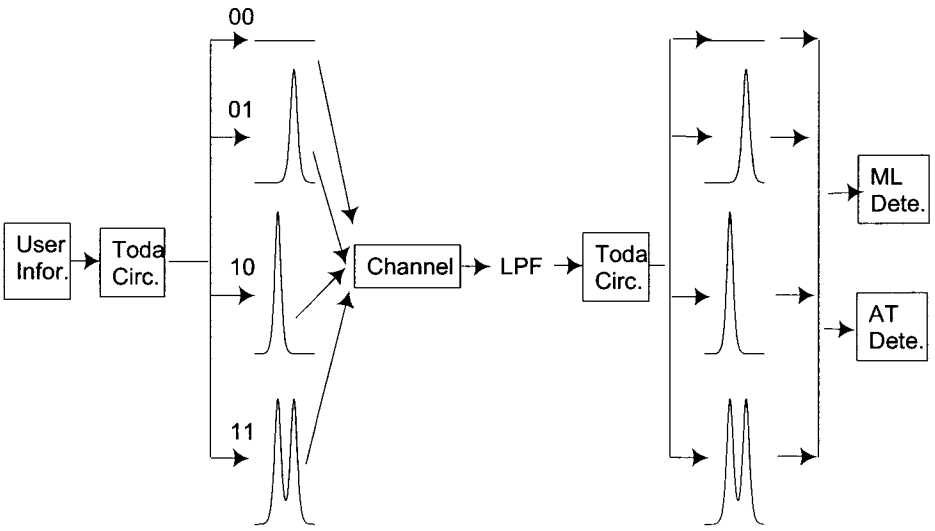

Figure 5.1: Soliton multiplexing system model

Maximum Likelihood Detection

While making use of the peak amplitudes of the solitons yields the AT detection, we can arrive at a detection scheme using the maximum likelihood (ML) principle [56] by examining the output waveform of the receiver Toda circuit and comparing it with the ideal transmitted signals. Unlike the amplitude detection scheme, peak alignment at the receiver output is not necessary for ML detection in a multiple user soliton system. However, for performing ML detection, while we should limit our detection period to the essential duration of the composite soliton of $x_3(t)$, we should make the distinction between $x_1(t)$ and $x_2(t)$ representing $\{10\}$ and $\{01\}$ respectively as large as

possible while assuring that the 99% energy durations of both are within the essential duration of the composite soliton. Since the detection period is limited to the range of $[0, T_c]$, we will then align $x_1(t)$ such that the essential duration of the single soliton starts at 0, whereas for $x_2(t)$, the essential duration of the single soliton finishes at T_c. This alignment of the soliton pulses at the transmitter is referred to as SADM2 and is denoted by $\{x_{2i}(t)\}$. With AWGN during transmission, the output of the short ($N \leq 5$) receiving Toda circuit will no longer be the ideally SADM2-aligned signal, rather it can be approximated by $\tilde{x}_{2i}(t)+\tilde{n}_{2i}(t)$, $i = 0, \cdots, 3$, where $\tilde{n}_{2i}(t)$ is the noise at the output of the receiver circuit when $x_{2i}(t)$ is transmitted. The received signal and noise is then compared with the expected signal pulse shapes, i.e., $\{\tilde{x}_{2i}(t)\}$, at the output of the Toda circuit and ML detection is applied by choosing the expected signal shape closest to the noisy received signal. An example of the SADM2 signal alignment system with the amplitude of two single solitons being 5 and 4 respectively is shown in Fig. 5.2. The 99%-energy durations of s_1, s_2 calculated from $3.14/\beta_1$ and $3.14/\beta_2$ are given by 4.4406, 4.9648, respectively. The essential time duration of s_c can be calculated from Eq. (5.4) and is given by 9.7707. Since s_c is in the duration of $[0, 9.7707]$, the initial phase shifts of the two constituent solitons are the same as those of SADM1. For SADM2 signal alignment, we allocate s_1 in the duration of $[0, 4.4406]$. Since the 99%-energy duration of s_2 is to finish at the instant 9.7707, we assign s_2 in the duration $[4.8059, 9.7707]$. Thus, at the transmitter, the initial phase shifts of the two single solitons s_1 and s_2 can be calculated as $\phi_{s1} = 4.4406\beta_1/2 = 1.57$ and $\phi_{s2} = (9.7707 + 4.8059)\beta_2/2 = 4.6095$ respectively. Fig. 5.2 shows the three SADM2-aligned nonzero waveforms at the transmitter and at the output of the receiver Toda circuit ($N = 1$). For comparison, we also show the corresponding three nonzero waveforms which are SADM1-aligned at the output of the Toda circuit. It can be seen from Fig. 5.2 that the differences in pulse positions between the transmitted signals and the signal at the output of the received Toda circuit are relatively small.

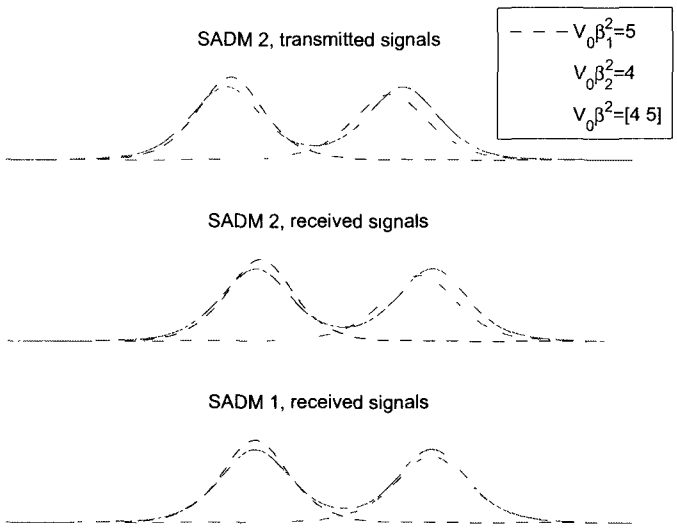

Figure 5.2: Transmitted and received signals in SADM

In this thesis, we apply AT detection to the peak (SADM1) aligned signals in noise. We also apply ML detection to both SADM1- and SADM2-aligned signals so that the results of two detection methods can be compared. For both detection methods, our receiver is equipped with an N-stage Toda circuit.

5.2 Efficiency of Soliton Data Transmission Systems

In Chapter 3, we have shown that the Time-bandwidth (T-B) product of a single soliton is a constant close to minimum value of 0.5, and that the T-B product of a composite soliton can be made close to the minimum value too if the parameters of constituent solitons are properly chosen. We now examine the T-B product of the transmission and multiplexing schemes of SADM1 and SADM2 proposed above and

compare it with well-established FDM system.

For an FDM system, Nyquist pulses are commonly used for transmission [22]. The spectral characteristics of the Nyquist pulse has a bandwidth of $(1+\alpha)B$ where α is the roll-off factor, and $B = 1/T_b$ with T_b being the bit period. Apart from the bandwidth of the pulse, the FDM signals also require a guard band between the adjacent pulse spectra. This guard band is usually taken as 20% of B. Therefore, for an FDM system having N multiplexed user signals, the total bandwidth required is given by $W = (1+\alpha+.2)BN$. For two users, an FDM system using a Nyquist pulse with $\alpha = .2$ has a T-B product of $T_bW = 2.8$ while that with $\alpha = .5$ has a T-B product of $T_bW = 3.4$.

For the two-user SADM system, the time-multiplexed signals are {00, 01, 10, 11} which are represented by combinations of zero and single solitons, or by a composite soliton which are aligned in two forms: SADM1 and SADM2 as described in the previous section. If we denote the essential durations and essential bandwidths of the single and composite solitons s_1, s_2, s_c by T_{E1}, T_{E2}, T_{Ec} and F_{E1}, F_{E2}, F_{Ec} respectively, then the required T-B product for either of the SADM systems is the product of the maximum duration and the maximum bandwidth required by four representing signals, i.e.,

$$\Pi_{DB} = \max(T_{E1}, T_{E2}, T_{Ec}) \times \max(F_{E1}, F_{E2}, F_{Ec}) \tag{5.6}$$

We carry out the calculation of the necessary SADM T-B product of Eq. (5.6) as follow: It has been shown in Chapter 3 that the essential duration and the essential bandwidth of a single soliton $s(\tau) = V_0\beta^2\text{sech}^2(\beta\tau)$ are given by $T_E = \frac{3.14}{\beta}$ and $F_E = 0.3931\beta$, respectively, and the T_{Ec} and F_{Ec} of a composite soliton whose constituents are s_1 and s_2 can be also readily evaluated numerically (Section 3.3). To study the variation of Π_{DB} in Eq. (5.6), we first fix the value of the controlling parameter β_1 for s_1 so that $V_0\beta_1^2$ is a constant and that the corresponding T_{E1} and F_{E1} can be calculated right away. We then vary the amplitude $V_0\beta_2^2$ of the other single soliton s_2. For the

fixed value of $V_0\beta_1^2$ and for each value of $V_0\beta_2^2$, we calculate the corresponding T_{E2} and F_{E2} of s_2 as well as numerically evaluating the corresponding essential duration and bandwidth of the composite soliton s_c of which s_1 and s_2 are the constituents. Selecting the largest product so obtained as in Eq. (5.6) yields the corresponding necessary SADM T-B product.

Fig. 5.3 shows the variation of Π_{DB} for values of $V_0\beta_1^2 = 1, 2, 3, 4, 5$. It can be observed that for any choice of $V_0\beta_1^2$, there are ample choices of $V_0\beta_2^2$ which will result in a T-B product substantially less than either of the values (2.8 or 3.4) for the FDM system. For example, for $V_0\beta_1^2 = 3$, we can choose $V_0\beta_2^2 = 6$ to achieve a minimum T-B product of 2.5 which is respectively 10.71% and 26.47% less than those of the FDM systems with 0.2 and 0.5 as guard-band factors. However, in choosing the constituent soliton parameters we have to consider the following: As discussed in the previous section, to maintain the twin-peak structure of the composite soliton for convenience in detection, it is important to choose the constituent solitons which are close in amplitude. However, it can be observed from Fig. 5.3 that for a fixed $V_0\beta_1^2$, the closer is $V_0\beta_2^2$ to $V_0\beta_1^2$, the larger is Π_{DB}. Also, as discussed in Section 5.1.1 above, as long as $\beta_2 < \beta_{th}$, then the resulting composite soliton will retain its twin peak structure. Thus, for a given $V_0\beta_1^2$, it appears that we should choose β_2 so that Π_{DB} is close to the minimum while maintaining $\beta_2 < \beta_{th}$. The values of β_{th} can be found in Fig. 3.8. We also notice that as β_2 moves away from the value of β_1, the T-B product decreases quickly to a minimum and gradually increases again. This is because as β_1 and β_2 become larger in their difference, the essential durations of the two solitons become larger, rendering the product of the maximum duration and maximum bandwidth larger. For example, we fix the amplitude of $V_0\beta_1^2$ to be 5. We observe from Fig. 5.3 that a minimum Π_{DB} of value 2.55 is attained when $V_0\beta_2^2 = 7.5$. Thus, $\beta_2/\beta_1 = \sqrt{1.5} = 1.2247$ for minimum T-B product. A glance at Fig. 3.8 gives $\beta_{th}/\beta_1 = 1.78$ for $V_0\beta_1^2 = 5$. Thus, our optimum choice of β_2 is well within the limit

to maintain a twin peak structure in the resulting composite soliton. On the other hand, we also note from Chapter 3 that the closer is β_2 to β_{th}, the closer together are the twin peaks in time. This may cause difficulty in the alignment of the signals for AT detection as described above. Therefore, for a fixed value of $V_0\beta_1^2$, a good choice of $V_0\beta_2^2$ has to take into consideration the factors of *keeping the T-B product low while maintaining the twin peak structure of the resulting composite soliton to be well separated and clearly distinguishable.*

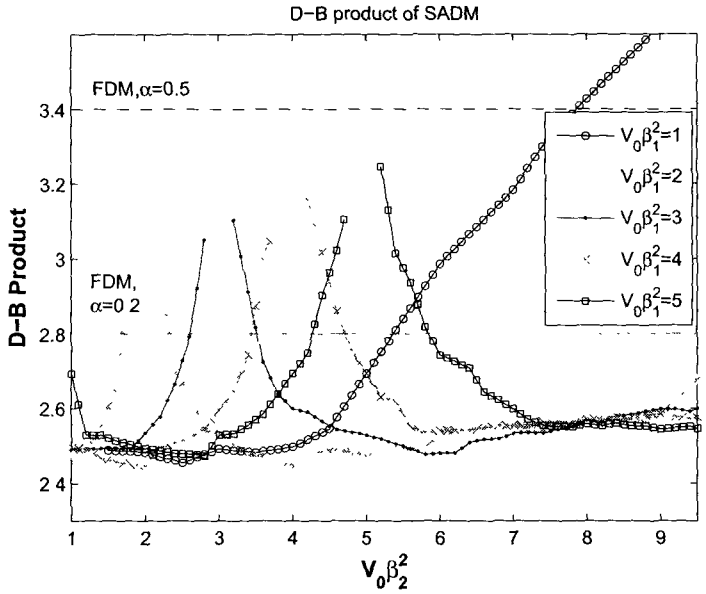

Figure 5.3: T-B product comparison

5.3 Detection Performance of the Single User System

In this section, we investigate the performance of the single user soliton communication system and apply both the AT and the ML detections to the transmitted

solitons. Since the Toda circuit is employed at the receiver, the output signal and noise properties developed in Chapter 4 will be applied in the development of the analysis.

In a single user soliton system, the transmitted signals are given by Eq. (5.2) and the received signal is expressed as $y(t) = x_i(t) + n(t), i = 0, 1$ with the input noise $n(t)$ being zero-mean white Gaussian having PSD $\mathcal{N}_0/2$. For a relatively short receiving Toda circuit, it has been shown in Chapter 4 that the output of the circuit can be written as

$$\tilde{y}(t) = \tilde{x}_i(t) + \tilde{n}_i(t) \qquad i = 0, 1 \tag{5.7}$$

where $\tilde{x}_i(t)$ is the output signal and $\tilde{n}_i(t)$ is the output noise of the receiving Toda circuit.

5.3.1 Amplitude Threshold Detection

AT detection is applied to the output signal $\tilde{y}(t)$ of the receiver N-staged Toda circuit at the instant t_0 where the peak of the soliton $s(t)$ is expected to occur. To apply the AT detection to the single user system, we set up a threshold to which the receiver circuit output sample $\psi_y = \tilde{y}(t_0)$ is compared. Assuming '0' and '1' are of equal probability, the optimum threshold can be determined numerically by the intersecting point of the probability density functions (PDF) $p(\psi_y|0)$ and $p(\psi_y|1)$ [43]. We have seen from Section 4.3 that if the input sample to a relatively short Toda circuit is Gaussian noise or a signal plus Gaussian noise, the output noise is approximately Gaussian with the mean being close to that of the input, while the variance may be reduced from that of the input noise. Therefore, for the output sample measured at t_0 in a single user system in which '0' is represented by no signal and '1' is represented by a soliton pulse of amplitude $V_0\beta^2$, a close approximation to the optimum threshold can be located at $A_{\text{th}} = V_0\beta^2/2$. For circuit input being either white Gaussian noise

$n(t)$ with zero-mean and PSD $\mathcal{N}_0/2$, or $s(t)$ (with amplitude $V_0\beta^2$) plus $n(t)$, the variance of the output noise at the sample instant can be calculated from Eq. (4.18). Denoting the output variance at the sample instant by σ_{01}^2 and σ_{02}^2 corresponding to user information 0 and 1 being transmitted, respectively. The probability of "false alarm" (a transmitted '0' mistaken as a '1') is given by

$$P_{FA} = \frac{1}{\sqrt{2\pi\sigma_{01}^2}} \int_{A_{\text{th}}}^{\infty} \exp(-\frac{\zeta^2}{2\sigma_{01}^2}) d\zeta = Q\left(\frac{\mathrm{V}_0\beta^2}{2\sqrt{\sigma_{01}^2}}\right)$$

where $Q(z) \triangleq \int_z^{\infty} \frac{1}{\sqrt{2\pi}} \exp\left(-\frac{\zeta^2}{2}\right) d\zeta$. The probability of "missing" (a transmitted '1' mistaken as a '0') is given by

$$P_M = \frac{1}{\sqrt{2\pi\sigma_{02}^2}} \int_{-\infty}^{A_{\text{th}}} \exp\left(-\frac{(\zeta - V_0\beta^2)^2}{2\sigma_{02}^2}\right) d\zeta = Q\left(\frac{V_0\beta^2 - A_{th}}{\sqrt{\sigma_{02}^2}}\right)$$

Assuming '0' and '1' are equally likely, the bit-error-rate (BER) of the single soliton system is

$$P_e = \frac{1}{2}(P_{FA} + P_M) = \frac{1}{2}\left[Q\left(\frac{\mathrm{V}_0\beta^2}{2\sqrt{\sigma_{01}^2}}\right) + Q\left(\frac{V_0\beta^2 - A_{\text{th}}}{\sqrt{\sigma_{02}^2}}\right)\right] \tag{5.8}$$

Effects of Low-Pass Filter

Instead of employing the Toda circuit directly at the receiver of the soliton system to receive the noise corrupted signal, we can apply a low-pass filter (LPF) before the Toda cirucit to filter out the noise outside the pass-band of the signal. The output of the LPF can then be passed into the Toda circuit. To examine the effects of the receiver LPF on the signal detection, we need to compare the bandwidth of the LPF with that of the Toda circuit. To allow the signal to pass through without distortion, while suppressing the noise component outside the frequency band of the signal, the bandwidth of the LPF should be chosen to be the same as that of the signal. We have shown that for a single soliton with parameter β, the single-sided bandwidth

containing 99% energy is given by

$$B_s = 0.3931\beta \tag{5.9}$$

Therefore, the bandwidth of the LPF employed in a single soliton system is also equal to B_s. It has been shown in Chapter 4 that based on Volterra series, the response of the Toda circuit at the early stages can be characterized by the linear, second-order and third-order transfer functions of the circuit, i.e., $H_1(f)$, $H_2(f_1, f_2)$ and $H_3(f_1, f_2, f_3)$. To examine qualitatively the effect of the Toda circuit on the input signal and noise, we ignore the higher order terms and treat the Toda circuit as a linear filter having transfer suction $H_1(f)$. The single-sided bandwidth of this approximated low-pass Toda circuit can be calculated as

$$B_{TC} = \int_0^\infty |H_1^2(f)| \mathrm{d}f \approx 0.334 \tag{5.10}$$

Comparing Eq. (5.9) and Eq. (5.10), we can expect that when $\beta < 0.8497$, the bandwidth of the LPF is smaller than that of the linearized Toda circuit, therefore, the effects of the LPF in filtering the noise outside the signal bandwidth will be dominant compared to that of the Toda circuit. The corresponding AT detection performance can then be approximated by:

$$P_{e1} = Q\left(\frac{\mathrm{V}_0\beta^2}{2\sqrt{2B_s\mathcal{N}_0/2}}\right) = Q\left(\frac{\mathrm{V}_0\beta^2}{2\sqrt{0.3931\beta\mathcal{N}_0}}\right) \tag{5.11}$$

With the approximation given in Eq. (5.10), the output noise variance of the Toda circuit, i.e., σ_{0i}^2, $i = 1, 2$ in Eq. (5.8) can be calculated as $\sigma_{01}^2 = \sigma_{02}^2 \approx 2 \times 0.334\mathcal{N}_0/2$, Eq. (5.8) can be rewritten as:

$$P_{e2} = Q\left(\frac{\mathrm{V}_0\beta^2}{2\sqrt{\sigma_{01}^2}}\right) = Q\left(\frac{\mathrm{V}_0\beta^2}{2\sqrt{\sigma_{02}^2}}\right) = Q\left(\frac{\mathrm{V}_0\beta^2}{2\sqrt{0.334\mathcal{N}_0}}\right) \tag{5.12}$$

Comparing Eq. (5.11) with Eq. (5.12), it can be seen that for single soliton system with low soliton amplitude, i.e., $\beta < 0.8497$, the receiver employing a LPF will give

better AT detection performance than the receiver employing only the Toda circuit. This will be verified in the section of numerical results. When $\beta > 0.8497$, the bandwidth of the LPF is larger than that of the approximated linear Toda circuit. In this case, the output of the LPF is re-filtered by the Toda circuit with smaller bandwidth, therefore, the effect of the LPF will be negligible comparing to that of the Toda circuit and the AT detection performance can be approximated by Eq. (5.8). This can also be observed in the section of numerical results.

5.3.2 ML Detection

In a single soliton system, $x_1(t) = 0$ or a single soliton $x_2(t) = s(t)$ is transmitted according to user information. The noise corrupted transmitted signal, i.e., $x_i(t) + n(t)$, $i = 1, 2$ is received by a Toda circuit, where $n(t)$ is the white Gaussian noise with zero mean and PSD $\mathcal{N}_0/2$. The output of the N-staged receiver Toda circuit is given by $\tilde{x}_i(t) + \tilde{n}_i(t)$. From Eq. (4.15) and Eq. (4.16), we obtain that $\tilde{x}_1(t) = 0$ and for short Toda circuits, $\tilde{x}_2(t)$ can be closely approximated by the soliton output at the Nth stage of the Toda circuit which, in turn, can be obtained directly by substituting the correct value of N into Eq. (5.1). From Fig. 4.11, it can be seen that within the pass-band, i.e., $|\omega| < 2$, the power spectral density (PSD) of the noise $\tilde{n}_1(t)$ can be approximated to be a constant, that is, the noise can be assumed to be white. From Fig. 4.14, we can see that the pass-band of the noise $\tilde{n}_2(t)$ is similar to that of the $\tilde{n}_1(t)$. While the PSD of $\tilde{n}_2(t)$ oscillates slightly within the pass-band, comparing Fig. 4.11 with Fig. 4.14, we can see that the difference is relatively small, therefore, we can approximate the PSD of $\tilde{n}_2(t)$ by that of $\tilde{n}_1(t)$. Focusing on the pass-band of the signal, the problem of the ML detection of the single user soliton system can now be formulated as a general ASK scheme with either zero or $\tilde{x}_2$ being transmitted and the additive noise being white. The PSD of the noise, denoted by $\eta_{\tilde{n}}$ can be numerically evaluated according to the procedure in Section 4.3.

The ML detection of the single user soliton system can be performed by a matched filter. The impulse response of the matched filter is chosen to be $g(t) = \tilde{x}_2(T_b - t)$, where T_b denotes the pulse duration of signal $\tilde{x}_2(t)$. The output of the matched filter is sampled at kT_b, $k = 1, 2 \cdots$ and compared with the threshold $E_s/2$, where E_s is the energy of the signal $\tilde{x}_2(T_b - t)$. Assuming '0' and '1' are equally likely in the system, the bit-error-rate (BER) of the single soliton system can be obtained as [43]

$$P_e = Q\left(\sqrt{\frac{E_s}{4\eta_{\tilde{n}}}}\right) \tag{5.13}$$

5.3.3 Numerical Experiments

In this section, we simulate the detection performance of a single user soliton system, in which the transmitted signal of the system is selected at random from either $x(t) = 0$ or $x(t) = s(t)$ where $s(t)$ is a soliton pulse of amplitude $V_0\beta^2$. The transmitted signal mixed with AWGN with zero-mean and PSD $\mathcal{N}_0/2$ is received by a Toda circuit. The signal-to-noise ratios (SNR) at the input of the receiver circuit is defined as

$$\rho = (E_s/2)/(\mathcal{N}_0/2) \tag{5.14}$$

The operation of the receiving Toda circuit is simulated numerically by the Runge-Kutta solution of Eq. (5.1). Both the AT and the ML detection methods are applied to the output of the Toda circuit. The error rates of the two detection methods are then measured.

Fig. 5.4 shows the BER performance at various SNR of the single-user soliton system transmitting zero or a soliton of amplitude $V_0\beta^2 = 4$ and employing either the AT detection or the ML detection at the receiver. The corresponding analytic probability of error expressed in Eq. (5.8) and Eq. (5.13) are plotted for comparison. It can be observed that for both the AT and ML detections, the theoretical results match the numerical results very well. It is also observed that as expected,

ML detection performs better than AT detection in general. We also plot the theoretical performance of binary amplitude shift keying (ASK) [22] signalling scheme. Comparing the ML detection performance for the soliton system with the theoretical ASK scheme, we can see that the performance are very close. This is because at the early stages, the nonlinearity of the Toda circuit is relatively small and the linear part dominates the characteristics of the Toda circuit, therefore, the circuit performs similar to a linear low-pass filter, which will not affect the ML detection performance of the system. Other simulation tests of the ML detection have also been carried out using soliton pulses of various amplitudes for transmission. Similar observations have been obtained, indicating that the ML detection performance of single soliton system is relatively independent of the soliton parameters.

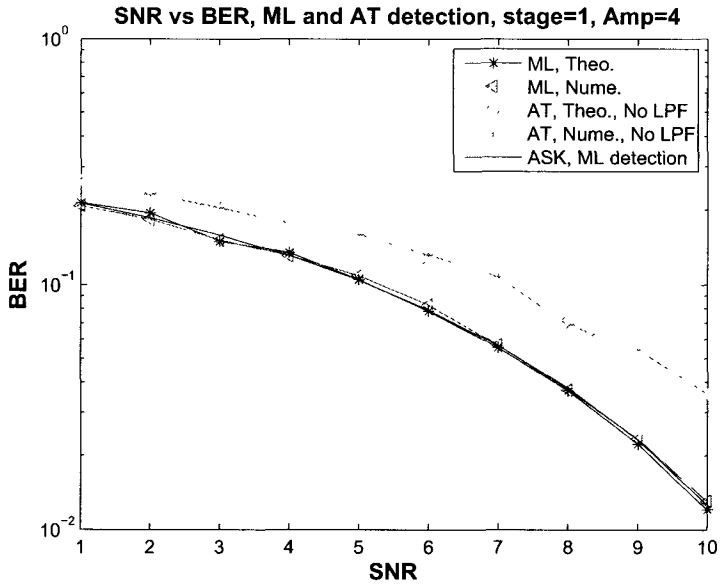

Figure 5.4: BER of single soliton system, ML and AT detection, $V_0\beta^2 = 4$, stage=1

While ML detection performance of the single soliton system is relatively independent of soliton parameters, we will show in the following that the AT detection

performance indeed varies with the parameter of soliton, furthermore, employing a LPF before the Toda circuit at the receiver may help to improve the AT detection performance.

We consider the AT detection performance of a single soliton system with the low, medium and high amplitudes, respectively. For comparison, we also show the theoretical AT detection performance of an ASK system having the baseband waveform being a single soliton with parameter β, a Raised Cosine pulse with the roll-off factor $\gamma_{rc} = 0.5$ and a Gaussian pulse. The time duration of the Raised Cosine and the Gaussian pulse is set to be the same as that of the single soliton, i.e. $T = 3.14/\beta$. The bandwidth of the Raised Cosine can then be calculated: $B_{rc} = (1 + \gamma_{rc})/2T$. The 99%-energy bandwidth of the Gaussian pulse can be calculated numerically. The Raised Cosine and the Gaussian pulse are both normalized such that the energy is the same as that of the single soliton. A LPF with the pass-band being the same as that of the corresponding transmitted signal is employed at the receiver of the ASK system. For the ASK system transmitting a single soliton with amplitude being $V_0\beta^2$, the performance of the AT detection with LPF is given by:

$$P_{es} = Q\left(\frac{V_0\beta^2}{2\sqrt{2(0.3931\beta)\mathcal{N}_0/2}}\right)$$

Assuming the amplitude of the Raised Cosine is A_{rc}, the performance of the corresponding AT detection with LPF can be calculated such that:

$$P_{eRC} = Q\left(\frac{A_{rc}}{2\sqrt{2B_{rc}\mathcal{N}_0/2}}\right)$$

Assuming the amplitude of the Gaussian pulse is A_g and assuming the bandwidth of the pulse is B_g, the performance of the corresponding AT detection with LPF can be calculated such that:

$$P_{eg} = Q\left(\frac{A_g}{2\sqrt{2B_g\mathcal{N}_0/2}}\right)$$

The ML detection performance of the ASK scheme is also shown for comparison.

Case 1: Low amplitude ($V_0\beta^2 = 1$)

Fig. 5.5 shows the AT detection performance of a single soliton system with low amplitude, e.g. $V_0\beta^2 = 1$. It can be seen from Fig. 5.5 that the performance of the soliton system employing the LPF is much better than that without LPF being employed. Comparing to the ASK scheme with LPF, we can see that the soliton system with LPF and Toda circuit performs similarly to that of the ASK scheme with soliton signal. This is because for input soliton with low amplitude, the bandwidth of the LPF is smaller than that of the approximated Toda circuit, therefore, the effects of the linear LPF dominates that of the Toda circuit.

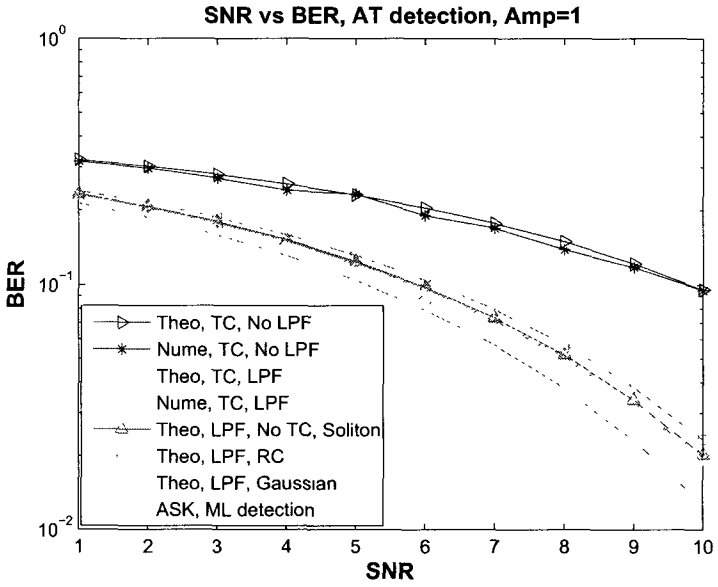

Figure 5.5: BER of single soliton system, AT detection, $V_0\beta^2 = 1$, stage=1

Case 2: Medium amplitude ($V_0\beta^2 = 4$)

Fig. 5.6 shows the AT detection performance of a single soliton system with medium amplitude, e.g. $V_0\beta^2 = 4$. It can be seen from Fig. 5.6 that similar to Case 1, the

performance of the soliton system employing the LPF is still better than that without LPF being employed, indicating the effects of the linear LPF still dominates the effects of the Toda circuit in this case. However, we can also see that the performance of the system employing only Toda circuit has improved comparing to that in Case 1, showing the filtering effects of the Toda circuit increases.

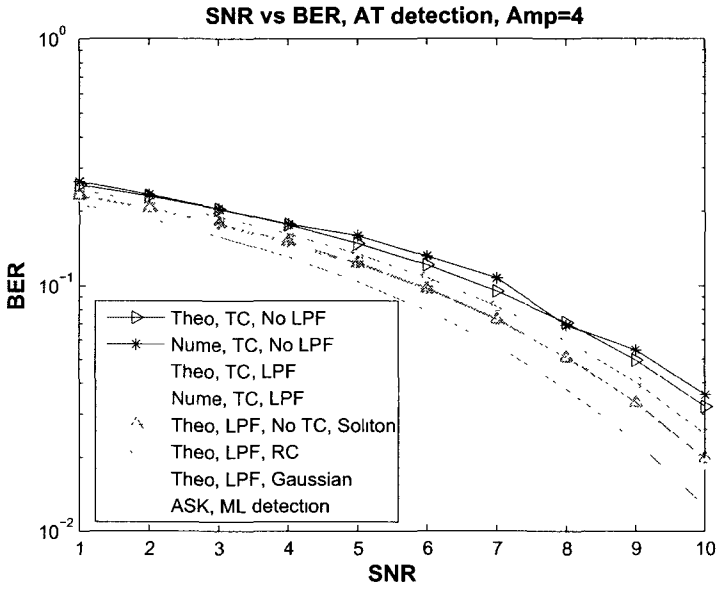

Figure 5.6: BER of single soliton system, AT detection, $V_0\beta^2 = 4$, stage=1

Case 3: High amplitude ($V_0\beta^2 = 10$)

Fig. 5.7 shows the AT detection performance of a single soliton system with high amplitude, e.g. $V_0\beta^2 = 10$. It can be seen from Fig. 5.7 that different from previous two cases, the performance of the soliton system employing the LPF is very close to that without LPF being employed. Comparing to the traditional ASK scheme using soliton (with LPF), we can see that the soliton system with Toda circuit performs much better. This is because for input soliton with high amplitude, the bandwidth of

the signal is larger than that of the approximated Toda circuit, therefore, the effects of the Toda circuit dominates that of the LPF and filters the received signal with smaller bandwidth and results in better detection performance. Comparing to the performance of the ML detection in Fig. 5.7, we can see that while ML performs better than AT detection in general, the difference can be relatively small. Therefore, in practice, the AT detection may be desirable for its simplicity in computation complexity.

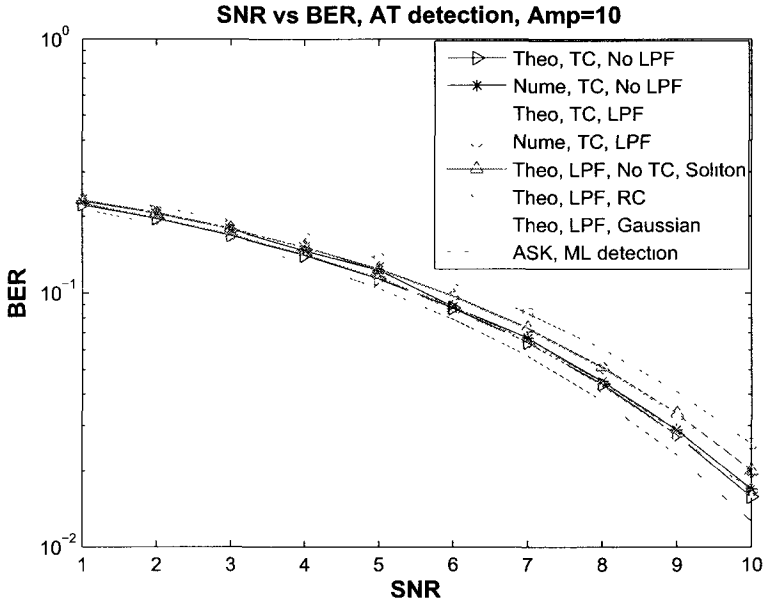

Figure 5.7: BER of single soliton system, AT detection, $V_0\beta^2 = 10$, stage=1

It can also be seen that comparing to traditional ASK scheme using Raised Cosine pulse or Gaussian pulse, the proposed soliton system with Toda circuit has better AT performance. This is partly due to the noise-filtering effects of the Toda circuit. Compared to the ASK scheme using Raised Cosine pulse, the better AT detection performance of the soliton system is also due to the small T-B product of the single soliton pulse.

We also try to examine the performance of the single soliton system being detected at late stages of the Toda circuit. However, we observe that both the ML detection and the AT detection will deteriorate when applied at late stages of the circuit. This is due to the distortion in the phase shift of the output signal caused by the input noise. Therefore, in this thesis, we only focus on the detection at the early stages of the Toda circuit.

5.4 Detection of Multiplexed Solitons

In this section, we investigate the detection performance of the two-user soliton multiplexing system employing the two different signal alignments SADM1 and SADM2. Both of the AT and ML detection methods are applied to the SADM1 signalling. We also apply the ML detection on SADM2. For a two-user multiplexed soliton system, the transmitted signals are given by Eqs. (5.5), where the signals $\{x_i(t)\}$ are aligned either as $\{x_{1i}(t)\}$ (SADM1 alignment) or $\{x_{2i}(t)\}$ (SADM2 alignment). We have also seen that for a two-user multiplexed signal, the two constituent soliton signals $s_1(t)$ and $s_2(t)$ should have comparable amplitudes. At the receiver, the transmitted signal is mixed with AWGN of zero mean and PSD $\mathcal{N}_0/2$. For a relatively short receiving Toda circuit, we have seen that the output can be written as

$$\tilde{y}(t) = \tilde{x}_{ki}(t) + \tilde{n}_{ki}(t) \qquad k = 1, 2, \qquad i = 0, \cdots, 3 \tag{5.15}$$

where $\tilde{x}_{ki}(t)$ and $\tilde{n}_{ki}(t)$ are respectively the output signal and noise of the receiving Toda circuit.

5.4.1 Amplitude Threshold Detection

As described in Sec. 5.1.2, we apply AT detection to a SADM1 aligned signal at the output of the receiver N-staged Toda circuit at t_1 and t_2 corresponding to the instants

at which the twin peaks of $s_c(t)$ are expected to occur. Two thresholds at each of the detection time instants t_1 and t_2 need to be chosen so that the receiver circuit output samples $\psi_{y1} = \tilde{y}(t_1)$ and $\psi_{y2} = \tilde{y}(t_2)$ are compared with these thresholds. The purpose of setting these thresholds at t_1 and t_2 is to detect if a single or composite soliton peak exists at each of these instants. It has been shown in Chapter 4 that at these peak instants, the output noise of a short Toda circuit with input being a combination of zero mean Gaussian noise of PSD $\mathcal{N}_0/2$ and a single (or composite) soliton of amplitude $V_0\beta^2$ (or A_c) will have an approximate mean of $V_0\beta^2$ (or A_c), and an approximate variance of calculated from Eq. (4.18). However, the peak value at t_1 may be $V_0\beta_1^2$ or A_c, and the peak value at t_2 may be $V_0\beta_2^2$ or A_c. These possible values have to be distinguished from 0. Thus, assuming the four bit-pairs are equally likely, a safe threshold for each of these instants is half the average of the two peak values, i.e.,

$$A_{\text{th1}} = \frac{1}{2}\left[(V_0\beta_1^2 + A_c)/2\right], \qquad A_{\text{th2}} = \frac{1}{2}\left[(V_0\beta_2^2 + A_c)/2\right] \tag{5.16}$$

where A_{th1} and A_{th2} are respectively the thresholds at t_1 and t_2 and A_c can be precalculated by numerically searching for the peak value in Eq. (3.5).

To analyze the BER performance for the two-user multiplexed soliton system with AT detection, we denote the variance of the output noise by σ_{ij}^2, $i = 0, 1, \cdots 3$, $j = 1, 2$, where index i corresponds to different signals, i.e., x_0, x_1, x_2, x_3 being transmitted, index j represents information of differen users been detected at time instants t_1 and t_2, respectively. Using the thresholds in Eq. (5.16) and following similar reasoning as the case for single user, the probability of false alarm and missing for User 1 in the multiplexed system are given by

$$\begin{aligned} P_{FA1} &= \frac{1}{2}\left[Q\left(\frac{A_{\text{th1}}}{\sqrt{\sigma_{01}^2}}\right) + Q\left(\frac{A_{\text{th1}}}{\sqrt{\sigma_{11}^2}}\right)\right] \\ P_{M1} &= \frac{1}{2}\left[Q\left(\frac{V_0\beta_1^2 - A_{\text{th1}}}{\sqrt{\sigma_{21}^2}}\right) + Q\left(\frac{A_c - A_{\text{th1}}}{\sqrt{\sigma_{31}^2}}\right)\right] \end{aligned}$$

Assuming '0' and '1' are equally likely for both users, the probability of error for User 1 is

$$\begin{aligned} P_{e1} &= P_{FA1} \cdot P(0) + P_{M1} \cdot P(1) \\ &= \frac{1}{4}\left[Q\left(\frac{A_{\text{th1}}}{\sqrt{\sigma_{01}}}\right) + Q\left(\frac{A_{\text{th1}}}{\sqrt{\sigma_{11}}}\right)\right] + \frac{1}{4}\left[Q\left(\frac{V_0\beta_1^2 - A_{\text{th1}}}{\sqrt{\sigma_{21}}}\right) + Q\left(\frac{A_c - A_{\text{th1}}}{\sqrt{\sigma_{31}}}\right)\right] \end{aligned} \tag{5.17}$$

Similarly, the probability of false alarm and missing for User 2 are given by

$$\begin{aligned} P_{FA2} &= \frac{1}{2}\left[Q\left(\frac{A_{\text{th2}}}{\sqrt{\sigma_{02}^2}}\right) + Q\left(\frac{A_{\text{th2}}}{\sqrt{\sigma_{22}^2}}\right)\right] \\ P_{M2} &= \frac{1}{2}\left[Q\left(\frac{V_0\beta_2^2 - A_{\text{th2}}}{\sqrt{\sigma_{12}^2}}\right) + Q\left(\frac{A_c - A_{\text{th2}}}{\sqrt{\sigma_{32}^2}}\right)\right] \end{aligned}$$

The probability of error for User 2 is

$$\begin{aligned} P_{e2} &= P_{FA2} \cdot P(0) + P_{M2} \cdot P(1) \\ &= \frac{1}{4}\left[Q\left(\frac{A_{\text{th2}}}{\sqrt{\sigma_{02}}}\right) + Q\left(\frac{A_{\text{th2}}}{\sqrt{\sigma_{22}}}\right)\right] + \frac{1}{4}\left[Q\left(\frac{V_0\beta_2^2 - A_{\text{th2}}}{\sqrt{\sigma_{12}}}\right) + Q\left(\frac{A_c - A_{\text{th2}}}{\sqrt{\sigma_{32}}}\right)\right] \end{aligned} \tag{5.18}$$

5.4.2 ML Detection

The output in Eq. (5.15) can be generically written as $\tilde{y}(t) = \tilde{x}_i(t) + \tilde{n}_i(t)$, $i = 0, \cdots, 3$ regardless of whether SADM1 or SADM2 alignment is used. It has been shown in Chapter 4 that for a short receiving Toda circuit, $\tilde{x}_i(t)$ is closely approximated by the ideal (no noise) output signal of the circuit for the corresponding input $x_i(t)$. For a given number of stages N, this ideal output can be obtained easily from Eq. (5.1) for an input involving single solitons ($x_1(t)$ and $x_2(t)$), and from Eq. (3.4) for an input involving a composite soliton ($x_3(t)$). These calculated quantities approximating $\tilde{x}_i(t)$ can now be used to facilitate the detection process. Similar to the ML detection of the single user system, we approximate the PSD of the output noise $\tilde{n}_i(t)$ for $i = 1$

to 3 by that of $\tilde{n}_0(t)$ and denote the PSD by $\eta_{\tilde{n}}$. Applying ML detection on $\tilde{y}(t)$, we obtain [43]

$$\hat{x}_i(t) = \arg\min_{\tilde{x}_i(t)} \left\{ \int_{t_{s1}}^{t_{s2}} [\tilde{y}(t) - \tilde{x}_i(t)]^2 \mathrm{d}t \right\} \qquad i = 0, 1, 2, 3 \tag{5.19}$$

To evaluate the probability of error of the SADM system, let ε_{ij} denote the event that $x_j(t)$ is detected while $x_i(t)$ is transmitted. For $i \neq j$, this constitutes an error. From Eq. (5.19), this occurs if $\int_{t_{s1}}^{t_{s2}} [\tilde{y}(t) - \tilde{x}_i(t)]^2 \mathrm{d}t > \int_{t_{s1}}^{t_{s2}} [\tilde{y}(t) - \tilde{x}_j(t)]^2 \mathrm{d}t$ which, by substituting $\tilde{y}$ in, can be written as

$$\int_{t_{s1}}^{t_{s2}} \tilde{n}_i(t)[\tilde{x}_j(t) - \tilde{x}_i(t)]\mathrm{d}t > \frac{1}{2} \int_{t_{s1}}^{t_{s2}} [\tilde{x}_i(t) - \tilde{x}_j(t)]^2 \, \mathrm{d}t \triangleq \frac{1}{2} D_{ij}^2 \tag{5.20}$$

We now define $\zeta_0 \triangleq \int_{t_{s1}}^{t_{s2}} \tilde{n}_i(t)[\tilde{x}_j(t) - \tilde{x}_i(t)]\mathrm{d}t$. Since $\tilde{n}_i(t)$ is approximately a zero-mean, stationary white Gaussian process ($E[\tilde{n}_i(\tau_1)\tilde{n}_i(\tau_2)] \approx \eta_{\tilde{n}}^2 \delta(\tau_1 - \tau_2)$), ζ_0 is a zero-mean Gaussian random variable with variance given by

$$\begin{aligned} \sigma_{\zeta_0}^2 &= \int_{t_{s1}}^{t_{s2}} \int_{t_{s1}}^{t_{s2}} E[\tilde{n}_i(\tau_1)\tilde{n}_i(\tau_2)] \\ &\quad \{\tilde{x}_j(\tau_1) - \tilde{x}_i(\tau_1)\}\{\tilde{x}_j(\tau_2) - \tilde{x}_i(\tau_2)\}\mathrm{d}\tau_1 \mathrm{d}\tau_2 = \eta_{\tilde{n}} D_{ij}^2 \end{aligned}$$

Thus, the probability of ε_{ij} occurring is the probability of ζ greater than $\frac{1}{2}D_{ij}^2$, i.e.,

$$P_{ij} = \frac{1}{\sqrt{2\pi\eta_{\tilde{n}} D_{ij}^2}} \int_{\frac{1}{2}D_{ij}^2}^{\infty} \exp\left(-\frac{\zeta^2}{2\eta_{\tilde{n}} D_{ij}^2}\right) d\zeta = Q\left(\sqrt{\frac{D_{ij}^2}{4\eta_{\tilde{n}}}}\right) \tag{5.21}$$

We note that due to the approximate properties of $\tilde{n}_i(t)$, $P_{ij} = P_{ji}$, Thus, by evaluating Eq. (5.21) for $i, j = 0, 1, 2, 3$, with $i \neq j$, we can obtain the probabilities of all the error events ε_{ij}. However, since the transmitted symbol from each user is represented by only one bit, not all the errors in the bit-pair constitute an error in a particular user's transmission. For example, ε_{01} represents that $b_1 b_2 = \{00\}$ is mistaken as $\hat{b}_1 \hat{b}_2 = \{01\}$; however, since the first bit $\hat{b}_1$ is the same as the transmitted first bit b_1, there is no error in the detected message for User 1. Hence, the events

that cause error in User 1 are: $\{\varepsilon_{02}, \varepsilon_{03}, \varepsilon_{12}, \varepsilon_{13}, \varepsilon_{20}, \varepsilon_{21}, \varepsilon_{30}, \varepsilon_{31}\}$, and those that cause error in User 2 are: $\{\varepsilon_{01}, \varepsilon_{03}, \varepsilon_{10}, \varepsilon_{12}, \varepsilon_{21}, \varepsilon_{23}, \varepsilon_{30}, \varepsilon_{32}\}$. From this, together with the assumption that the signals x_i are equiprobable, i.e. $P(x_i) = \frac{1}{4}$, the BER of User 1 and User 2 can be written as

$$P_{e1} = (P_{02} + P_{03} + P_{12} + P_{13} + P_{20} + P_{21} + P_{30} + P_{31})/4 \quad (5.22a)$$

$$P_{e2} = (P_{01} + P_{03} + P_{10} + P_{12} + P_{21} + P_{23} + P_{30} + P_{32})/4 \quad (5.22b)$$

The overall probability of error is given by $P_e = (P_{e1} + P_{e2})/2$. Note that with the corresponding substitutions of $\tilde{x}_{ki}(t)$ and $\tilde{n}_{ki}(t)$, the above analysis is applicable to both SADM1 and SADM2 signals.

5.4.3 Numerical Experiments

We now examine the performance of a two-user soliton multiplexing system by simulation and compare the experimental results to the above performance analysis. For the two-user SADM system, the transmitted signal is selected at random from $x_i(t)$, $i = 0, 1, 2, 3$ which are constructed using two constituent solitons of amplitudes $V_0\beta_1^2$ and $V_0\beta_2^2$ and are aligned either in SADM1 or in SADM2 format. The transmitted signal with AWGN (zero-mean, PSD $\mathcal{N}_0/2$) is received by a one-staged ($N = 1$) Toda circuit. The operation of the receiving Toda circuit is obtained numerically by the Runge-Kutta solution of the circuit. At the output of the receiving Toda circuit, we apply both the AT and the ML detections if the transmitted signal is SADM1-aligned, whereas only the ML detection is applied if it is a SADM2 signal. The simulation results of the performance of the two-user SADM system are compared with the theoretical evaluation of probabilities of error for both User 1 and User 2 in Eq. (5.17) and Eq. (5.18) for AT detection and in Eqs. (5.22a) and (5.22b) for ML detection.

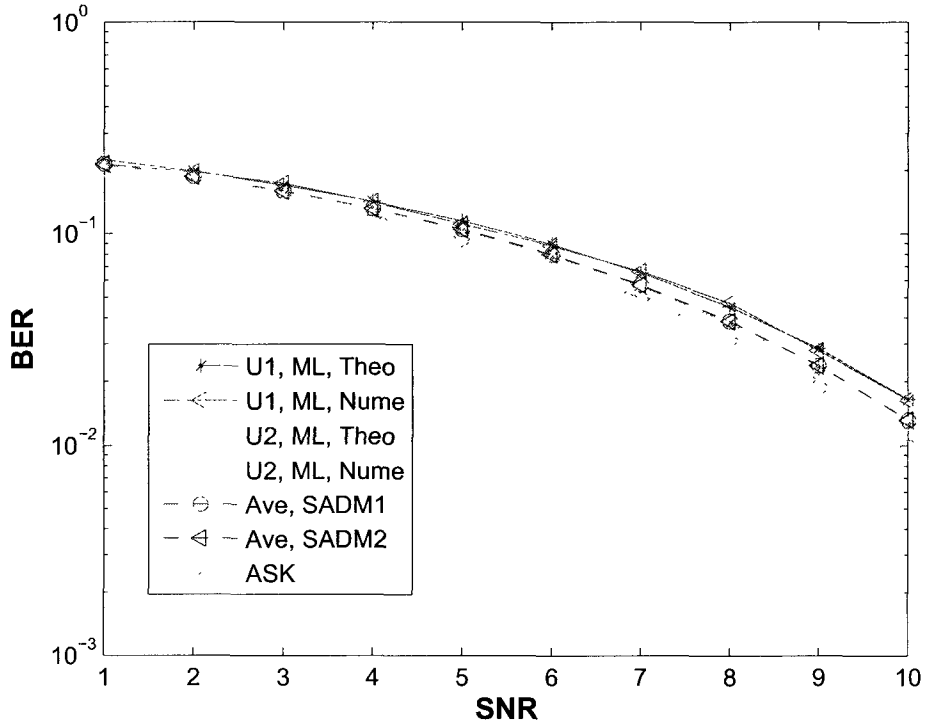

Figure 5.8: BER of the two users in a soliton multiplexing system – AT and ML detection

Fig. 5.8 shows the ML detection performance of the theoretical probabilities of error comparing to the BER obtained from the simulations of a SADM system using two constituent solitons of amplitudes $V_0\beta_1^2 = 5$ and $V_0\beta_2^2 = 4$, respectively, for User 1 and User 2. It can be clearly observed that the simulation results of each user agree very well with the theoretical evaluation. In Fig. 5.8, we also plot the average ML detection performance of two users of both SADM1- and SADM2-aligned systems together with the theoretical ML detection performance of the ASK scheme. As expected from Fig. 5.2, the ML detection performance of the SADM1- and SADM2-aligned systems are very close. The performance of both system is also very similar to that of the ASK scheme. This is because the nonlinearity of the Toda circuit

is relatively weak at the early stages, therefore the circuit simply exhibits low-pass characteristics. It can also be verified that the average ML detection performance of the two user soliton system varies very little with the parameters of the solitons.

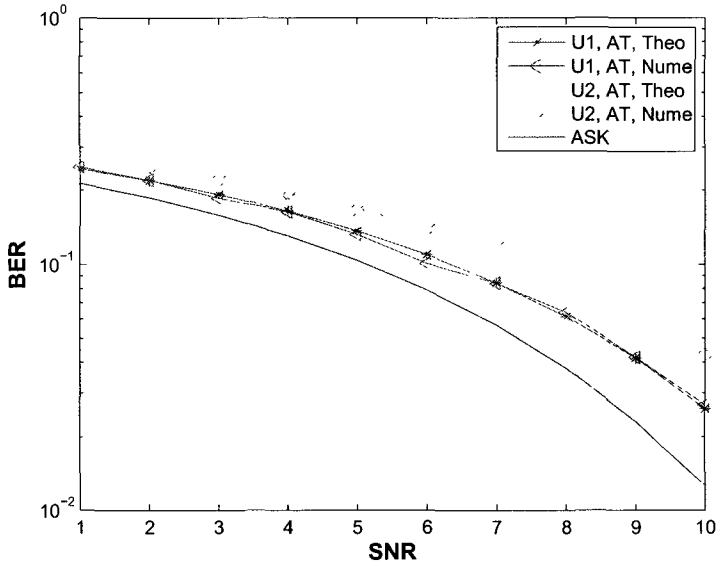

Figure 5.9: Average BER of soliton multiplexing system, stage=1

Fig. 5.9 shows the theoretical and numerical performance of the AT detection (without LPF) for a SADM1-aligned system using two constituent solitons of amplitudes $V_0\beta_1^2 = 5$ and $V_0\beta_2^2 = 4$, respectively. It can be clearly observed that the simulation results of each user agree very well with the theoretical evaluation. Similar to the single soliton system, the AT detection performance of a two user soliton system may be improved if we apply a LPF before the Toda circuit at the receiver. We compare the AT detection performance of the SADM1-aligned system with and without LPF for different set of soliton parameters. The results are shown in Fig. 5.10 to Fig. 5.12 with the amplitudes of the two constituent solitons being chosen as [2 1], [5 4] and [10 9], respectively. For comparison, the AT detection performance of a soliton

multiplexing system without Toda circuit at the receiver is also plotted together with the ML detection performance of the theoretical ASK scheme. It can be seen from Fig. 5.10 to Fig. 5.12 that the AT detection performance depends on the parameters of the soliton system. The system of high soliton amplitudes achieves better performance than that of low soliton amplitudes. For the amplitudes of two constituent solitons being 10 and 9, respectively, the AT detection performance of User 1 is very close to the ML detection performance of the ASK. While the performance of User 2 is worse than that of ASK, the difference is relatively small. Therefore, for its simplicity, the AT detection may be still desirable in practice. It can also be seen that similar to the single soliton system, for the soliton multiplexing system with low amplitudes, the LPF plays a dominant role compared to that of the Toda circuit. While for the soliton system with high amplitudes, the Toda circuit dominates the LPF and offers better performance compared to the system with no Toda circuit being employed.

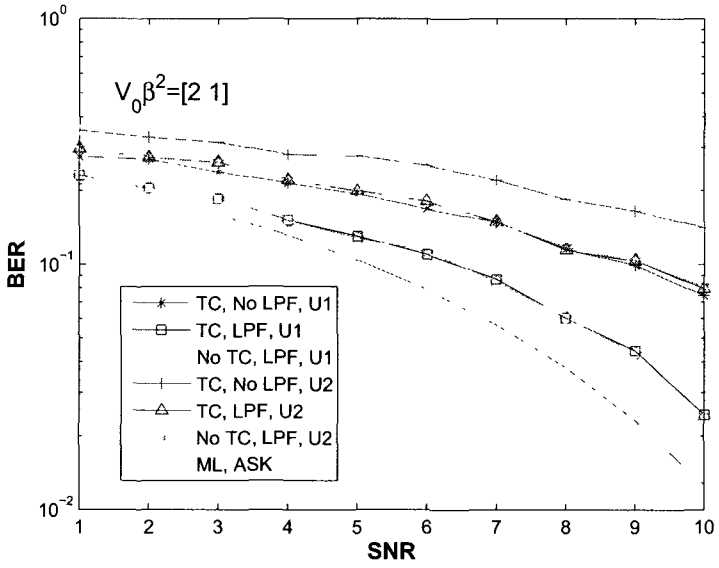

Figure 5.10: Average BER of soliton multiplexing system, stage=1

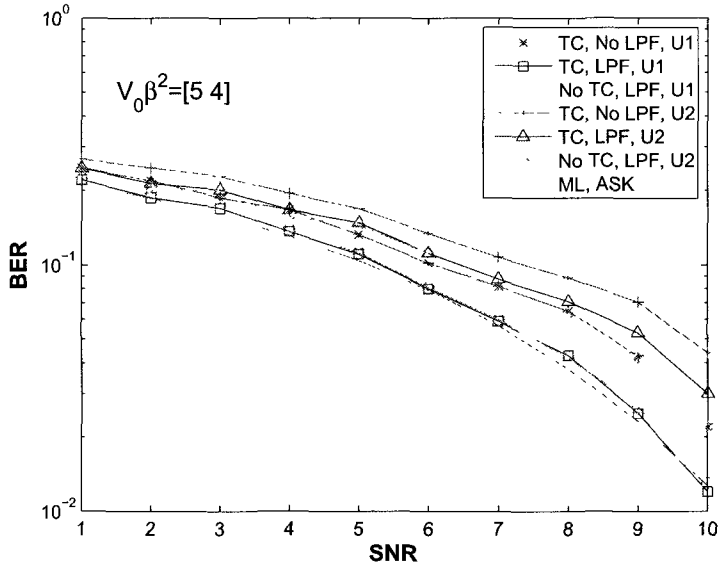

Figure 5.11: Average BER of soliton multiplexing system, stage=1

5.5 Timing Error of Single Soliton System

In previous sections of this chapter, we propose a soliton communication system in which the Toda circuit is applied at the receiver of the soliton system. We show that the multiplexing soliton system enjoys high bandwidth efficiency. The ML detection performance of the system is comparable to that of the traditional ASK scheme while the AT detection performance of the system is improved due to the noise filtering effects of the Toda circuit. In this section, a common problem in digital communication system, i.e., symbol synchronization will be examined. Focusing on ASK scheme, the detection performance of a single soliton system under timing error is studied. Aimed at examining the property of the soliton itself, in the single soliton ASK system studied in this section, we do not employ the Toda circuit at the receiver. The ASK signal is detected using ML method which is performed by a matched filter at the receiver. The system performance under the condition that there exists small

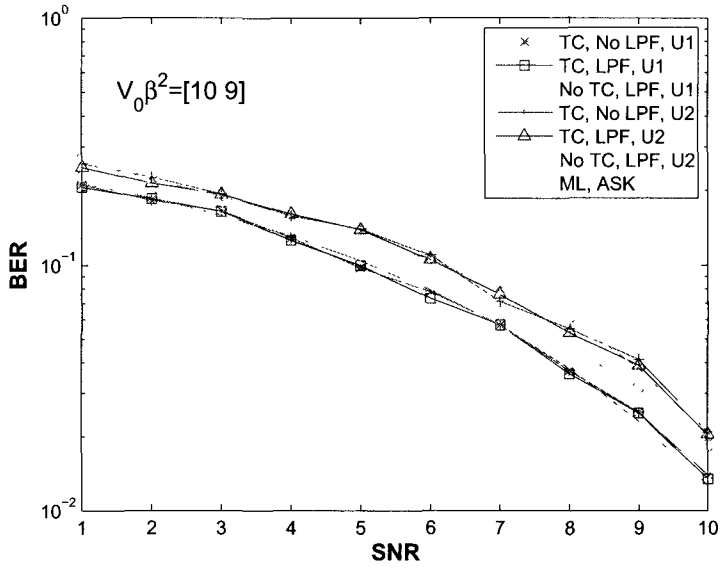

Figure 5.12: Average BER of soliton multiplexing system, stage=1

timing error of the matched filter is studied. For comparison, we also evaluate the detection performance of the ASK scheme using both the Raised Cosine pulse and the rectangular pulse under same timing error and compare the performance with that of the soliton system. We will show that in the case that there exists small timing error at the output of the matched filter, the ASK system employing the single soliton waveform is more robust in performance than those using Raised Cosine and rectangular waveforms.

Assuming the transmitted signal of the ASK scheme is given by $x_{a0}(t) = 0$ and $x_{a1}(t) = s_a(t)$, where $s_a(t)$ is the baseband waveform and assuming the channel noise $n_a(t)$ is white Gaussian with zero-mean, PSD $\mathcal{N}_0/2$, the received signal is therefore $y_a(t) = x_{ai}(t) + n_a(t)$, $i = 0, 1$. Denoting the time duration of the signal $s_a(t)$ by T_a, the impulse response of the matched filter is given by $h_a(t) = s_a(T_a - t)$. Denoting the energy of $s_a(t)$ by E_a, in the case of no timing-error, the output of the matched filter

is sampled at the multiples of the time instance T_a and compared with a threshold $E_a/2$. In practice, there may exist small timing error at the receiver, in this thesis, for simplicity, we only consider the case of constant timing error, i.e., the detection time instants shifts to $(k-1)T_a + (1-\gamma)T_a,\ k = 1, 2\cdots$, where $|\gamma| < 1$ is a small constant.

For the transmission of a '0', $y_a(t) = n_a(t)$. Denoting the transfer function of the matched filter as $H_a(f)$, the output sampling of the matched filter will be zero-mean, white Gaussian noise. The noise variance, denoted by σ_{ao}^2, is the same for different sampling time and is given by

$$\sigma_{a0}^2 = \frac{\mathcal{N}_0}{2}\int_{-\infty}^{\infty}|H_a(f)|^2 df = E_s \cdot \frac{\mathcal{N}_0}{2}$$

The probability of "false alarm" is given by

$$P_{FA} = \frac{1}{\sqrt{2\pi\sigma_{a0}^2}}\int_{\frac{E_s}{2}}^{\infty}\exp\Big(-\frac{\zeta^2}{2\sigma_{a0}^2}\Big)d\zeta = Q\left(\sqrt{\frac{E_s}{4\mathcal{N}_0/2}}\right)$$

For a '1' transmitted, $y_a(t) = s_a(t) + n_a(t)$. The output sampling of the matched filter includes both signal component and noise component. The noise component is the same as the case that a '0' is transmitted. The output of the signal component, denoted as E_1 is given by

$$E_1 = \int_0^{(1-\gamma)T_a} s_a(\tau)h_a\big((1-\gamma)T_a - \tau\big)d\tau$$

The probability of "missing" is given by

$$P_M = \frac{1}{\sqrt{2\pi\sigma_{a0}^2}}\int_{-\infty}^{E_s/2}\exp\left(-\frac{(\zeta - E_1)^2}{2\sigma_{a0}^2}\right)d\zeta = Q\left(\frac{E_1 - E_s/2}{\sqrt{E_s\mathcal{N}_0/2}}\right)$$

Assuming '0' and '1' are equally likely, the bit-error-rate (BER) of the single soliton system is

$$P_e = \frac{1}{2}\left(P_{FA} + P_M\right) = \frac{1}{2}Q\left(\sqrt{\frac{E_s}{4\mathcal{N}_0/2}}\right) + \frac{1}{2}Q\left(\frac{E_1 - E_s/2}{\sqrt{E_s\mathcal{N}_0/2}}\right) \qquad (5.23)$$

In Fig. 5.13 and Fig. 5.14, the BER performance at various SNR of the ASK scheme calculated from Eq. (5.23) are plotted with the receiver timing error being 0.1 and 0.2, respectively. The system waveform is chosen to be a single soliton with amplitude $V_0\beta^2 = 4$, a rectangular pulse and Raised Cosine pulse with roll-off factor being 0.5, respectively. The time duration containing 99% energy of the soliton is calculated and those of the rectangular pulse and the Raised Cosine pulse are chosen to be the same. The amplitudes of the Raised Cosine pulse and the rectangular pulse are normalized such that the energy of these pulses is the same as that of the soliton. It can be clearly seen from Fig. 5.13 and Fig. 5.14 that under small timing error, the ML detection performance of the ASK scheme employing single soliton is better than those of rectangular pulse and Raised Cosine pulse. This result indicates that the use of soliton pulse is more robust against receiver timing error.

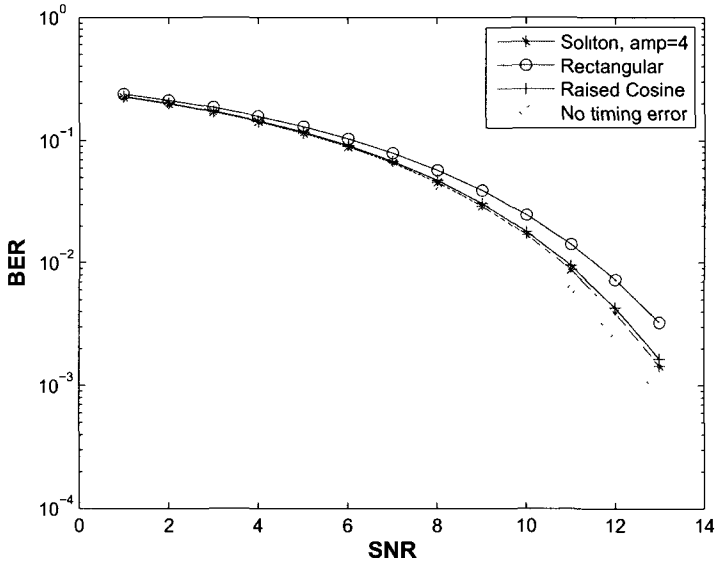

Figure 5.13: BER of ASK, timing error=0.1

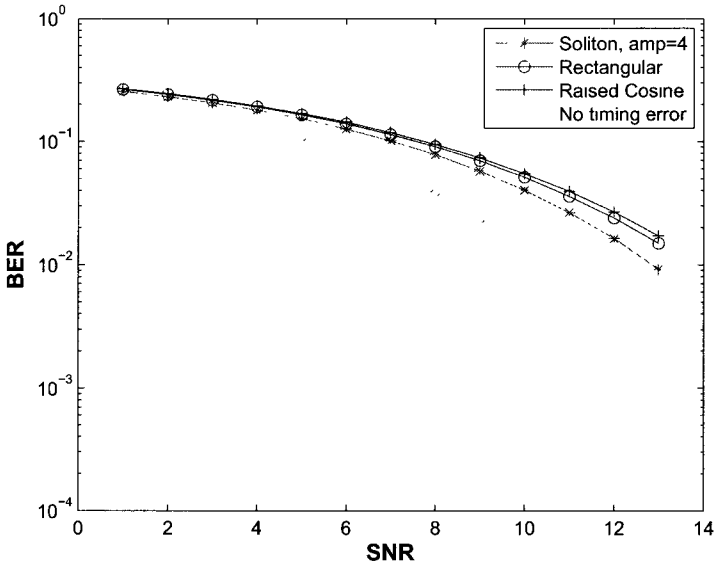

Figure 5.14: BER of ASK, timing error=0.2

5.6 Summary

In this chapter, we apply the Toda soliton to communication and propose a OOK soliton communication system for both the single-user and multi-user transmission. In a single user system, either a single soliton or zero is transmitted. In a two-user soliton multiplexing system, a single soliton with two different parameters, a composite soliton or zero is transmitted. The communication channel model is chosen to be the common AWGN channel. At the receiver, the Toda circuit is employed as a nonlinear noise filter. We propose the AT and the ML methods of detecting the transmitted solitons. The detection performance of these systems have been analyzed and compared with the traditional ASK scheme. We show that while being detected at the early stages of the Toda circuit, the ML detection performance of the soliton system is similar to the ML detection of the traditional ASK scheme. The AT detection performance of the soliton system with large amplitude is better than that

of the traditional ASK scheme using soliton pulse, Raised-Cosine pulse and Gaussian pulse. The better AT detection performance is due to the high bandwidth efficiency of the soliton signal and the noise-filtering effects of the Toda circuit. While the performance of the ML detection is better than that of the AT detection in general, the difference is relatively small (as shown in Fig. 5.7 and Fig. 5.12), therefore, the AT detection is still desirable due to its simplicity.

We also study the bandwidth efficiency of the soliton multiplexing system and show that it is superior to the traditional FDM system using Raised-Cosine pulse. The property of high bandwidth efficiency of the soliton system results in a high capacity in transmission comparing to the FDM system. Focusing on the property of single soliton, we also study the ML detection performance of a traditional ASK scheme with receiver timing error. We show that compared to other pulses, such as Raised-Cosine and Rectangular pulse, soliton pulse is more robust against receiver timing error.

Chapter 6

Toda Circuit Sensitivity to Imperfection

From the governing equation of the LC Toda circuit, i.e., Eq. (3.2) and the corresponding soliton equation, i.e., Eq. (3.3), it can be seen that the parameters of the inductor and the linear capacitor of the Toda circuit also characterize the properties of the circuit solution soliton. As a matter of fact, it can be shown that to support a stable propagation of the Toda soliton, the parameters of the inductor and the linear capacitor of the Toda circuit should be exactly the same as those of the input soliton. In the case that there exist parameter difference between the Toda circuit and the input soliton, the soliton might be distorted while propagating along the circuit. The problem of the Toda circuit response to an input soliton with mismatched parameters is designated as a mismatch problem.

The mismatch problem is of particular importance in the soliton communication system we propose in Chapter 5. In both the single user and the multiple user soliton communication systems, single solitons and composite solitons of particular parameters are stored at the transmitter and are transmitted according to the user information. At the receiver, Toda circuit with same parameters of the inductor and

the linear capacitor are employed as a nonlinear receiver allowing the propagation of the solitons while suppressing the channel noise. In practice, due to the imperfect circuit technology or inaccurate knowledge of the circuit information, the parameters of the receiver Toda circuit may not be exactly the same as those of the transmitted soliton signals. In this case, a mismatch problem may occur when the transmitted solitons are received by Toda circuit. In this chapter, we study the mismatched Toda circuit response to the input single solitons and analyze the distortion effects of the input signals. The discussion can be extended to the case of circuit input being a composite soliton in a straightforward manner.

To study the response problem of the mismatched Toda circuit analytically, we need to solve the initial problem of the governing equation of the circuit, which turns out to be inadmissible due to the nonlinearity and discreteness of the governing equation. In Section 2.3, we have shown that Toda lattice equation can be approximated by KdV equation under the condition of small input. In this chapter, we will show that the governing equation of the perturbed Toda circuit can be approximated by a perturbed KdV equation. The response problem of the perturbed Toda circuit can then be approximated by the propagation problem of the perturbed KdV equation, which can then be solved through some known results. The results calculated from the KdV approximation are compared with those obtained from the Runge-Kutta method. The amplitude distortion of the input soliton is also verified through the inverse scattering transform of the Toda lattice in Section 6.2. In Section 6.3, we numerically examine the effects of the receiver mismatched Toda circuit on the performance of both single user and multiplexing soliton system.

6.1 Korteweg-de Vries Equation Approximation

The governing equation of the LC Toda circuit with the inductance of the inductor being L and the capacitance of the linear capacitor being C_0 is given in Eq. (3.2). For convenience, it is rewritten in the following:

$$\frac{\mathrm{d}^2}{\mathrm{d}t^2}\log\left(1+\frac{V_n(t)}{V_0}\right)=\frac{V_{n-1}(t)-2V_n(t)+V_{n+1}(t)}{LC_0V_0} \tag{6.1}$$

Assuming there exists inductor mismatch in the Toda circuit, and the inductance of the inductor is perturbed into $L(1+\epsilon_L)$, where ϵ_L is the parameter denoting mismatch effects and is assumed to be small in this thesis, i.e., $|\epsilon_L| \ll 1$. Substituting L by $L(1+\epsilon_L)$ in Eq. (6.1), we obtain the governing equation of the perturbed Toda circuit:

$$\frac{\mathrm{d}^2}{\mathrm{d}t^2}\log\left(1+\frac{V_n(t)}{V_0}\right)=\frac{V_{n-1}(t)-2V_n(t)+V_{n+1}(t)}{(1+\epsilon)LC_0V_0} \tag{6.2}$$

Similarly, in the case of linear capacitor perturbation, C_0 in Eq. (3.2) should be replaced by the perturbed capacitance of the capacitor, i.e., $C_0(1+\epsilon_C)$, we obtain the governing equation of the perturbed Toda circuit:

$$\frac{\mathrm{d}^2}{\mathrm{d}t^2}\log\left(1+\frac{V_n(t)}{V_0}\right)=\frac{V_{n-1}(t)-2V_n(t)+V_{n+1}(t)}{(1+\epsilon_C)LC_0V_0} \tag{6.3}$$

It is clear that for $\epsilon_L = \epsilon_C$, Eq. (6.3) turns out to be in the same form as Eq. (6.2). This indicates the inductor perturbation and the linear capacitor perturbation result in equivalent effects of the Toda circuit, therefore, the same circuit response to input solitons can be expected. For convenience, we only consider the case of inductor perturbation in this thesis. The results obtained in this thesis can also be extended to both problems of inductor and linear capacitor perturbation.

As we have mentioned before, it may be mathematically intractable to analyze the problem of the perturbed Toda circuit response to input signal directly. In the following, we show that the perturbed Toda circuit can be approximated by the

perturbed KdV equation, the general propagation problem of which has been treated [26, 27].

Rewriting Eq. (6.2) as

$$\frac{\mathrm{d}^2}{\mathrm{d}t^2}\log\left(1+\frac{V_n(t)}{V_0}\right)=\frac{V_{n-1}(t)-2V_n(t)+V_{n+1}(t)}{LC_0V_0}-\frac{\epsilon}{1+\epsilon}\frac{V_{n-1}(t)-2V_n(t)+V_{n+1}(t)}{LC_0V_0} \tag{6.4}$$

Similar to the approximation of the Toda lattice equation by the KdV equation in Section 2.3, under the condition of small $\frac{V_n(t)}{V_0}$, we make following approximation:

$$\log\big(1+\frac{V_n(t)}{V_0}\big)\approx\frac{V_n}{V_0}-\frac{V_n^2}{2V_0^2} \tag{6.5}$$

Denoting $v_m=\frac{1}{\sqrt{LC_0}}$, $u=-\frac{2}{vV_0}V$, where v is an arbitrary parameter, we apply the Gardner-Morikawa transformation [8]:

$$\xi=v^{1/2}(n-v_mt),\quad \tau=v^{3/2}\frac{v_m}{24}t \tag{6.6}$$

Substituting Eq. (6.5) and (6.6) into Eq. (6.4) and choosing $v=1$, we obtain:

$$u_\tau-6uu_\xi+u_{\xi\xi\xi}=\frac{\epsilon}{1+\epsilon}u_{\xi\xi\xi} \tag{6.7}$$

The r.h.s. of Eq. (6.7) can be regarded as a perturbation term, therefore, we call Eq. (6.7) a perturbed KdV equation. Recalling the original KdV equation as shown in Eq. (2.22):

$$u_\tau-6uu_\xi+u_{\xi\xi\xi}=0 \tag{6.8}$$

It has been shown in previous chapters that the single soliton solution of Eq. (6.8) can be expressed as:

$$u(\tau,\xi)=-2\beta^2\mathrm{sech}^2(\beta\xi-4\beta^3\tau) \tag{6.9}$$

where, the parameter β characterizes the amplitude and the width of the KdV soliton and does not change with time, i.e.

$$\frac{d\beta}{d\tau}=0 \tag{6.10}$$

It clear from Eq. (6.9) that the displacement parameter ξ corresponding to the peak occurrence of the soliton is:

$$\xi = 4\beta^2\tau \tag{6.11}$$

Substituting Eq. (6.6) into Eq. (6.9), we obtain:

$$V_n(t) = V_0\beta^2\text{sech}^2((\beta + \frac{\beta^3}{6})t/\sqrt{LC_0} - \beta n) \tag{6.12}$$

Under the condition of small soliton amplitude, i.e. small β, Eq. (6.12) approximates the Toda soliton as expressed in Eq. (3.3) very well. It is shown in [1, 26, 27] that under small perturbation, if the input to a system characterized by Eq. (6.7) is a single soliton, the output can still be approximated by a single soliton or a waveform similar to a single soliton and for a general perturbed KdV equation:

$$u_\tau - 6uu_\xi + u_{\xi\xi\xi} = \epsilon R(u)$$

where $R(u)$ is a given function of $u(\tau, \xi)$, it has been proved in [27] that both the amplitude parameter β and the phase shift ξ vary with time and the dynamics can be characterized as:

$$\frac{d\beta}{d\tau} = -\frac{\epsilon}{4\beta}\int_{-\infty}^{\infty} R(u_s)\text{sech}^2(a)da \tag{6.13}$$

$$\frac{d\xi}{d\tau} = 4\beta^2 - \frac{\epsilon}{4\beta^3}\int_{-\infty}^{\infty} R(u_s)(a + \frac{1}{2}\sinh 2a)\text{sech}^2(a)da \tag{6.14}$$

where u_0 is the soliton solution of Eq. (6.8), i.e., $u_0 = -2\beta^2\text{sech}^2(\beta\xi - 4\beta^3\tau)$ and $a = \beta\xi - 4\beta^3\tau$. Applying the above results in the propagation problem of Eq. (6.7), we replace ϵ in Eq. (6.13) and (6.14) by $\frac{\epsilon_L}{1+\epsilon_L}$ and substitute

$$R(u_0) = u_{\xi\xi\xi} = -16\beta^5\text{sech}^2(a)\tanh(a) + 16\beta^5\text{sech}^4(a)\tanh(a) \tag{6.15}$$

into Eq. (6.13) and (6.14). As the integration function of Eq. (6.13) is a odd function and the integral is in a symmetric region, we obtain

$$\frac{d\beta}{d\tau} = 0 \tag{6.16}$$

$$\begin{aligned}\frac{d\xi}{d\tau} &= 4\beta^2 - \frac{\epsilon}{(1+\epsilon)4\beta^3} \\ &\quad \cdot \int_{-\infty}^{\infty} (-16\beta^5 \mathrm{sech}^2(a)\tanh(a) + 16\beta^5 \mathrm{sech}^4(a)\tanh(a))(a + \frac{1}{2}\sinh 2a)\mathrm{sech}^2(a)da \\ &= 4\beta^2 + \frac{16\beta^5\epsilon}{(1+\epsilon)4\beta^3} \int_{-\infty}^{\infty} (a\mathrm{sech}^4(a)\tanh(a) + \frac{1}{2}\mathrm{sech}^4(a)\tanh(a)\sinh(2a) \\ &\quad -a\mathrm{sech}^6(a)\tanh(a) - \frac{1}{2}\sinh(2a)\mathrm{sech}^6(a)\tanh(a))da \\ &= 4\beta^2(1 + \frac{\epsilon}{1+\epsilon}\frac{5}{9}) \end{aligned} \tag{6.17}$$

Eq. (6.16) shows that the amplitude parameter β of the input soliton is a constant and does not change with time. This result indicates that under small circuit perturbation, the amplitude of the soliton is maintained at a constant. From Eq. (6.17), we obtain

$$\xi(\tau) = 4\beta^2(1 + \frac{\epsilon}{1+\epsilon}\frac{5}{9})\tau + \xi_0 \tag{6.18}$$

where the integration constant ξ_0 is the initial phase shift and can be assumed to be zero. Comparing Eq. (6.18) with Eq. (6.11) and taking into account of Eq. (6.6), we obtain the expression of the perturbed Toda soliton:

$$V_n(t) = V_0\beta^2\mathrm{sech}^2\big((\beta + \frac{\beta^3}{6})t/\sqrt{LC_0} - \beta n - \beta\frac{\epsilon}{1+\epsilon}\frac{5}{9}t\big) \tag{6.19}$$

Comparing Eq. (6.19) with Eq. (6.12), it is clear that the perturbation of the Toda circuit affects both the width and the propagation velocity of the soliton. The time instance corresponding to the peak of the output soliton at stage n can be obtained by setting the term inside sech function to be zero and is shown to be:

$$t_n = \frac{\beta n\sqrt{LC_0}}{(\beta + \frac{\beta^3}{6} - \beta\frac{5\epsilon}{9(1+\epsilon)})} \tag{6.20}$$

For input soliton with small amplitude, we can approximate $\beta + \frac{\beta^3}{6} \approx \beta$, therefore, t_n can be rewritten as:

$$t_n = \frac{n\sqrt{LC_0}}{1 - \frac{5\epsilon}{9(1+\epsilon)}} \tag{6.21}$$

Comparing Eq. (6.21) to t_n in Eq. (6.12), i.e., $t_n \approx n\sqrt{LC_0}$, it is clear that positive ϵ_L in the perturbed Toda circuit results in a larger t_n, which causes a slower propagation rate of the soliton.

We now apply Runge-Kutta method described in Section 4.2 to examine the response problem of the perturbed Toda circuit by replacing L in Eq. (4.14) with $L(1+\epsilon)$. Without loss of generality, we assume $L = 1$ and $C_0 = 1$. Setting the input as a single soliton with amplitude 1 and 4 respectively to the perturbed Toda circuit, circuit outputs at different stages are examined and the corresponding amplitude of the output soliton is plotted in Fig. 6.1. The perturbation coefficient ϵ is chosen to be 0.1 and 0.5. It is clear that for small input amplitude, i.e. $V_0\beta^2 = 1$ and small ϵ, i.e. $\epsilon = 0.1$, the perturbation of the soliton amplitude is very small. Denote the parameter of the output soliton by β', we obtain $\frac{\beta'}{\beta} \approx 0.99$. This result is agreement with that of Eq. (6.16). Three other curves in Fig. 6.1 show that for larger input amplitude or larger ϵ, the difference between input amplitude and output amplitude is more obvious and cannot be ignored. This indicates that the approximation of the perturbed Toda circuit by the perturbed KdV equation in these cases results in larger error. It is also observed from Fig. 6.1 that for positive ϵ, the output amplitude of soliton is less than that of input soliton. In Fig. 6.2, we plot the amplitudes of the output soliton for circuit mismatch coefficient ϵ being negative. The amplitude parameters of Fig. 6.2 are chosen to be the same as those of Fig. 6.1. It can be seen that negative ϵ will result in the increase of the amplitude of the output soliton. The analysis of the response of the mismatched circuit with positive or negative ϵ is similar, therefore, in the following, we only focus on the case for positive ϵ for simplicity. That for circuit with negative ϵ can be extended in a straightforward manner.

For the amplitude of the input soliton being 1, the time instants corresponding to the peak of the output soliton at different circuit stages are plotted in Fig. 6.3. The theoretical results calculated from Eq. (6.20) are compared with numerical results.

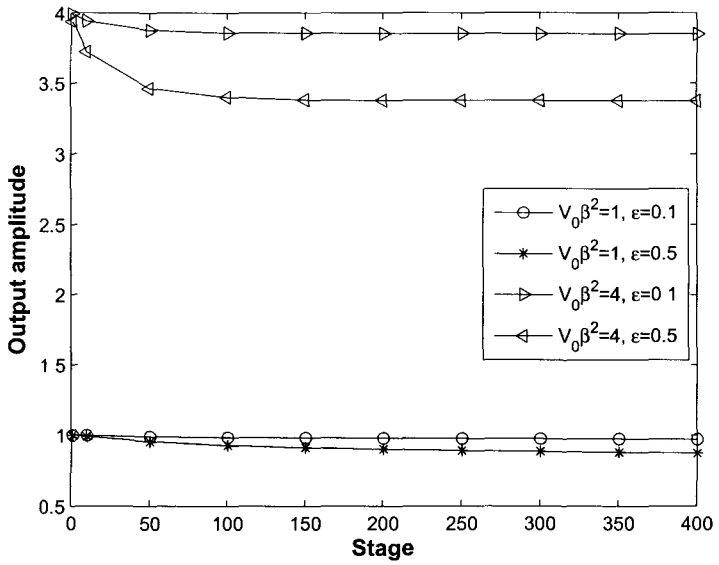

Figure 6.1: Amplitude of output soliton versus circuit stage, positive ϵ

The perturbation coefficient ϵ is chosen to be 0.1 and 0.5. It can be seen from Fig. 6.3 that the theoretical results match the numerical ones perfectly even for large ϵ, i.e. $\epsilon = 0.5$, indicating the KdV approximation is very accurate in calculating phase shift for small input amplitude. Fig. 6.4 is similar to Fig. 6.3 except the amplitude of the input soliton is chosen to be 4. It can be seen from Fig. 6.4 that there is small discrepancy between the theoretical results and those of numerical ones for both $\epsilon = 0.1$ and $\epsilon = 0.5$. However, the difference is relatively small especially for $\epsilon = 0.1$, indicating that the KdV approximation method can still be feasible.

Fig. 6.1 to 6.4 show that the approximation of the perturbed Toda circuit by the perturbed KdV equation is relatively accurate for the amplitude of the input soliton being relatively small and for small circuit mismatch coefficient. However, for large amplitude of the input soliton or large circuit mismatch coefficient, it introduces relatively large error especially in calculating the amplitude of the output soliton. From Fig. 6.1, we observe that with the increase of the circuit stage, the amplitude of

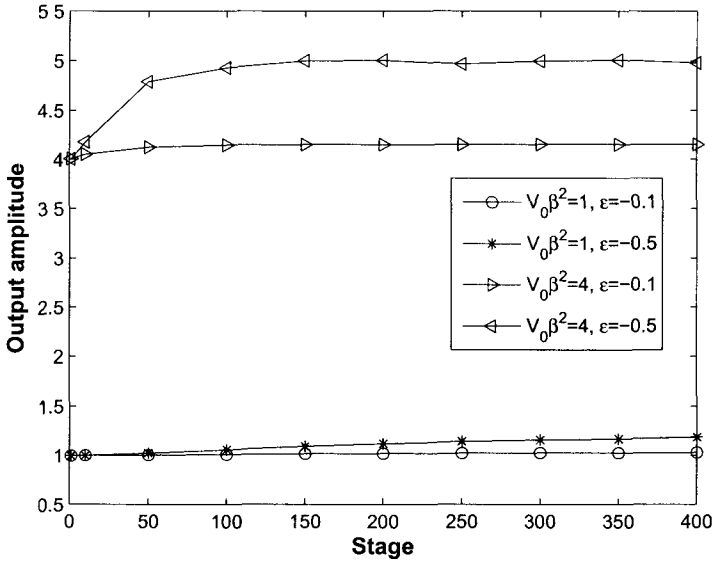

Figure 6.2: Amplitude of output soliton versus circuit stage, negative ϵ

the output soliton decreases at the early stages and then settles to a stable value at late circuit stages. This observation can be verified by calculating circuit response to input soliton with other amplitudes. Applying this result in examining the dependence of the amplitude parameter of the output soliton on circuit mismatch coefficient ϵ, we focus on the parameter of the output soliton at late circuit stages, i.e., the output waveform has become relatively stable, in which case, for a given input soliton and a mismatch coefficient ϵ, a stable value is capable to characterize the amplitude parameter of the output soliton. Furthermore, for the amplitudes of the output soliton at early stages, this stable value can be applied as a lower bound (for positive ϵ). Denoting the parameter of the output soliton as $\tilde{\beta}$ and applying polynomial fitting, we obtain,

$$\beta - \tilde{\beta} \approx 0.2\epsilon\beta^{1.35} \tag{6.22}$$

In Fig. 6.5, $(\beta - \tilde{\beta})/\beta^{1.35}$ versus ϵ is plotted for two different amplitude of input soliton, i.e. $V_0\beta^2 = 1$ and $V_0\beta^2 = 4$. Two curves in Fig. 6.5 is very close to a straight

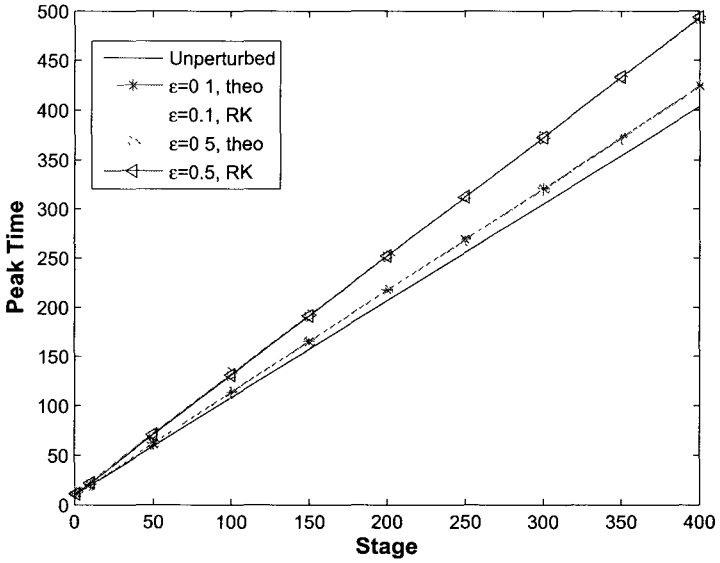

Figure 6.3: Peak occurrence time instance vs stage, $V_0\beta^2 = 1$

line with slope being 0.2, showing the fitting error in Eq. (6.22) is negligible.

6.2 Applying Inverse Scattering Method

We have mentioned in Section 2.2.2 that the inverse scattering method of the Toda lattice solves the initial problem of the lattice. In particularly, given the circuit states at all the stages n at time $t = 0$, it can calculate the circuit states in all the stages at any time $t = t_0$. For the problem of the Toda circuit response to an input signal, we are interested in the propagation characteristics of the signal from the early stages to the later stages of the circuit, that is, given the time domain characteristics of the circuit input at stage $n = 0$, to calculate the time domain characteristics of the circuit output at any later stages $n = n_0$. This problem is different as the one which the IST of the Toda circuit addresses, however, from Eq. (3.3), we can clearly observe the duality of the time variable t and the circuit stage n, therefore, we can

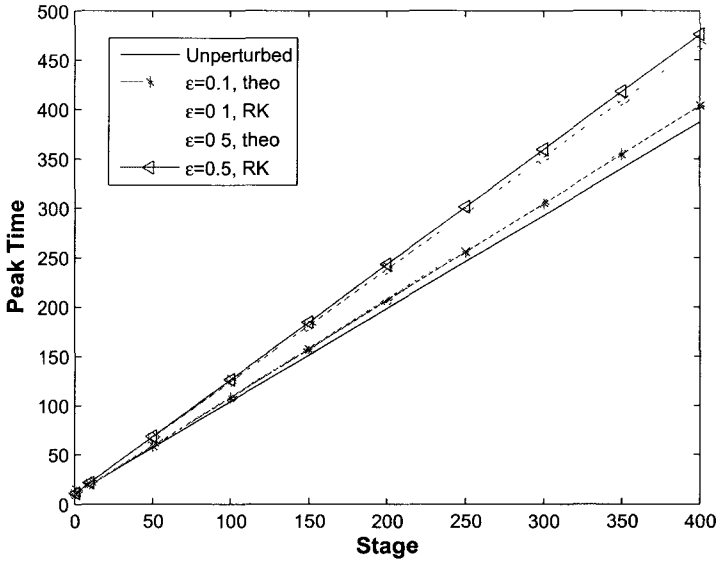

Figure 6.4: Peak occurrence time instance vs stage, $V_0\beta^2 = 4$

still expect some qualitative results by applying IST. This intuition is verified by numerical results.

The mismatch problem of the LC Toda circuit is similar to the initial problem of a Toda spring lattice with the mass of particles perturbed. The perturbed Toda lattice is also called impure lattice. Most research works on the solution of an impure Toda lattice focus on the lattice with the mass of only one particle being impure, that is, the mass of all the particles in the lattice were 1 except the zeroth particle, of which the mass perturbed into $\frac{1}{1+\epsilon}$, i.e.

$$m_n = \begin{cases} \frac{1}{1+\epsilon}, & n = 0 \\ 1, & \text{otherwise} \end{cases}$$

where ϵ is a small number. The problem has been studied numerically in [35, 37, 57] and also analytically in [61], where the author applied the perturbation theory [34] and the IST of the Toda lattice and proved that under the assumption that the perturbed lattice response to a single soliton is still a soliton, the amplitude parameter β of the

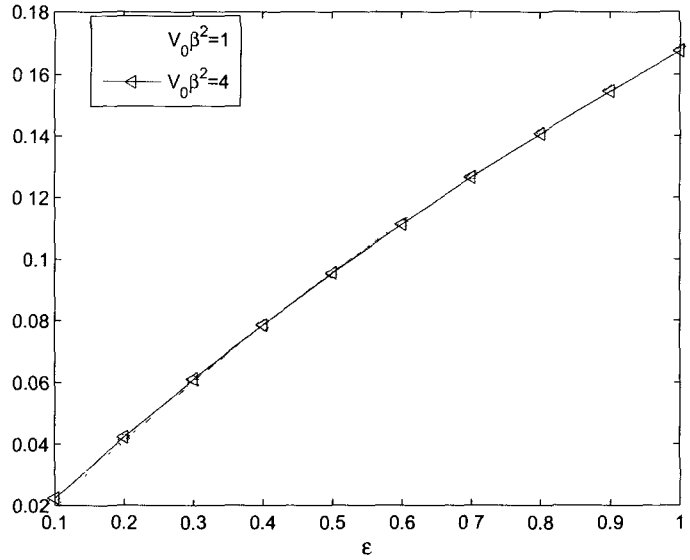

Figure 6.5: $(\beta - \tilde{\beta})/\beta^{1.35}$ vs ϵ

output soliton can be expressed as

$$\beta = \beta_0 + \epsilon C + \bigcirc(\epsilon^2) \tag{6.23}$$

where β_0 is the amplitude parameter of the input soliton and C is a constant independent on time. Eq. (6.23) shows for small ϵ, the variation of input and output soliton is linear in ϵ.

The Toda spring lattice with the mass of one particle being perturbed corresponded to a perturbed LC Toda circuit with one inductor or one linear capacitor perturbation. In our mismatch problem, we assume all the inductors are perturbed from L_0 to $L_0(1+\epsilon)$ or all the linear capacitors are perturbed from C_0 to $C_0(1+\epsilon)$. In this section, we will show that as a generalized scenario of the problem treated in [61], the result obtained in [61] can indeed be generalized to our problem. Following a common practice of the IST of Toda lattice [53], we define

$$a(n) = \frac{1}{2}\exp\left(-\frac{Q_n - Q_{n-1}}{2}\right), \quad b(n) = -\frac{L_0(1+\epsilon)\dot{Q}_n}{2} \tag{6.24}$$

where $\dot{Q}_n$ denotes the derivative of Q_n over time. The time derivative of $a(n)$ and $b(n)$ can be calculated and expressed as following:

$$\dot{a}(n) = \frac{[b(n+1) - b(n)]a(n)}{(1+\epsilon)} \approx (1-\epsilon)[b(n+1) - b(n)]a(n)$$

$$\dot{b}(n) = 2[a(n)^2 - a(n-1)^2]$$

Introducing linear operator $\mathcal{L}$, we rewrite Eqs. (6.24) into the form of linear Schrödinger equation:

$$\mathcal{L}Q(n) = a(n-1)Q(n-1) + a(n)Q(n+1) + b(n)Q(n)$$

We denote the continuous eigenvalue of $\mathcal{L}$ by $\lambda = \frac{z+z^{-1}}{2}$ and corresponding to each eigenvalue , we have two eigen-function $\phi(n,z)$ and $\psi(n,z)$. Using a similar procedure as in [61], we can show that $\alpha(z)$, the reciprocal of which is defined as the transmission coefficient, changes with time as follows:

$$\begin{aligned}\dot{\alpha}(z) &= \frac{2\epsilon}{z - z^{-1}} \sum_{n=-\infty}^{\infty} b(n)[a(n-1)\{\phi(n-1,z)\psi(n,z) + \phi(n,z)\psi(n-1,z)\} \\ &\quad -a(n)\{\phi(n,z)\psi(n+1,z) + \phi(n+1,z)\psi(n,z)\}] \qquad (6.25)\end{aligned}$$

It has been proved [16] that for un-perturbed Toda lattice $\dot{\alpha}(z) = 0$, which indicates the time invariance of soliton parameter and explains the stable propagation of soliton along the lattice. It is difficult to see how the parameters of the solitons are perturbed from Eq. (6.25). In the following, we will examine the perturbation of the rth discrete eigenvalues of $\mathcal{L}$, which corresponds to the soliton solutions of the system.

Denoting the discrete eigenvalue of $\mathcal{L}$ by $\lambda_r = \frac{z_r + z_r^{-1}}{2}$, $r = 1..N$, where N is the total number of solitons in the lattice, from Eq. (6.25) we can obtain the time variation of z_r:

$$\dot{z}_r = \frac{4\epsilon z_r}{z_r - z_r^{-1}} C_r^2 \sum_{n=-\infty}^{\infty} b(n)[a(n-1)\phi_r(n-1) - a(n)\phi_r(n+1)]\phi_r(n) \qquad (6.26)$$

We assume that only one Toda soliton exists in the lattice, i.e., $r = N = 1$. Now, we introduce C_1 and $A(n)$ such that

$$C_1 = [\sum_{n=-\infty}^{\infty} \phi_1^2(n)]^{-1}$$

$$A(n) = -\frac{(z_1^2 - 1)^{1/2}}{Dz_1^n + (Dz_1^n)^{-1}}$$

where $D = (z_1^2 - 1)^{1/2}/C_1$. We can rewrite Eq. (6.26) as

$$\begin{aligned} \dot{z}_1 &= \frac{4\epsilon z_1}{z_1 - z_1^{-1}} C_1^2 \sum_{n=-\infty}^{\infty} b(n)[a(n-1)\phi_r(n-1) - a(n)\phi_r(n+1)]\phi_1(n) \\ &= \frac{\epsilon}{z_1} \sum_{n=-\infty}^{\infty} \left[A(n-1)^3 A(n) - A(n-1)A(n)^3\right] \end{aligned} \tag{6.27}$$

Applying perturbation theory [34], we express

$$z_1 = z_1^{(0)} + \epsilon z_1^{(1)} + \epsilon^2 z_1^{(2)} + \cdots \tag{6.28}$$

where $z_1^{(0)}$ is the parameter of the original soliton and $\dot{z}_1^{(0)} = 0$. Differentiating Eq. (6.28) and combining Eq. (6.27), we obtain

$$\dot{z}_1 = \epsilon \dot{z}_1^{(1)} + \epsilon^2 \dot{z}_1^{(2)} + \cdots = \frac{\epsilon}{z_1} \sum_{n=-\infty}^{\infty} \left[A(n-1)^3 A(n) - A(n-1)A(n)^3\right] \tag{6.29}$$

Applying first order perturbation theory, we obtain,

$$z_1^{(1)} = \int \frac{\epsilon}{z_1} \sum_{n=-\infty}^{\infty} \left[A(n-1)^3 A(n) - A(n-1)A(n)^3\right] dt \tag{6.30}$$

The variation of $z_1^{(1)}$ in time can then be calculated as:

$$z_1^{(1)}(\infty) - z_1^{(1)}(-\infty) = \frac{1}{z_1} \sum_{n=-\infty}^{\infty} \int_{-\infty}^{\infty} \left[A(n-1)^3 A(n) - A(n-1)A(n)^3\right] dt \tag{6.31}$$

It can be proved that (see Appendix B)

$$z_1^{(1)}(\infty) - z_1^{(1)}(-\infty) = 0$$

Eq. (6.32) shows after the soliton becomes stable, i.e., $t \rightarrow \infty$, it is first order perturbation coefficient does not change. Denoting $z_1^{(1)}(\infty) = z_1^{(1)}(-\infty) = C_1$, where C_1 is a constant, we obtain,

$$z_1 = z_1^{(0)} + \epsilon C_1 + \bigcirc(\epsilon^2) \tag{6.32}$$

Under the assumption of small ϵ and recall the relation of z_1 and β [53], we can obtain

$$\beta = \beta_0^{(0)} + \epsilon C_2 + \bigcirc(\epsilon^2) \tag{6.33}$$

where C_2 is a constant. Eq. (6.33) clearly shows that the result presented in [61] can be generalized to the Toda lattice with any continuous section of perturbations. In the other words, increasing the number of the perturbed components in the Toda lattice does not change the form of the dependence of the soliton parameters on the perturbation coefficient. The difference of β and β_0 is still linear in ϵ, this result is agreement with that of Eq. (6.22).

6.3 Detection Performance of Soliton System with Mismatched Circuit

In previous sections, we study the response of mismatched Toda circuit to input soliton, and show that the circuit mismatch may result in the distortion of input soliton. In this section, we numerically examine the effects of the receiver mismatched Toda circuit on the performance of both single user and multiplexing soliton system. For the single user soliton system, the amplitude of the single soliton is chosen to be 10. For the multiplexing soliton system, the amplitudes of the two constituent solitons are chosen to be 10 and 9, respectively. Two cases of Toda circuit mismatch are considered, i.e., $\epsilon = 0.1$ and $\epsilon = 0.5$, respectively.

In Fig. 6.6 and Fig. 6.7, we show the AT and ML detection performance of a single soliton system with a mismatched Toda circuit. For comparison, we also show

the corresponding detection performance of the system with perfectly matched Toda circuit. It can be seen that as expected, for a small mismatch, i.e., $\epsilon = 0.1$, the performance deterioration of the soliton system with mismatched Toda circuit is relatively small. However, for a larger mismatch coefficient, i.e., $\epsilon = 0.5$, the deterioration of both AT and ML detection performance is obvious compared to the system with matched Toda circuit.

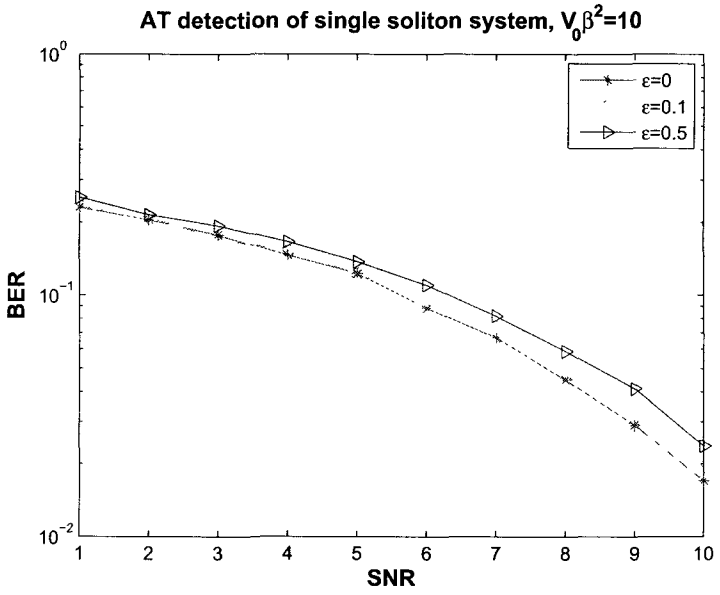

Figure 6.6: BER of single soliton system with mismatched circuit, AT detection, $V_0\beta^2 = 10$

Fig. 6.8 and Fig. 6.9 show the AT and ML detection performance of a multiplexing soliton system with a mismatched Toda circuit. It can be seen from the figures that similar to the single soliton system, the effects of the slightly mismatched Toda circuit on the system detection performance is relatively small, while the mismatched Toda circuit with a larger mismatch coefficient causes severe deterioration in the system performance. It can be verified that the results obtained for both single and multiplexing soliton system can be extended to the systems with solitons of other

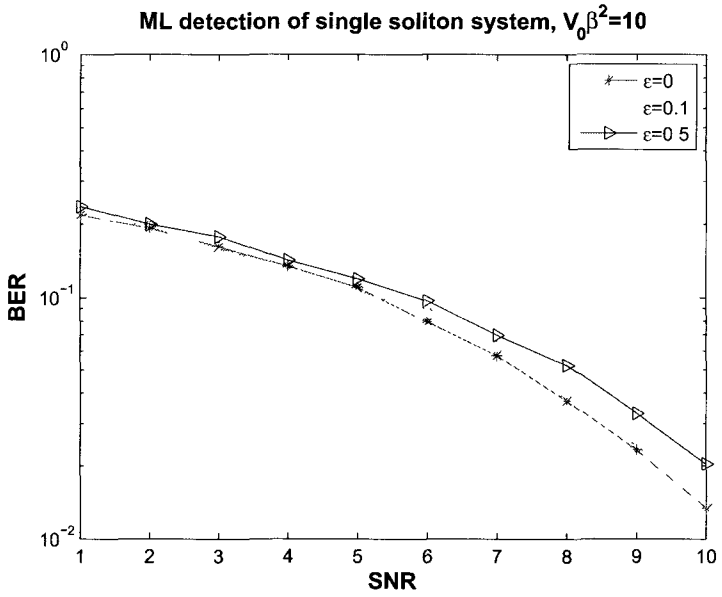

Figure 6.7: BER of single soliton system with mismatched circuit, ML detection, $V_0\beta^2 = 10$

amplitude parameters.

6.4 Summary

In this chapter, we study the response of the mismatched Toda circuit to input single soliton. Applying both KdV approximation method and the IST of Toda lattice, we show that for small circuit mismatch coefficient, e.g. $\epsilon = 0.1$ and for the input soliton with small amplitude, e.g. $V_0\beta^2 \approx 1$, the circuit mismatch only results in small distortion of the output phase shift, while the amplitude of the input soliton remains unchanged. For large mismatch coefficient or high input soliton amplitude, both the amplitude and the phase shift of the input soliton are distorted and the distortion increases with the increase of the input soliton amplitude and the mismatch coefficient. The detection performance of the soliton system with mismatched Toda

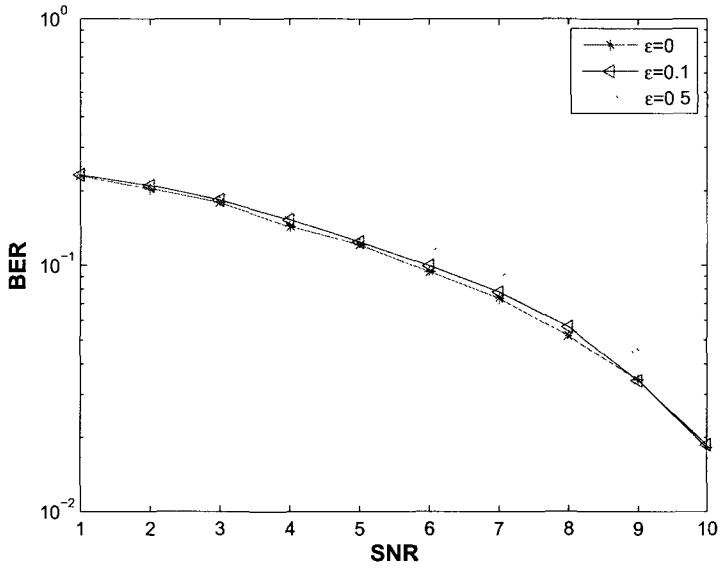

Figure 6.8: Average BER of multiplexing soliton system with mismatched circuit, AT detection, $V_0\beta^2 = [10\ 9]$

circuit is also studied. It is shown that the small mismatch of the Toda circuit will not affect the detection performance of the soliton system severely, while large mismatch of Toda circuit may severely deteriorate the detection accuracy in the soliton system.

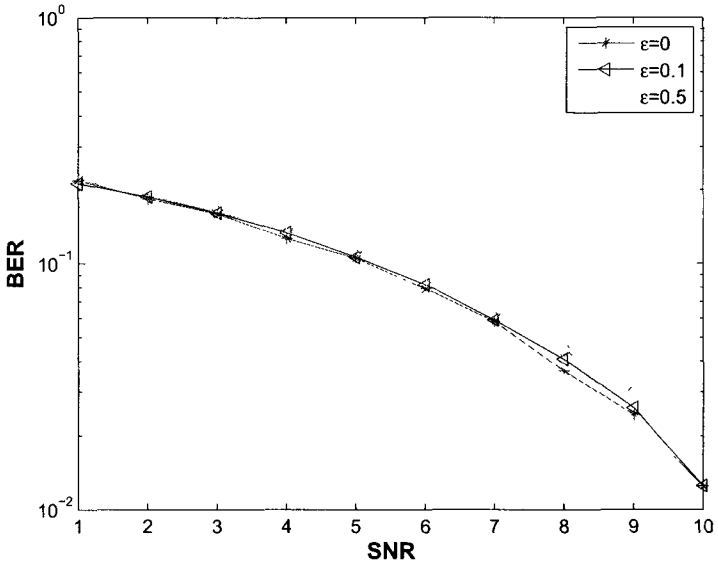

Figure 6.9: Average BER of multiplexing soliton system with mismatched circuit, ML detection, $V_0\beta^2 = [10\ 9]$

Chapter 7

Conclusion and Future Work

In this thesis, we examine the properties of the Toda solitons including the time and frequency domain characteristics, the time-bandwidth characteristics and the signal energy. We show that the single soliton is unimodal in both time and frequency characteristics and the characteristics of the composite soliton varies with the relative parameters of the two constituent solitons. Depending on the ratio of the parameters of the two constitute solitons, the resulting composite soliton might have two entirely different shapes. Fixing the parameter of one constitute soliton, the threshold of the parameter of another constitute soliton corresponding to the shape variation of the composite soliton has been examined.

The time-domain and frequency-domain efficiency of the Toda soliton pulses are studied in this thesis. We show that the T-B product of single Toda soliton is a constant close to optimal T-B product which is achieved by Gaussian pulse. The T-B product of the composite soliton depends on the parameters of two constituent solitons and can be as small as that of the single soliton for properly chosen parameters. These results indicate the high energy localization of both single Toda soliton and composite Toda soliton. Another important factor of pulses, i.e., pulse energy has also been examined for both single and composite Toda solitons. We have shown

that the energy of the single Toda soliton is a monotonic function of its parameter β. The energy of the composite soliton depend on the parameters of the two constituent solitons and is always smaller than the sum of two single solitons. The condition of the maximum energy saving of the composite soliton has been examined.

We then study the properties of the Toda circuit. In particular, we focus on the Toda circuit responses to stochastic inputs at both early stages and late stages. We have demonstrated that at the early stages, the Toda circuit exhibits weak nonlinearity and can be analyzed by the Volterra series. At late stages, the approximation error of the Volterra series increases due to the increase of the circuit nonlinearity. For higher accuracy, we apply Runge-Kutta method in this case. We have shown that high nonlinearity of the Toda circuit tend to transform circuit input into the combination of soliton(s), transients and oscillations.

These properties of the Toda soliton and the Toda circuit are then applied fundamentally in wireless communication system and we propose the single-user and multi-user OOK signalling schemes employing Toda solitons as information carriers in data communications. The bandwidth efficiency of the soliton multiplexing system have been calculated and shown to be superior to the traditional FDM system. For the soliton OOK schemes, we also propose the AT and the ML methods of detecting the transmitted solitons. The detection performance of these systems have been analyzed and compared with the traditional on-off keying scheme commonly used in wireless optical and optical fiber systems. We show that while being detected at the early stages of the Toda circuit, the ML detection performance of the soliton system is similar to the ML detection of the traditional ASK due to the weak nonlinearity of the circuit. On the other hand, the low-pass filtering effects of the Toda circuit helps the soliton system to achieve a better AT detection performance compared to the systems without the Toda circuit, especially for systems transmitting soliton with large parameters. Compared to the ASK system with other waveforms such as the

commonly-used Raised-cosine pulse, we show that the soliton system performs better in AT detection resulted from the high energy localization property of the soliton and the extra noise filtering effects of the receiver Toda circuit. It should be mentioned that while the ML detection performance of the soliton system is similar to that of the ASK scheme, the high bandwidth efficiency of the soliton signals results in a high capacity of the soliton system compared to ASK systems using other waveforms such as commonly-used Raised-Cosine waveforms.

Instead of employing Toda circuit at the receiver of the soliton system, we also study a single soliton ASK system without applying the Toda circuit and focus on the detection performance under receiver timing error. For comparison, we also study the ML detection performance of the ASK system with other commonly-used waveforms including a Raised Cosine pulse with roll-off factor 0.5 and a rectangular pulse. It has been shown that the ASK system with single soliton has better performance compared to those using other waveforms, demonstrating the robustness of the soliton signal against receiver timing error.

The mismatch problem of the Toda circuit is also addressed in this thesis, specifically, we study the response of the mismatched Toda circuit to input single soliton. We show that when circuit mismatch coefficient and the parameter of the input soliton are small, the circuit mismatch only results in small distortion of the output phase shift, while the amplitude of the input soliton remains unchanged. For large mismatch or large input soliton, both the amplitude and the phase shift of the input soliton are distorted and the amplitude distortion increases with the increase of the input soliton amplitude and the mismatch coefficient. This result indicates that large mismatch of Toda circuit may severely affect detection accuracy in soliton system. This property in turn can be applied to offers relative information security: From Eqs. (3.3) and Eqs. (3.5), it can be seen that a Toda circuit with particular values of inductor and linear capacitor only supports stable propagation of solitons of the same

parameter values. Departure from these values in the receiver Toda circuit results in gross distortions of the solitons in both amplitudes and pulse shapes while propagating along the Toda circuit causing errors in detection. Thus, a soliton system may also offer additional security in transmission from users not having the exact knowledge of the Toda circuit parameters.

It can also be shown that soliton multiplexing system also has simpler implementation comparing to traditional multiplexing system. For the traditional multiplexing system, such as FDM or wave division multiplexing (WDM) system, filters are applied at the receiver to isolate signals from different users. These filters have to be different and separated, thus increasing the complexity of the receiver. However, in SADM, different soliton waveforms are chosen to represent user information and at the receiver, a single relative simple Toda circuit is applied followed by a detector and no channel filters are needed to separate signals from different users. This provides the advantage of simplifying the receiver implementation.

7.1 Future works

A common property of many classes of solitons is that solitons can be generated through exciting soliton-supporting systems with rectangular pulses and solitons enjoy special propagation properties while transmitting along the system. In particular for Toda soliton, its corresponding soliton-supporting system is the Toda lattice which can be realized by a LC Toda circuit. In our communication model of the soliton system, a Toda circuit is employed at the transmitter to generate Toda soliton and at the receiver to filter out noise. Instead of employing an analog Toda circuit, an alternative while more convenient way of generating and processing soliton signals can be the digital signal processing (DSP) technology [30]. Similar to Runge-Kutta method, other algorithms for simulating the Toda circuit can also be realized by

computer languages such as C language or Matlab and be embedded in a discrete signal processor. The algorithms function in such way that the processor performs exactly as a discrete Toda circuit with both of its input and output being discrete.

In the soliton system model we propose in this thesis, soliton OOK was proposed as information carriers because, as can be clearly seen from Eq. (3.3) and Eq. (3.4), a Toda circuit only supports positive pulses. Any negative input pulse transmitting along the Toda circuit will be distorted. However, if the circuit output is detected at the early stages of the Toda circuit, because the circuit exhibits weak nonlinearity, we can expect the distortion due to negative input pulses of relatively low amplitude will be small. This can be illustrated in Fig. 7.1 in which the input to the Toda circuit, a single Toda soliton of amplitude 4, and the output at stage $N = 1$ are both shown. Indeed, it can be observed that the distortion of the pulse within the essential duration of the original soliton is relatively small. This observation indicates the possibility of employing Phase Shift Keying (PSK) technique in the soliton system. It can be expected that the PSK soliton system will performs better than ASK soliton system due to its larger distance of separation of the signals.

In this thesis, we have propose an OOK soliton communication system and demonstrate its high bandwidth efficiency and relative robustness to channel noise for AT detection. The robustness of the single soliton signal to timing error is also verified. A laboratory model of a soliton communication system should be built to demonstrate its practical feasibility and advantages over conventional schemes.

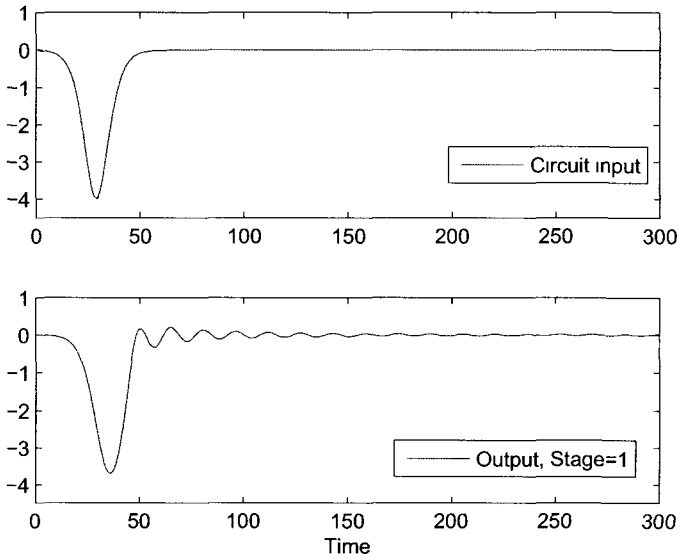

Figure 7.1: Negative soliton output, stage=1

Appendix A

Correlation and Variance of Output Noise

The output noise of the Toda circuit is given by

$$\tilde{n} = n \otimes h_1 + [(n \circ n) + 2(s \circ n)] \otimes h_2 + [(n \circ n \circ n) + 3(s \circ n \circ n + s \circ s \circ n)]$$

Denoting

$$\begin{aligned}
a(t) &= n \otimes h_1 = \int_{-\infty}^{\infty} h_1(t-\tau_1) n(\tau_1) d\tau_1 \\
b_1(t) &= (n \circ n) \otimes h_2 = \int_{-\infty}^{\infty} \int_{-\infty}^{\infty} h_2(t-\tau_1, t-\tau_2) n(\tau_1) n(\tau_2) d\tau_1 d\tau_2 \\
b_2(t) &= 2(s \circ n) \otimes h_2 = 2 \int_{-\infty}^{\infty} \int_{-\infty}^{\infty} h_2(t-\tau_1, t-\tau_2) s(\tau_1) n(\tau_2) d\tau_1 d\tau_2 \\
c_1(t) &= (n \circ n \circ n) \otimes h_3 \\
&= \int_{-\infty}^{\infty} \int_{-\infty}^{\infty} \int_{-\infty}^{\infty} h_3(t-\tau_1, t-\tau_2, t-\tau_3) n(\tau_1) n(\tau_2) n(\tau_3) d\tau_1 d\tau_2 d\tau_3 \\
c_2(t) &= 3(s \circ n \circ n) \otimes h_3 \\
&= 3 \int_{-\infty}^{\infty} \int_{-\infty}^{\infty} \int_{-\infty}^{\infty} h_3(t-\tau_1, t-\tau_2, t-\tau_3) s(\tau_1) n(\tau_2) n(\tau_3) d\tau_1 d\tau_2 d\tau_3 \\
c_3(t) &= 3(s \circ s \circ n) \otimes h_3 \\
&= 3 \int_{-\infty}^{\infty} \int_{-\infty}^{\infty} \int_{-\infty}^{\infty} h_3(t-\tau_1, t-\tau_2, t-\tau_3) s(\tau_1) s(\tau_2) n(\tau_3) d\tau_1 d\tau_2 d\tau_3
\end{aligned}$$

The correlation of $\tilde{n}$ at time instants t_1 and t_2 is given by:

$$\begin{aligned}
r_{\tilde{n}\tilde{n}}(t_1,t_2) &= E[(a(t_1)+b_1(t_1)+b_2(t_1)+c_1(t_1)+c_2(t_1)+c_3(t_1)) \\
&\quad (a(t_2)+b_1(t_2)+b_2(t_2)+c_1(t_2)+c_2(t_2)+c_3(t_2))] \\
&= E[a(t_1)a(t_2)]+E[b_1(t_1)b_1(t_2)]+E[b_2(t_1)b_2(t_2)]+E[c_1(t_1)c_1(t_2)] \\
&+ E[c_2(t_1)c_2(t_2)]+E[c_3(t_1)c_3(t_2)]+E[a(t_1)b_1(t_2)]+E[a(t_1)b_2(t_2)] \\
&+ E[a(t_1)c_1(t_2)]+E[a(t_1)c_2(t_2)]+E[a(t_1)c_3(t_2)]+E[b_1(t_1)b_2(t_2)] \\
&+ E[b_1(t_1)c_1(t_2)]+E[b_1(t_1)c_2(t_2)]+E[b_1(t_1)c_3(t_2)]+E[b_2(t_1)c_1(t_2)] \\
&+ E[b_2(t_1)c_2(t_2)]+E[b_2(t_1)c_3(t_2)]+E[c_1(t_1)c_2(t_2)]+E[c_1(t_1)c_3(t_2)] \\
&+ E[c_2(t_1)c_3(t_2)]+E[a(t_2)b_1(t_1)]+E[a(t_2)b_2(t_1)]+E[a(t_2)c_1(t_1)] \\
&+ E[a(t_2)c_2(t_1)]+E[a(t_2)c_3(t_1)]+E[b_1(t_2)b_2(t_1)]+E[b_1(t_2)c_1(t_1)] \\
&+ E[b_1(t_2)c_2(t_1)]+E[b_1(t_2)c_3(t_1)]+E[b_2(t_2)c_1(t_1)]+E[b_2(t_2)c_2(t_1)] \\
&+ E[b_2(t_2)c_3(t_1)]+E[c_1(t_2)c_2(t_1)]+E[c_1(t_2)c_3(t_1)]+E[c_2(t_2)c_3(t_1)]
\end{aligned} \tag{A.1}$$

Applying the properties of white Gaussian noise [44], the terms in Eq. (A.1) can be calculated as:

$$E[a(t_1)a(t_2)] = E\left[\int_{-\infty}^{\infty}\int_{-\infty}^{\infty} h_1(t_1-\tau_1)h_1(t_2-\tau_2)n(\tau_1)n(\tau_2)d\tau_1 d\tau_2\right] = \frac{\mathcal{N}_0}{2}\int_{-\infty}^{\infty} h_1^2(\tau_1)d\tau_1$$

$$\begin{aligned}
E[b_1(t_1)b_1(t_2)] &= E\left[\int_{-\infty}^{\infty}\cdots\int_{-\infty}^{\infty} h_2(t_1-\tau_1,t_1-\tau_2)h_2(t_2-\tau_3,t_2-\tau_4)n(\tau_1)n(\tau_2)n(\tau_3)n(\tau_4)\right. \\
&\quad \left. d\tau_1\cdots d\tau_4\right] = \left(\frac{\mathcal{N}_0}{2}\right)^2\int_{-\infty}^{\infty}\int_{-\infty}^{\infty}\Big(h_2(\tau_1,\tau_1)h_2(\tau_2,\tau_2)+2h_2^2(\tau_1,\tau_2)\Big)d\tau_1 d\tau_2
\end{aligned}$$

$$\begin{aligned}
E[b_2(t_1)b_2(t_2)] &= 4E\left[\int_{-\infty}^{\infty}\cdots\int_{-\infty}^{\infty} h_2(t_1-\tau_1,t_1-\tau_2)h_2(t_2-\tau_3,t_2-\tau_4)s(\tau_1)n(\tau_2)s(\tau_3)\right. \\
&\quad \left. n(\tau_4)d\tau_1\cdots d\tau_4\right] = 4\cdot\frac{\mathcal{N}_0}{2}\left[\int_{-\infty}^{\infty}\cdots\int_{-\infty}^{\infty} h_2(t_1-\tau_1,t_1-\tau_2)\right. \\
&\quad \left. h_2(t_2-\tau_3,t_2-\tau_2)s(\tau_1)s(\tau_3)d\tau_1\cdots d\tau_3\right]
\end{aligned}$$

$$
\begin{aligned}
E[c_1(t_1)c_1(t_2)] &= E\Bigg[\int_{-\infty}^{\infty}\cdots\int_{-\infty}^{\infty} h_3(t_1-\tau_1,t_1-\tau_2,t_1-\tau_3)h_3(t_2-\tau_4,t_2-\tau_5,t_2-\tau_6) \\
&\quad n(\tau_1)n(\tau_2)n(\tau_3)n(\tau_4)n(\tau_5)n(\tau_6)d\tau_1\cdots d\tau_6\Bigg] \\
&= \left(\frac{\mathcal{N}_0}{2}\right)^3\int_{-\infty}^{\infty}\cdots\int_{-\infty}^{\infty}\Big(9h_3(t_1-\tau_1,t_1-\tau_1,t_1-\tau_2)h_3(t_2-\tau_2,t_2-\tau_3,t_2-\tau_3 \\
&+ 6h_3(t_1-\tau_1,t_1-\tau_2,t_1-\tau_3)h_3(t_2-\tau_1,t_2-\tau_2,t_2-\tau_3)\Big)\mathrm{d}\tau_1\mathrm{d}\tau_2\mathrm{d}\tau_3 \\
E[c_2(t_1)c_2(t_2)] &= 9E\Bigg[\int_{-\infty}^{\infty}\cdots\int_{-\infty}^{\infty} h_3(t_1-\tau_1,t_1-\tau_2,t_1-\tau_3)h_3(t_2-\tau_4,t_2-\tau_5,t_2-\tau_6) \\
&\quad s(\tau_1)n(\tau_2)n(\tau_3)s(\tau_4)n(\tau_5)n(\tau_6)d\tau_1\cdots d\tau_6\Bigg] \\
&= 9\left(\frac{\mathcal{N}_0}{2}\right)^2\int_{-\infty}^{\infty}\cdots\int_{-\infty}^{\infty}\Big[h_3(t_1-\tau_1,t_1-\tau_2,t_1-\tau_2)h_3(t_2-\tau_4,t_2-\tau_3,t_2-\tau_3) \\
&+ 2h_3(t_1-\tau_1,t_1-\tau_2,t_1-\tau_3)h_3(t_2-\tau_4,t_2-\tau_2,t_2-\tau_3)\Big]s(\tau_1)s(\tau_4)\mathrm{d}\tau_1\cdots\mathrm{d}\tau_4 \\
E[c_3(t_1)c_3(t_2)] &= 9E\Bigg[\int_{-\infty}^{\infty}\cdots\int_{-\infty}^{\infty} h_3(t_1-\tau_1,t_1-\tau_2,t_1-\tau_3)h_3(t_2-\tau_4,t_2-\tau_5,t_2-\tau_6) \\
&\quad s(\tau_1)s(\tau_2)n(\tau_3)s(\tau_4)s(\tau_5)n(\tau_6)d\tau_1\cdots d\tau_6\Bigg] \\
&= 9\cdot\frac{\mathcal{N}_0}{2}\int_{-\infty}^{\infty}\cdots\int_{-\infty}^{\infty}\Big[h_3(t_1-\tau_1,t_1-\tau_2,t_1-\tau_3)h_3(t_2-\tau_4,t_2-\tau_5,t_2-\tau_3) \\
&\quad s(\tau_1)s(\tau_2)s(\tau_4)s(\tau_5)\Big]\mathrm{d}\tau_1\cdots\mathrm{d}\tau_5 \\
E[a(t_1)b_1(t_2)] &= E\Bigg[\int_{-\infty}^{\infty}\cdots\int_{-\infty}^{\infty} h_1(t_1-\tau_1)n(\tau_1)h_2(t_2-\tau_2,t_2-\tau_3)n(\tau_2)n(\tau_3)d\tau_1\cdots d\tau_3\Bigg] \\
&= E[b_1(t_1)a(t_2)] = 0 \\
E[a(t_1)b_2(t_2)] &= 2E\Bigg[\int_{-\infty}^{\infty}\cdots\int_{-\infty}^{\infty} h_1(t_1-\tau_1)n(\tau_1)h_2(t_2-\tau_2,t_2-\tau_3)s(\tau_2)n(\tau_3)d\tau_1\cdots d\tau_3\Bigg] \\
&= 2\cdot\frac{\mathcal{N}_0}{2}\Bigg[\int_{-\infty}^{\infty}\int_{-\infty}^{\infty} h_1(t_1-\tau_1)h_2(t_2-\tau_2,t_2-\tau_1)s(\tau_2)d\tau_1d\tau_2\Bigg] \\
E[b_2(t_1)a(t_2)] &= 2E\Bigg[\int_{-\infty}^{\infty}\cdots\int_{-\infty}^{\infty} h_1(t_2-\tau_1)n(\tau_1)h_2(t_1-\tau_2,t_1-\tau_3)s(\tau_2)n(\tau_3)d\tau_1\cdots d\tau_3\Bigg] \\
&= 2\cdot\frac{\mathcal{N}_0}{2}\Bigg[\int_{-\infty}^{\infty}\int_{-\infty}^{\infty} h_1(t_2-\tau_1)h_2(t_1-\tau_2,t_1-\tau_1)s(\tau_2)d\tau_1d\tau_2\Bigg]
\end{aligned}
$$

$$
\begin{aligned}
E[a(t_1)c_1(t_2)] &= E\Bigg[\int_{-\infty}^{\infty}\cdots\int_{-\infty}^{\infty} h_1(t_1-\tau_1)n(\tau_1)h_3(t_2-\tau_2,t_2-\tau_3,t_2-\tau_4) \\
&\quad n(\tau_2)n(\tau_3)n(\tau_4)d\tau_1\cdots d\tau_4\Bigg] \\
&= 3\left(\frac{\mathcal{N}_0}{2}\right)^2\left[\int_{-\infty}^{\infty}\int_{-\infty}^{\infty}\Big[h_1(\tau_1)h_3(\tau_1,\tau_2,\tau_2)\Big]d\tau_1 d\tau_2\right] = E[c_1(t_1)a(t_2)] \\
E[a(t_1)c_2(t_2)] &= 3E\Bigg[\int_{-\infty}^{\infty}\cdots\int_{-\infty}^{\infty} h_1(t_1-\tau_1)n(\tau_1)h_3(t_2-\tau_2,t_2-\tau_3,t_2-\tau_4) \\
&\quad s(\tau_2)n(\tau_3)n(\tau_4)d\tau_1\cdots d\tau_4\Bigg] = E[c_2(t_1)a(t_2)] = 0 \\
E[a(t_1)c_3(t_2)] &= 3E\Bigg[\int_{-\infty}^{\infty}\cdots\int_{-\infty}^{\infty} h_1(t_1-\tau_1)n(\tau_1)h_3(t_2-\tau_2,t_2-\tau_3,t_2-\tau_4) \\
&\quad s(\tau_2)s(\tau_3)n(\tau_4)d\tau_1\cdots d\tau_4\Bigg] \\
&= 3\cdot\frac{\mathcal{N}_0}{2}\int_{-\infty}^{\infty}\int_{-\infty}^{\infty}\Big[h_1(t_1-\tau_1)h_3(t_2-\tau_2,t_2-\tau_3,t_2-\tau_1)s(\tau_2)s(\tau_3)\Big]d\tau_1\cdots d\tau_3 \\
E[c_3(t_1)a(t_2)] &= 3E\Bigg[\int_{-\infty}^{\infty}\cdots\int_{-\infty}^{\infty} h_1(t_2-\tau_1)n(\tau_1)h_3(t_1-\tau_2,t_1-\tau_3,t_1-\tau_4) \\
&\quad s(\tau_2)s(\tau_3)n(\tau_4)d\tau_1\cdots d\tau_4\Bigg] \\
&= 3\cdot\frac{\mathcal{N}_0}{2}\int_{-\infty}^{\infty}\int_{-\infty}^{\infty}\Big[h_1(t_2-\tau_1)h_3(t_1-\tau_2,t_1-\tau_3,t_1-\tau_1)s(\tau_2)s(\tau_3)\Big]d\tau_1\cdots d\tau_3 \\
E[b_1(t_1)b_2(t_2)] &= 2E\Bigg[\int_{-\infty}^{\infty}\cdots\int_{-\infty}^{\infty} h_2(t_1-\tau_1,t_1-\tau_2)n(\tau_1)n(\tau_2)h_2(t_2-\tau_3,t_2-\tau_4) \\
&\quad s(\tau_3)n(\tau_4)d\tau_1\cdots d\tau_4\Bigg] = E[b_2(t_1)b_1(t_2)] = 0 \\
E[b_1(t_1)c_1(t_2)] &= E\Bigg[\int_{-\infty}^{\infty}\cdots\int_{-\infty}^{\infty} h_2(t_1-\tau_1,t_1-\tau_2)n(\tau_1)n(\tau_2)h_3(t_2-\tau_3,t_2-\tau_4,t_2-\tau_5) \\
&\quad n(\tau_3)n(\tau_4)n(\tau_5)d\tau_1\cdots d\tau_5\Bigg] = E[c_1(t_1)b_1(t_2)] = 0
\end{aligned}
$$

$$
\begin{aligned}
E[b_1(t_1)c_2(t_2)] &= 3E\Bigg[\int_{-\infty}^{\infty}\cdots\int_{-\infty}^{\infty} h_2(t_1-\tau_1,t_1-\tau_2)n(\tau_1)n(\tau_2) \\
&\quad h_3(t_2-\tau_3,t_2-\tau_4,t_2-\tau_5)s(\tau_3)n(\tau_4)n(\tau_5)d\tau_1\cdots d\tau_5\Bigg] \\
&= 3\left(\frac{\mathcal{N}_0}{2}\right)^2\Bigg[\int_{-\infty}^{\infty}\cdots\int_{-\infty}^{\infty}\Big[h_2(t_1-\tau_1,t_1-\tau_1)h_3(t_2-\tau_3,t_2-\tau_2,t_2-\tau_2) \\
&+ 2h_2(t_1-\tau_1,t_1-\tau_2)h_3(t_2-\tau_3,t_2-\tau_1,t_2-\tau_2)\Big]s(\tau_3)d\tau_1\cdots d\tau_3\Bigg] \\
E[c_2(t_1)b_1(t_2)] &= 3E\Bigg[\int_{-\infty}^{\infty}\cdots\int_{-\infty}^{\infty} h_2(t_2-\tau_1,t_2-\tau_2)n(\tau_1)n(\tau_2) \\
&\quad h_3(t_1-\tau_3,t_1-\tau_4,t_1-\tau_5)s(\tau_3)n(\tau_4)n(\tau_5)d\tau_1\cdots d\tau_5\Bigg] \\
&= 3\left(\frac{\mathcal{N}_0}{2}\right)^2\Bigg[\int_{-\infty}^{\infty}\cdots\int_{-\infty}^{\infty}\Big[h_2(t_2-\tau_1,t_2-\tau_1)h_3(t_1-\tau_3,t_1-\tau_2,t_1-\tau_2) \\
&+ 2h_2(t_2-\tau_1,t_2-\tau_2)h_3(t_1-\tau_3,t_1-\tau_1,t_1-\tau_2)\Big]s(\tau_3)d\tau_1\cdots d\tau_3\Bigg] \\
E[b_1(t_1)c_3(t_2)] &= 3E\Bigg[\int_{-\infty}^{\infty}\cdots\int_{-\infty}^{\infty} h_2(t_1-\tau_1,t_1-\tau_2)n(\tau_1)n(\tau_2) \\
&\quad h_3(t_2-\tau_3,t_2-\tau_4,t_2-\tau_5)s(\tau_3)s(\tau_4)n(\tau_5)d\tau_1\cdots d\tau_5\Bigg] = E[c_3(t_1)b_1(t_2)] = 0 \\
E[b_2(t_1)c_1(t_2)] &= 2E\Bigg[\int_{-\infty}^{\infty}\cdots\int_{-\infty}^{\infty} h_2(t_1-\tau_1,t_1-\tau_2)s(\tau_1)n(\tau_2) \\
&\quad h_3(t_2-\tau_3,t_2-\tau_4,t_2-\tau_5)n(\tau_3)n(\tau_4)n(\tau_5)d\tau_1\cdots d\tau_5\Bigg] \\
&= 6\left(\frac{\mathcal{N}_0}{2}\right)^2\int_{-\infty}^{\infty} h_2(t_1-\tau_1,t_1-\tau_2)h_3(t_2-\tau_2,t_2-\tau_3,t_2-\tau_3)d\tau_1\cdots d\tau_3
\end{aligned}
$$

$$
\begin{aligned}
E[c_1(t_1)b_2(t_2)] &= 2E\Bigg[\int_{-\infty}^{\infty}\cdots\int_{-\infty}^{\infty} h_2(t_2-\tau_1,t_2-\tau_2)s(\tau_1)n(\tau_2) \\
&\quad h_3(t_1-\tau_3,t_1-\tau_4,t_1-\tau_5)n(\tau_3)n(\tau_4)n(\tau_5)d\tau_1\cdots d\tau_5\Bigg] \\
&= 6\left(\frac{\mathcal{N}_0}{2}\right)^2\int_{-\infty}^{\infty} h_2(t_2-\tau_1,t_2-\tau_2)h_3(t_1-\tau_2,t_1-\tau_3,t_1-\tau_3)d\tau_1\cdots d\tau_3 \\
E[b_2(t_1)c_2(t_2)] &= 6E\Bigg[\int_{-\infty}^{\infty}\cdots\int_{-\infty}^{\infty} h_2(t_1-\tau_1,t_1-\tau_2)s(\tau_1)n(\tau_2) \\
&\quad h_3(t_2-\tau_3,t_2-\tau_4,t_2-\tau_5)s(\tau_3)n(\tau_4)n(\tau_5)d\tau_1\cdots d\tau_5\Bigg] = E[c_2(t_1)b_2(t_2)] = 0 \\
E[b_2(t_1)c_3(t_2)] &= 6E\Bigg[\int_{-\infty}^{\infty}\cdots\int_{-\infty}^{\infty} h_2(t_1-\tau_1,t_1-\tau_2)s(\tau_1)n(\tau_2) \\
&\quad h_3(t_2-\tau_3,t_2-\tau_4,t_2-\tau_5)s(\tau_3)s(\tau_4)n(\tau_5)d\tau_1\cdots d\tau_5\Bigg] \\
&= 6\cdot\frac{\mathcal{N}_0}{2}\Bigg[\int_{-\infty}^{\infty}\cdots\int_{-\infty}^{\infty} h_2(t_1-\tau_1,t_1-\tau_2)s(\tau_1) \\
&\quad h_3(t_2-\tau_3,t_2-\tau_4,t_2-\tau_2)s(\tau_3)s(\tau_4)d\tau_1\cdots d\tau_4\Bigg] \\
E[c_3(t_1)b_2(t_2)] &= 6E\Bigg[\int_{-\infty}^{\infty}\cdots\int_{-\infty}^{\infty} h_2(t_2-\tau_1,t_2-\tau_2)s(\tau_1)n(\tau_2) \\
&\quad h_3(t_1-\tau_3,t_1-\tau_4,t_1-\tau_5)s(\tau_3)s(\tau_4)n(\tau_5)d\tau_1\cdots d\tau_5\Bigg] \\
&= 6\cdot\frac{\mathcal{N}_0}{2}\Bigg[\int_{-\infty}^{\infty}\cdots\int_{-\infty}^{\infty} h_2(t_2-\tau_1,t_2-\tau_2)s(\tau_1) \\
&\quad h_3(t_1-\tau_3,t_1-\tau_4,t_1-\tau_2)s(\tau_3)s(\tau_4)d\tau_1\cdots d\tau_4\Bigg] \\
E[c_1(t_1)c_2(t_2)] &= 3E\Bigg[\int_{-\infty}^{\infty}\cdots\int_{-\infty}^{\infty} h_3(t_1-\tau_1,t_1-\tau_2,t_1-\tau_3)n(\tau_1)n(\tau_2)n(\tau_3) \\
&\quad h_3(t_2-\tau_4,t_2-\tau_5,t_2-\tau_6)s(\tau_4)n(\tau_5)n(\tau_6)d\tau_1\cdots d\tau_6\Bigg] = E[c_2(t_1)c_1(t_2)] = 0
\end{aligned}
$$

$$
\begin{aligned}
E[c_1(t_1)c_3(t_2)] &= 3E\Bigg[\int_{-\infty}^{\infty}\cdots\int_{-\infty}^{\infty} h_3(t_1-\tau_1,t_1-\tau_2,t_1-\tau_3)n(\tau_1)n(\tau_2)n(\tau_3) \\
&\quad h_3(t_2-\tau_4,t_2-\tau_5,t_2-\tau_6)s(\tau_4)s(\tau_5)n(\tau_6)d\tau_1\cdots d\tau_6\Bigg] \\
&= 9\left(\frac{\mathcal{N}_0}{2}\right)^2\int_{-\infty}^{\infty}\cdots\int_{-\infty}^{\infty} h_3(t_1-\tau_1,t_1-\tau_2,t_1-\tau_2) \\
&\quad h_3(t_2-\tau_1,t_2-\tau_3,t_2-\tau_4)s(\tau_3)s(\tau_4)d\tau_1\cdots d\tau_4 \\
E[c_3(t_1)c_1(t_2)] &= 3E\Bigg[\int_{-\infty}^{\infty}\cdots\int_{-\infty}^{\infty} h_3(t_2-\tau_1,t_2-\tau_2,t_2-\tau_3)n(\tau_1)n(\tau_2)n(\tau_3) \\
&\quad h_3(t_1-\tau_4,t_1-\tau_5,t_1-\tau_6)s(\tau_4)s(\tau_5)n(\tau_6)d\tau_1\cdots d\tau_6\Bigg] \\
&= 9\left(\frac{\mathcal{N}_0}{2}\right)^2\int_{-\infty}^{\infty}\cdots\int_{-\infty}^{\infty} h_3(t_2-\tau_1,t_2-\tau_2,t_2-\tau_2) \\
&\quad h_3(t_1-\tau_1,t_1-\tau_3,t_1-\tau_4)s(\tau_3)s(\tau_4)d\tau_1\cdots d\tau_4 \\
E[c_2(t_1)c_3(t_2)] &= 9E\Bigg[\int_{-\infty}^{\infty}\cdots\int_{-\infty}^{\infty} h_3(t_1-\tau_1,t_1-\tau_2,t_1-\tau_3)s(\tau_1)n(\tau_2)n(\tau_3) \\
&\quad h_3(t_2-\tau_4,t_2-\tau_5,t_2-\tau_6)s(\tau_4)s(\tau_5)n(\tau_6)d\tau_1\cdots d\tau_6\Bigg] = E[c_3(t_1)c_2(t_2)] = 0
\end{aligned}
$$

Arranging the terms in the order of $\frac{\mathcal{N}_0}{2}$, Eq. (A.1) can be rewritten as Eq. (4.19), where,

$$
\begin{aligned}
\tilde{R}_1(t_1,t_2) &= E[a(t_1)a(t_2)] + E[b_2(t_1)b_2(t_2)] + E[c_3(t_1)c_3(t_2)] + E[a(t_1)b_2(t_2)] \\
&+ E[b_2(t_1)a(t_2)] + E[a(t_1)c_3(t_2)] + E[c_3(t_1)a(t_2)] + E[b_2(t_1)c_3(t_2)] \\
&+ E[c_3(t_1)b_2(t_2)] \\
\tilde{R}_2(t_1,t_2) &= E[b_1(t_1)b_1(t_2)] + E[c_2(t_1)c_2(t_2)] + E[a(t_1)c_1(t_2)] + E[c_1(t_1)a(t_2)] \\
&+ E[b_1(t_1)c_2(t_2)] + E[c_2(t_1)b_1(t_2)] + E[b_2(t_1)c_1(t_2)] + E[c_1(t_1)b_2(t_2)] \\
&+ E[c_1(t_1)c_3(t_2)] + E[c_3(t_1)c_1(t_2)] \\
\tilde{R}_3(t_1,t_2) &= E[c_1(t_1)c_1(t_2)]
\end{aligned}
$$

The output noise variance at time instant t_0 is given by $r_{\tilde{n}\tilde{n}}(t_0, t_0)$ and can be expressed as Eq. (4.18), where

$$\begin{aligned}
\tilde{a}_1 &= E[a(t_0)^2] \\
\tilde{V}_1(t_0) &= E[b_2(t_0)^2] + E[c_3(t_0)^2] + 2E[a(t_0)b_2(t_0)] + 2E[a(t_0)c_3(t_0)] + 2E[b_2(t_0)c_3(t_0)] \\
\tilde{a}_2 &= E[b_1(t_0)^2] + 2E[a(t_0)c_1(t_0)] \\
\tilde{V}_2(t_0) &= E[c_2(t_0)^2] + 2E[b_1(t_0)c_2(t_0)] + 2E[b_2(t_0)c_1(t_0)] + 2E[c_1(t_0)c_3(t_0)] \\
\tilde{a}_3 &= E[c_1(t_0)^2]
\end{aligned}$$

Appendix B

Proof of Time Invariance $\dot{z}_1^{(1)}$

Proof: Introducing variable θ_1, such that $\xi^{n-1}(\xi^2-1)^{1/2} = \exp(\theta_1)$, we obtain

$$\begin{aligned} A(n-1) &= -\frac{(\xi^2-1)^{1/2}}{\xi^{n-1}(\xi^2-1)^{1/2}\exp\left[(\xi-\xi^{-1})t/2\right] + \xi^{-n+1}(\xi^2-1)^{-1/2}\exp\left[-(\xi-\xi^{-1})t/2\right]} \\ &= -\frac{(\xi^2-1)^{1/2}}{2}\mathrm{sech}\left(\frac{(\xi-\xi^{-1})}{2}t+\theta_1\right) \end{aligned}$$

Similarly, denote $\xi^n(\xi^2-1)^{1/2} = \exp(\theta_2)$, $A(n)$ can be expressed as:

$$A(n) = -\frac{(\xi^2-1)^{1/2}}{2}\mathrm{sech}(\frac{(\xi-\xi^{-1})}{2}t+\theta_2)$$

Denoting $\Delta\theta = \theta_2 - \theta_1$, we obtain

$$\int_{-\infty}^{\infty} A(n-1)^3 A(n)dt = \frac{2}{(\xi-\xi^{-1})}\frac{(\xi^2-1)^2}{2^4}\int_{-\infty}^{\infty}\mathrm{sech}^3(t_1)\mathrm{sech}(t_1+\Delta\theta)dt$$

$$\begin{aligned} \int_{-\infty}^{\infty} A(n-1)A(n)^3dt &= \frac{2}{(\xi-\xi^{-1})}\frac{(\xi^2-1)^2}{2^4}\int_{-\infty}^{\infty}\mathrm{sech}^3(t_1)\mathrm{sech}(t_1-\Delta\theta)dt \\ &= \int_{-\infty}^{\infty} A(n-1)^3A(n)dt \end{aligned}$$

Substituting Eq. (B.2) into Eq. (6.32), we obtain, $z_1^{(1)}(\infty) - z_1^{(1)}(-\infty) = 0$

Bibliography

[1] M. Lisak A. Bondeson and D. Anderson. Soliton perturbations: a variational principle for the soliton parameters. *Phys. Scrip.*, 20:479–485, 1979.

[2] M. J. Ablowitz and A. P. Clarkson. *Solitons, Nonlinear Evolution Equations and Inverse Scattering.* Number 149 in London Mathematical Society Lecture Note Series. Cambridge University Press, Cambridge, United Kingdom, 1991.

[3] G. P. Agrawal. *Fibre-optic Communication Systems.* Wiley Inter-Science, 1997.

[4] A.Hasegawa and F. D.Tappert. Transmission of stationary nonlinear optical pulses in dispersive dielectric fibers II: Normal dispersion. *Appl. Phys. Lett.*, 23:171–173, 1973.

[5] Y. L. Alpert. *Space Plasma.* Cambridge: Cambridge Univ. Press, 1990.

[6] S. Boyd and L. O. Chua. Uniqueness of a basic nonlinear structure. *IEEE Trans. Circuits Syst.*, CAS-30:648–651, Sept. 1983.

[7] S. Boyd and L. O. Chua. Uniqueness of circuits and systems containing one nonlinearity. *IEEE Trans. Autom. Control*, AC-32:674–681, June 1983.

[8] M. D. Kruskal C. S. Gardner, J. M. Green and R. M. Miura. Method for solving the korteweg de vries equation. *Phys. Rev. Letter*, 19:1095 – 1097, 1967.

[9] E. Carman, K. Giboney, and M. Case. 28-29 GHz distributed harmonic generation on a soliton nonlinear transmission line. *IEEE Microwave and Guided Wave Letters*, 1:28–31, Feb. 1991.

[10] R. Chai and K. M. Wong. Applications of solitons in data communications, Part I: Transmission properties of solitons. *Submitted to IEEE Trans. CAS-I*, 2007.

[11] R. Chai and K. M. Wong. Applications of solitons in data communications, Part II: A soliton data transmission system. *Submitted to IEEE Trans. CAS-I*, 2007.

[12] A. S. Davydov. *Solitons in Molecular Systems.* Holland: Kluwer Academic Publishers, 1985.

[13] P.G. Drazin and R.S. Johnson. *Solitons: An Introduction.* Cambridge University Press, 1990.

[14] L. N. Dworsky. *Modern Transmission Line Theory and Applications.* New York : Wiley, 1979.

[15] A. T. Filippov. *The Versatile Soliton.* Boston : Birkhäuser, 2000.

[16] H. Flaschka. On the Toda lattice - Inverse-Scattering solution. *Prog. of Theo. Phys.*, 51:703 – 716, Mar. 1974.

[17] I. S. Gradshteyn and I. M. Ryzhik. *Tables of Integrals, Series, and Products.* Academic Press, 1965.

[18] K. B. Hannsgen. *Volterra and Functional Differential Equations.* New York : M. Dekker, 1982.

[19] A. Hasegawa. *Optical Solitons in Fibers.* Springer-Verlag, 1989.

[20] A. Hasegawa and F. D.Tappert. Transmission of stationary nonlinear optical pulses in dispersive dielectric fibers I: Anomalous dispersion. *Appl. Phys. Lett.*, 23:142–144, 1973.

[21] H. Hasimoto. A soliton on a vortex filament. *J. Fluid Mech.*, 51:477–485, 1972.

[22] S. Haykin. *Communication Systems.* New York: John Wiley & Sons, 1994.

[23] R. Hirota and K. Suzuki. Theoretical and experimental studies of lattice solitons in nonlinear lumped networks. In *Proc. IEEE*, volume 61, pages 1483–1491, Oct. 1973.

[24] S. Hranilovic. *Wireless Optic Communication Systems.* New York : Springer, 2005.

[25] J. M. Kahn. Modulation and detection techniques for optical communication systems. *Optical Society of America, 2006.*

[26] V. I. Karpman and E. M. Maslov. Perturbation theory for solitons. *Sov. Phys. JETP*, 46:281–291, Aug. 1977.

[27] V. I. Karpman and E. M. Maslov. A perturbation theory for the korteweg-de vries equation. *Physics Letters*, 60A:307–308, Mar. 1977.

[28] D. J. Korteweg and G. de Vries. On the change of form of long waves advancing in a rectangular canal and on a new type of long stationary waves. *Phil. Mag.*, 5:422–443, Oct. 1895.

[29] Y. Kubota and T. Odagaki. Propogating of solitons in the Toda lattice with an impure segment. *Physical Review E*, 67:3133–3138, Mar. 2000.

[30] S. M. Kuo and W. Gan. *Digital Signal Processors : Architectures, Implementations, and Applications.* N.J. : Pearson Prentice Hall, 2005.

[31] G. L. Lamb. *Elements of Soliton Theory.* New York : John Wiley & Sons, 1980.

[32] G. L. Lamb. Analytical descriptions of ultrashort optical pulse propagation in a resonant medium. *Rev. Modern Phys.*, 43:99–124, 1971.

[33] J. H. Mathews. *Numerical Methods for Computer Science, Engineering, and Mathematics.* Prentice-Hall, 1987.

[34] J. A. Murdock. *Perturbations : Theory and Methods.* New York : Wiley, 1991.

[35] K. Nagahama and N. Yajima. Impurity localized modes of nonlinear lattice systems. *J. Phys. Soc. Jpn.*, 58:1539–1549, May 1989.

[36] H. Nagashima and Y. Amagishi. Experiment on the Toda lattice using nonlinear transmission lines. *JPSJ*, 45:680–688, Aug. 1978.

[37] A. Nakamura and S. Takeno. Scattering of a soliton by an impurity atom in the Toda lattice and localized modes. *Prog. Theor. Phys. 58*, 58:1074–1076, 1977.

[38] H. Gabriel N.K. Voulgarakis, D. Hennig and G.P. Tsironis. Polaronic electron transfer in β–sheet protein models. *J. Phys.: Condens. Matter*, 13:9821–9834, 2001.

[39] S. Novikov. *Theory of Solitons : the Inverse Scattering Methods.* New York: Consultants Bureau, 1984.

[40] P. J. Olver and D. H. Sattinger. *Solitons in Physics, Mathematics, and Nonlinear Optics.* New York : Springer-Verlag, 1990.

[41] L. A. Ostrovsky and Y. A. Stepanyants. Do internal solitons exist in the ocean. *Rev. of Geophysics*, 27:293–310, Mar. 1989.

[42] A. Papoulis. *Signal Analysis.* McGraw-Hill, 1977.

[43] J. G. Proakis. *Digital Communications.* McGraw-Hill, 2001.

[44] I. S. Reed. On a moment theorem for complex gaussian processes. *IRE Transactions on Information Theory*, pages 194–195, Apr. 1962.

[45] W. J. Rugh. *Nonlinear System Theory : the Volterra/Wiener Approach.* Johns Hopkins University Press, 1981.

[46] J.S. Russell. Report on waves. In *Proc. Roy. Soc., Edinburgh*, pages 319–320, 1844.

[47] I. W. Sandberg. The mathematical foundations of associated expansions for mildly nonlinear systems. *IEEE Trans. Circuits Syst.*, CAS-30:441–455, July 1983.

[48] A. C. Singer. *Signal Processing and Communication with Solitons.* Ph.D. dissertation. Massachusetts Institute of Technology, 1996.

[49] A. C. Singer, A. V. Oppenheim, and G. W. Wornell. Detection and estimation of multiplexed soliton signals. *IEEE Trans. Signal Processing*, 47:2768–2782, Oct. 1999.

[50] K. Suzuki, R. Hirota, and K. Yoshikawa. Amplitude-modulated soliton trains and coding-decoding applications. *IST J. Electronics*, 34:777–784, Oct. 1973.

[51] K. Suzuki, R. Hirota, and K. Yoshikawa. The properties of phase modulated soliton trains. *Japanese J. Applied Physics*, 12:361–365, Mar. 1973.

[52] J. R. Taylor. *Optical Solitons Theory and Experiment.* Cambridge University Press, 1992.

[53] M. Toda. *Theory of Nonlinear Lattices.* Springer-Verlag, 1988.

[54] M. Toda. Vibrations of a chain with nonlinear interactions. *J. Phys. Soc. Japan*, pages 431 – 436, 1967.

[55] C. J. Tranter. *Techniques of Mathematical Analysis.* The English Universities Press Ltd., 1961.

[56] H. L. Van Trees. *Detection, Estimation, and Modulation Theory.* John Wiley & Sons, 1968.

[57] S. Watanabe and M. Toda. Interaction of soliton with an impurity in nonlinear lattice. *J. Phys. Soc. Jpn.*, 50:3436–3442, Oct. 1981.

[58] D. Weiner and J. Spina. *Sinusoidal Analysis and Modeling of Weakly Nonlinear Circuits.* New York: Van Nostrand Reinhold, 1988.

[59] N. Wiener. *Nonlinear Problems in Random Theory.* Cambridge, Mass: M.I.T. Press, 1958.

[60] E. Witt and W. Lotko. Ion-acoustic solitary waves in a magnetized plasma with arbitrary electron equation of state. *Phys. Flouids*, 26:1983, 2176-2185.

[61] N. Yajima. Scattering of lattice solitons from a mass impurity. *Phys. Scrip.*, 20:431–434, 1979.

[62] V. E. Zakharov and A. B. Shabat. Exact theory of two-dimensional self-socusing and one-dimensional self-modulation of waves in nonlinear medis interaction of "solitons". *Sov. Phys. JETP*, 34:62–69, 1972.